GREENLAND EQUILIBRIUM LINE FROM ERS-1/2 SCATTEROMETERS AND SURFACE MASS BALANCE MODEL DATA

by

EMILY J. POWELL
(Under the Direction of Thomas L. Mote)

ABSTRACT

Long-term changes in the surface mass balance of the Greenland ice sheet are thought to respond directly to climate changes. Studies have shown increased thinning mainly along the southwest and northern margins, but thickening has been observed in the higher elevation accumulation regions. Knowledge of whether the overall change is positive or negative remains unclear. Therefore, this study compares data from the first and second Earth Remote Sensing (ERS-1/2) satellites and surface mass balance model data for the years 1992 to 1999. From ERS-1/2 data, the snow/ice zones are delineated and compared with accumulation, runoff, and surface mass balance estimates ascertained for this period. Results show substantial interannual variability between the data sets mainly along the periphery of the ice sheet in the southwest and northern margins. Surface mass balance estimates agreed within higher elevations, but disagreed in lower elevations of the ice sheet.

INDEX WORDS: Greenland ice sheet, Earth Remote Sensing Satellite, Equilibrium line, Surface mass balance

GREENLAND EQUILIBRIUM LINE FROM ERS-1/2 SCATTEROMETERS AND SURFACE MASS BALANCE MODEL DATA

by

EMILY J. POWELL

B.S., The University of Georgia, 2000

A Thesis Submitted to the Graduate Faculty of The University of Georgia in Partial Fulfillment of the Requirements for the Degree

MASTER OF SCIENCE

ATHENS, GEORGIA

2003

GREENLAND EQUILIBRIUM LINE FROM ERS-1/2 SCATTEROMETERS AND SURFACE MASS BALANCE MODEL DATA

by

EMILY J. POWELL

Major Professor:	Thomas L. Mote
Committee:	Andrew Grundstein
	Chor-pang Lo

Electronic Version Approved:

Maureen Grasso
Dean of the Graduate School
The University of Georgia
August 2003

ACKNOWLEDGEMENTS

There are a number of people I would like to mention that have contributed to the completion and success of this thesis. I would like to first acknowledge Dr. Thomas Mote, my major advisor, who provided me with invaluable expertise in the subject and helped tremendously in the research and writing processes and who initially introduced me to this topic. I wish to thank Dr. Andrew Grundstein for his commitment and flexibility during the last few months of my studies, and to Dr. Chor-pang Lo and Dr. Andrew Grundstein for their support and recommendations.

I want to express my gratitude to Dr. Edward Hanna who supplied me with data from his research. I would also like to mention Dr. Thomas Mote for providing me with data from his own research, as well as background material on the Greenland ice sheet from his personal experience. Additionally, I would like to acknowledge the NASA sponsored Scatterometer Climate Record Pathfinder project at Brigham Young University and the rich inventory of data that they have available. I wish to also mention, specifically, Dr. David Long and Dr. Mark Drinkwater whose work became an important component in this thesis.

TABLE OF CONTENTS

Page

LIST OF TABLES

Page

LIST OF FIGURES

Page

CHAPTER 1

INTRODUCTION

Monitoring the surface mass balance of the Greenland ice sheet is important in climate change research, particularly in understanding the ice sheet's relationship to global sea levels. Several studies have addressed the role Greenland plays in predictions of future sea level under various climate change scenarios; however, there is uncertainty as to whether the ice sheet as a whole is increasing or decreasing in mass. The Greenland ice sheet covers approximately 1.7 million square kilometers (Weidick, 1985), and the amount of ice contained in the ice sheet is equivalent to 6-7 meters of global sea level (Hvidberg, 2000). Abdalati and Steffen (2001) estimated the relationship between Greenland surface temperature and sea level rise to be 0.31 mm per year for a 1° C temperature increase. Other studies have estimated this relationship between Greenland temperature and sea level to be an increase of 0.6 mm per year of global sea level for a 1° C rise in surface temperature (Braithwaite and Olesen, 1989; Bindschadler, 1985). Over the last century, Greenland is suggested to have undergone melting approximately equal to 0.6 mm per year increase in sea levels (Mitrovica et al. 2001).

The mass conservation of an ice sheet is expressed as:

$$\partial V/\partial a = Qa - Qm - Qc + Q_B. \quad (1.1)$$

where, V represents the ice volume, a is equivalent to a one-year period, Qa is the annual surface accumulation, Qm is the annual loss by glacial surface runoff, Qc is the annual

loss by calving of icebergs, and Q_B is the annual balance at the bottom, where melting or freeze-up of ice occurs; all ice volumes are expressed in ice equivalents (Reeh, DCRS at the Technical University of Denmark). According to Reeh, Equation 1.1 suggests that the mass balance of Greenland may be determined by measuring the change in volume through monitoring changes in elevation, or by using the budget method, where each variable on the right hand side of the equation is determined separately.

The surface mass balance (SMB) of an ice sheet is simply the difference between net accumulation and net runoff (Hanna et al. 2002). Locations on the ice sheet where the net surface mass balance equals zero are said to be in a steady state and the total mass input is exactly balanced by the mass loss. Net accumulation is typically defined as solid precipitation minus sublimation or evaporation (Hanna et al. 2002), although accumulation comprises of other processes such as precipitation, condensation, and freezing of liquid water, that add snow or ice to a glacier. Runoff consists of meltwater, both surface runoff and refrozen meltwater. Net runoff, therefore, is defined as runoff of surface meltwater minus that part which refreezes on or in the ice before being lost (Hanna et al. 2002). Total ablation differs from net runoff in that ablation comprises of additional processes that also remove snow or ice from a glacier, such as evaporation or sublimation, wind ablation, and, most importantly, ice calving.

The equilibrium line (EL) serves as an important indicator of the state of the SMB, as it represents areas where accumulation is exactly balanced by ablation, or where the SMB is equal to zero. The EL, therefore, divides the ice sheet into an accumulation zone, where the net SMB is positive, and an ablation zone, where the net SMB is negative. Shifts in the location of this boundary are thought to relate strongly to climate

fluctuations, so monitoring changes in its location over an extended period of time can reveal information on how the ice sheet responds to changes in climate. Studying the effects that climate perturbations have on the location of the EL, Ambach (1993) found that a change in air temperature of +1 K produced a shift of the equilibrium line altitude (ELA) of + 87.5 meters, due to the fact that a rise in temperature leads to a prolongation of the ablation period.

The ice sheet responds to both temperature and precipitation, and as a warmer climate is expected to lead to enhanced precipitation, subsequently contributing to greater accumulation rates, determining the overall net change in the SMB of the ice sheet becomes challenging. Zwally (1989) suggested that as temperature and precipitation rise together, any change in the position of the EL would be small, since temperature and precipitation cause an opposite shift in the ELA, with a decrease and increase in the EL, respectively. Also, the short-term effect will likely be a growth in the ice sheet, since the majority of the ice sheet lies in the accumulation zone.

Because of the difficulty in obtaining accurate measurements of accumulation and ablation rates, it is advantageous to utilize data from multiple sources to more confidently assess the state of the SMB of the Greenland ice sheet. Therefore, this study will examine areas of accumulation and runoff across the Greenland ice sheet during the period 1992 to 1999 with data previously compiled by the Brigham Young University (BYU) Scatterometer Climate Record Pathfinder (SCP) project, and results from studies by Hanna et al. (2002) and Mote (2003). Altogether, this thesis utilizes data from the first and second Earth Remote Sensing (ERS-1/2) satellites, and annual net accumulation and runoff rates

derived primarily from SMB models for the years 1992 to 1999. A general map of Greenland illustrating the ice sheet outline is shown in Figure 1.1.

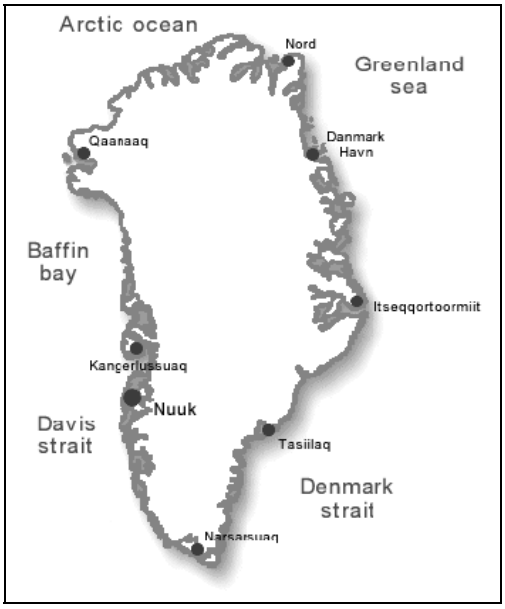

Figure 1.1 Map of Greenland showing the outline of the ice sheet and the exposed land in grey (http://www.dpc.dk/Res&Log/Links/InfoMaps.html).

The main goals of this thesis are to examine interannual variability in accumulation, net runoff, and therefore the location of the EL of the Greenland ice sheet and to determine the spatial and temporal changes to assess how the three data sets agree or disagree over this period. Monitoring the spatial variability of accumulation and ablation areas across the ice sheet over an extended period of time can provide indications of the ice sheet's response to climate change. Although this study does not employ a sufficient number of years to facilitate a true understanding of past climatological trends, it can contribute towards an understanding of the tools available to monitor the SMB. Therefore, this thesis is part of an ongoing effort to better understand the recent changing states of the SMB of the Greenland ice sheet.

CHAPTER 2

BACKGROUND

An understanding of the past, current, and future states of the SMB of the Greenland ice sheet is limited largely due to the complexity associated with obtaining reliable estimates of accumulation and ablation across the ice sheet. This section details results from past studies that have focused on acquiring more accurate estimates of Greenland SMB, accumulation, and net runoff rates, as well as a brief description of synoptic patterns that determine the spatial distribution of these mass balance components. Additionally, snow and ice zones of the Greenland ice sheet defined from radiometer and scatterometer data are discussed.

2.1 Surface mass balance

Understanding spatial and temporal surface mass balance changes is critical in predicting an ice sheet's response to climate change and in assessing its relationship with sea level. The mass balance at any given time is the sum of the accumulation and ablation rates, typically expressed in units of water equivalent, and the mass balance is commonly measured over a balance or budget year, represented as the time of maximum ablation from one year to the next. Difficulty arises when assessing the balance of an entire ice sheet or glacier, since the balance year is generally not the same at all areas and the

length of the balance year may vary from year-to-year. Additionally, the area of the ice sheet may change slightly within a balance year.

Obtaining measurements of the mass balance of the entire Greenland ice sheet would be difficult and expensive, but Bindschadler (1984) offered a way to circumvent this by studying individual drainage basins within the ice sheet. His study focused on the Jakobshavn Glacier basin located within the west central margin of the ice sheet. The Jakobshavn basin discharges between 4.8 and 7.6% of the annual net balance over Greenland. Results from his study indicated that the Jakobshavn Glacier was in approximate balance, based on radar altimeter data from the Seasat satellite from June to October 1978. He emphasized the importance of obtaining surface velocity and ice thickness measurements to assess the balance in localized areas. More recently, Mote (2000) looked at several transects along elevation gradients within the Greenland ice sheet to estimate ablation rates and mass balance using Scanning Multichannel Microwave Channel (SMMR) 37H brightness temperatures. This method was effective for determining the equilibrium line altitude along these transects, which can serve as an indication of climate change and change in the mass balance of the ice sheet.

During 1994 to 1999, a general thinning below about 2000 m elevation was found for the ice sheet (Krabill et al., 2000), and thickening rates were observed within higher elevation regions of the ice sheet during 1993 to 1997 (Thomas et al., 2000) using airborne laser altimetry data to monitor surface elevation changes. Krabill et al. (2000) further estimated a total net loss in ice volume of 51 km^3 per year for the entire Greenland ice sheet, equivalent to 0.13 mm per year sea-level rise for the period 1994 to 1999. The southern portion of the ice sheet underwent high interannual elevation changes, about 20

cm per year, whereas north of about 70° latitude there were considerably less elevation changes, about 10 cm per year.

Hanna et al. (2002) estimated accumulation and runoff for the period 1992 to 1998 using European Centre for Medium-Range Weather Forecasts (ECMWF) climate analysis data in meteorological and glaciological models, and their results showed considerable interannual and spatial variation in both accumulation and ablation rates. These estimates were averaged across the Greenland ice sheet mask from Abdalati and Steffen (1997), and accumulation ranged from 0.333 m (533 km^3) in 1992 to 0.232 m (371 km^3) in 1995, and annual runoff rates ranged from 0.049 m (78 km^3) in 1992 to 0.280 m (448 km^3) in 1998, when greatest surface melt runoff occurred in the lower elevation areas of the southwest. Therefore, surface mass balance measurements indicated that the ice sheet was in positive balance during most of the period from 1992 to 1997 and slightly negative during 1998. Thomas et al. (2000) found that, on average, higher elevation regions of the Greenland ice sheet were in balance during 1993 to 1997 using repeat Global Positioning System (GPS) measurements, although areas of both thickening and thinning were observed during the period. During the period 1988 to 1999, the SMB of Greenland was found to vary greatly both interannually and spatially across the ice sheet, with accumulation rates dominating the variability in the southeast, the runoff rate in the west, and neither component in the north (Mote, 2003).

2.2 Ablation rates

It is believed that the margins of the ice sheet are generally more sensitive to climate changes than areas further inland. Summer melting at two locations along the

margin of the Greenland ice sheet, namely Nordbogletscher and Qamanârssûp sermia (Figure 2.1), were expected to increase by about 0.5 m water a^{-1} for each degree rise in summer temperature, June-August (Braithwaite and Olesen, 1990). Further, Braithwaite and Olesen (1992) measured the ablation rate at the margin of the ice sheet at Qamanârssûp sermia and found that the increase in annual ice ablation was about 1 m water a^{-1} $°C^{-1}$, and ablation was expected to double here with a + 5° C temperature change. As mentioned above, Thomas et al. (2000) illustrated that much of the higher elevation regions of the ice sheet showed areas of both thickening and thinning, and they further suggested a general thinning is likely at lower elevation areas of the ice sheet.

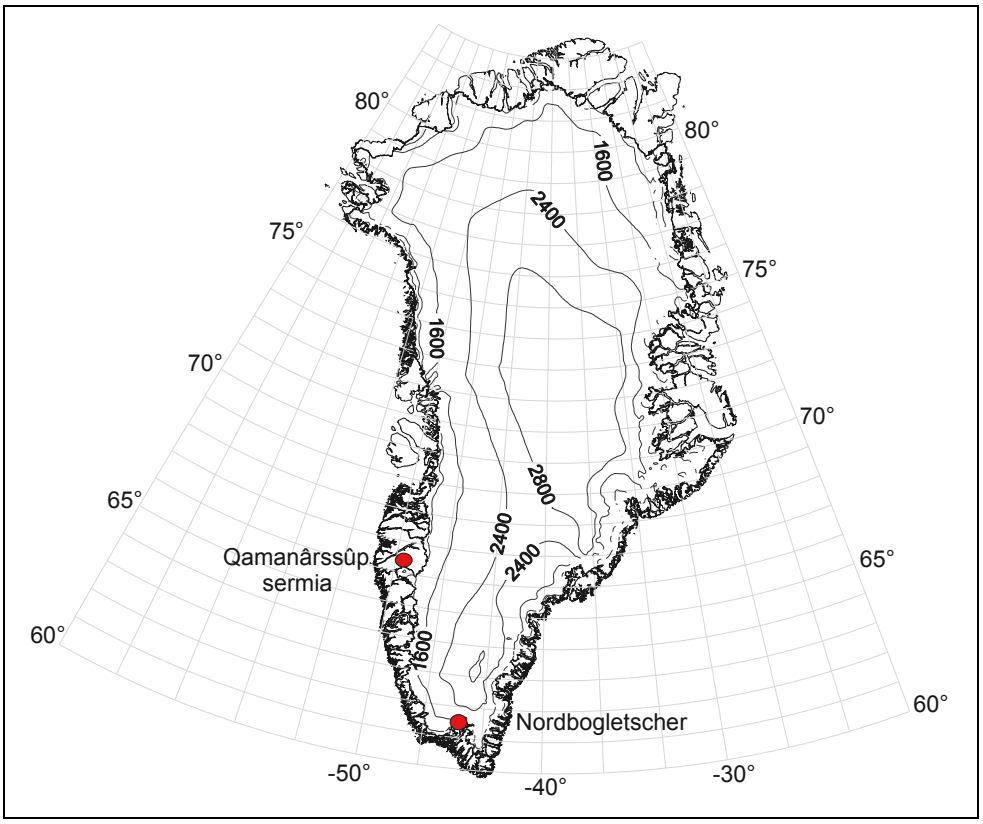

Figure 2.1 The locations of Nordbogletscher and Qamanârssûp sermia in southern Greenland, elevation contours are in meters.

Further, Krabill et al. (2000) indicated that thinning was experienced along approximately 70% of the coast during 1994 to 1999.

The Greenland ice sheet experienced an increasing areal melt extent trend of 1% per year over a 21-year period, 1979 – 1999, mainly in the western portion of the ice sheet, and a slight decrease in melt in the east (Abdalati and Steffen, 2001). Results from their study asserted that greatest melting of the ice sheet occurs in its shallow-sloped western edge, which also dominates the melt of the ice sheet as a whole. Conversely, the eastern side is characteristic of steeper slopes and a relatively lower melt area and is less important to the ice sheet melting as a whole. Mote and Anderson (1995) found a trend of increasing seasonally averaged daily melt extent of about 3.8% annually for the months May through August, with July and August accounting for 70% of the seasonal trend. They also observed the increase in mean melt extent to be confined to the west and southwest of the ice sheet, which is in agreement with results from Abdalati and Steffen (2001). Additionally, an increase in the spatial extent of ablation at higher elevations was observed along the southwestern flank of the ice sheet (Drinkwater et al. 2001).

Runoff and accumulation rates were examined by Mote (2003) for the period 1988 to 1999 in order to determine the cause of any changes in the SMB. These trends were then related to surface elevation changes. Mote (2003) observed a trend in surface elevation changes with a thinning generally below 2000 m a.s.l. However, in the south thinning was observed up to 2400 m, and in the north thinning was observed at lower elevations only up to between 1000 and 1200 m a.s.l. These findings were in general agreement with Krabill et al. (2000) who used laser altimetry measurements of thinning

and thickening across the ice sheet over a shorter period, 1993 to 1999. Thomas et al. (2000) discovered over the past few decades within higher elevations of the ice sheet, on average, thickening of 21 centimeters per year is observed in the southwest portion and thinning of 30 centimeters per year in the southeast portion of the ice sheet. The north showed a reversal with a general thickening in the east and thinning in the west. In addition, a comparison between the Seasat Scatterometer (SASS) from 1978, and NASA scatterometer (NSCAT) from 1996 revealed that the location and extent of the region of dry snow decreased due to an increase in the melt extent since 1978 (Drinkwater et al., 2001). It is believed that SMB changes may explain some portion, but not all, of the observed elevation changes on the Greenland ice sheet (Krabill et al., 2000).

2.3 Accumulation rates

An updated accumulation map of Greenland was developed for the period 1971 to 1990 using a combination of published historical data and data from the Program for Arctic Regional Climate Assessment (PARCA) that consisted of point accumulation estimates for over forty locations on the ice sheet (Bales et al. 2001). Certainty in these data varied across regions of the ice sheet with greatest uncertainty existing in areas with both large variances and large accumulation values, which were found in the west central and east central regions based on historical ice core and snow pit data. The pattern of accumulation mirrors that of precipitation, as Ohmura and Reeh (1991) found greatest precipitation along the east coast of the southern part of the ice sheet and accumulation estimates were typically greatest on the east-facing slope of the southern ice cap. These measurements were derived from a total of 251 snow pits and cores

obtained from the upper accumulation zone and precipitation measurements at thirty-five meteorological stations along the coastal regions. Obtaining more reliable estimates of accumulation and ablation rates has been of particular interest to reduce some of the existing uncertainties in the SMB of the Greenland ice sheet. Several studies have focused on obtaining more reliable measures of accumulation including, but not limited to, Ohmura and Reeh (1991), Drinkwater et al. (2001), McConnell et al. (2001), Hanna et al. (2001), and Bales et al. (2001).

The overall patterns of annual accumulation, consisting of solid precipitation minus sublimation or evaporation, and precipitation for the Greenland ice sheet are similar (Ohmura and Reeh, 1991; Long and Drinkwater, 1994). Within the southern part of Greenland, the east coast typically receives a greater amount of precipitation than the west coast. During the winter, the southeast slope of Greenland receives enhanced precipitation rates caused by inflow of water vapor from the Atlantic Ocean due to the Icelandic low circulation. In summer, southwesterly flow along the west coast of Greenland containing high water vapor results in a summer peak of precipitation. The northeast slope of the ice sheet is in a precipitation shadow from the dominant westerly flow and topography of the ice sheet. Local influences on the accumulation distribution across the ice sheet are described in greater detail by Ohmura and Reeh (1991).

McConnell et al. (2001) determined the relationship between accumulation and sea level by measuring snow accumulation rates over the southern Greenland ice sheet south of about 73° N latitude from 1975 to 1998. An increase of 37% was observed in accumulation during the calendar year 1995 to 1996, which corresponded to a drop in sea level of approximately 0.16 mm per year when taken alone. They concluded that typical

year-to-year variability in sea level caused by changes in snow accumulation within the high elevation regions of the southern ice sheet represents more than one third of the total estimated increase in sea level each year caused by Greenland mass balance changes.

2.4 Synoptic controls

The distribution of accumulation and ablation across Greenland are mostly controlled by large-scale atmospheric circulation patterns. Several studies have examined the roles of atmospheric circulation on the distribution of accumulation and ablation across the ice sheet, including Ohmura and Reeh (1991), Mote (1998a and 1998b), and Drinkwater et al. (2001). Summer to fall precipitation and summer ablation in the northwest region of Greenland are regulated by the strength of cyclonic activity over Baffin Bay, and any changes observed in these areas may be the result of shifts in large-scale atmospheric circulation (Drinkwater et al., 2001). For instance, during positive phases of the North Atlantic Oscillation (NAO), net precipitation is generally reduced over western Greenland. A large-scale reversal in the spatial pattern of accumulation along the northwestern part of Greenland is indicative of more frequent cyclonic activity in Baffin Bay and more frequent negative phases of the NAO (Drinkwater et al., 2001). The NAO accounted for approximately 55% of the interannual trend in melt extent for the entire ice sheet during 1979 to 1989, and the circulation characteristics were more efficient at explaining surface melt variations early in the summer season, May to August, for southern regions of the ice sheet and late in the season for northern regions (Mote, 1998a). As longer time-series data of

Greenland become available, the relationship between accumulation and ablation patterns with large-scale circulation anomalies may be evaluated in greater detail.

2.5 Greenland snow and ice zones

Several studies have partitioned the Greenland ice sheet into characteristic hydrologic regimes, and Benson (1962) produced initial measures of the snow and ice facies of Greenland. A zone or facies represents observable differences that distinguish one snow or ice unit from another, and the boundaries between each of these regions are distinguishable by strong gradients in surface properties. An illustration of the concept of ice facies implemented by Benson (1962) is shown in Figure 2.2 and a map of the original snow facies for Greenland in Figure 2.3. Benson based these regions on a collection of snow stratigraphy data of the ice sheet. Many studies have since contributed to Benson's glacier-facies classification scheme of various snow and ice zones of a glacier, including Benson (1967), Paterson (1981), and Williams et al. (1991), to name a few. Further, Williams et al. (1991) effectively demonstrated this evolution in the glacier-facies concept.

The dry snow zone dominates the central, interior portions of the ice sheet. The lower extent of the dry snow zone marks the location of the dry snow line (DSL) (Figure 2.2) where above this line negligible melting or percolation takes place (Benson, 1962). The region downslope of the dry snow zone is characteristic of downward percolating meltwater into the sub-surface layers of the ice sheet and is known as the percolation zone. The wet snow line (WSL) then bounds this region of percolating snow from the area downslope, the wet snow zone, where the surface is covered by wet or saturated

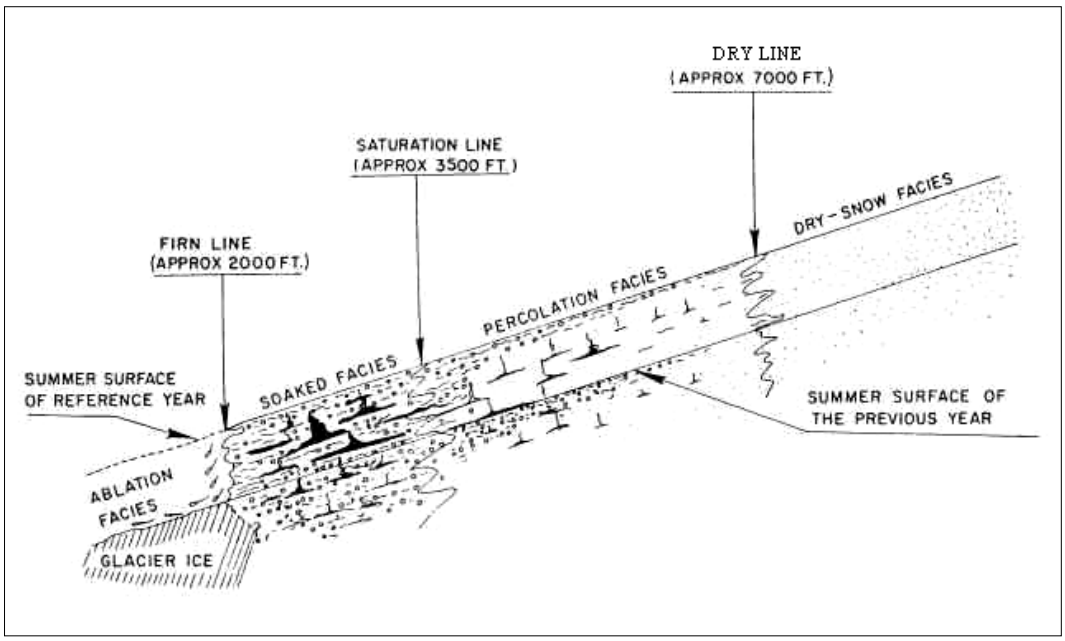

Figure 2.2 Generalized cross section of snow facies from Benson (1962). Negligible melt occurs in the dry snow zone, the percolation zone shows that percolation decreases with altitude and is minimal at the dry snow line, and snow cover is entirely gone at the end of the ablation season in the ablation zone.

snow at 0° C isotherm (Long and Drinkwater, 1994). The snow or firn line marks the lowest region of perennial snow found at the lower extent of the wet snow zone from the outer extent of the ice sheet or the area of bare glacial ice, defined as the ablation zone. During normal balance years, the EL is thought to closely approximate the location of the snow or firn line around mid-July, according to Long and Drinkwater (1994).

The dry and wet snow lines mark transitions between melting or freezing processes and, thus, change in the patterns of melting and accumulation (Long and Drinkwater, 1994). The dry and wet snow zones may be easily identifiable through the use of microwave satellite measurements that penetrate several meters into the snow and

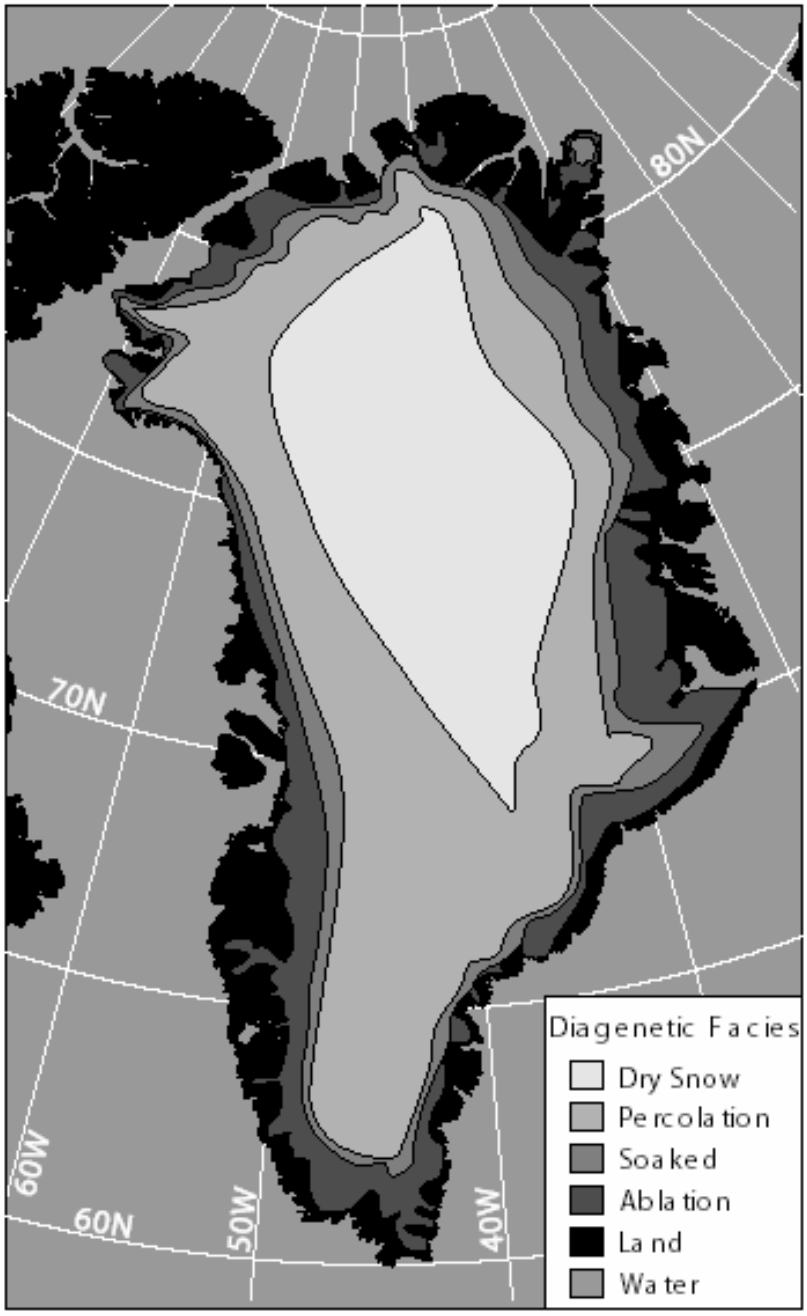

Figure 2.3 Illustration of the diagenetic facies on the Greenland ice sheet based on Benson (1962).

ice. Long and Drinkwater (1994) emphasized that microwave remote sensing demonstrates an effective means at which to infer surface characteristics by use of the 1.2 GHz L- and 5.3 GHz C-band microwave radar that are sensitive to variations in both surface and sub-surface snow characteristics. Several studies have presented these capabilities, including Rott et al. (1985), Swift et al. (1985), Bindschadler et al. (1987), Jezek et al. (1990, 1993), Long and Drinkwater (1994), and Drinkwater et al. (2001).

Additionally, satellite radar altimetry measurements on the ice sheet have provided valuable information about the characteristic behavior of dry versus wet snow within the various ice zones of Greenland. Partington et al. (1989) produced a classification of mean Greenland radar wave forms with latitude from altimeter radar echoes for the snow and ice regions defined by Benson (1962). Sample regions along the Greenland ice sheet from 72° to 64° N latitude were used to show the relationship of the relative importance of surface and volume scattering with latitude. In the dry snow zone, volume scattering was found to dominate, as the depth of penetration is generally much greater in a snowpack with low water content; whereas, in the soaked or wet snow zone surface scattering was dominant, as the penetration depth decreases.

2.6 Radar scatterometer snow and ice zones

Microwave remote sensing is an optimal method of acquiring a spatially and temporally detailed analysis of snow melt occurrences. Unlike visible and infrared remote sensing, microwave scatterometers and radiometers have the advantages of large spatial coverage in polar regions and are mostly uninhibited by clouds or rain. Although they were initially designed for analysis of wind over ocean, scatterometers

have been found to exhibit sensitivity to ice coverage as well (Long et al., 1993). A spaceborne scatterometer is a radar instrument designed to measure the radar backscatter of the surface of the earth. The radar backscatter behavior of snow is governed by various parameters like surface roughness, snow wetness, and stratification. Its sensitivity depends largely on the dielectric properties, such as the shape and size of ice particles and snow density. Thus, differences in the degree of backscatter vary seasonally and by snow type. Several studies have examined the snow and ice regions of the Greenland ice sheet using scatterometer data, including Swift et al. (1985), Long and Drinkwater (1994), Drinkwater et al. (2001).

Radar backscatter from airborne scatterometers over land and ice provide information on surface characteristics and ice conditions, and is, therefore, useful in acquiring measurements of accumulation and runoff. Drinkwater et al. (2001) used 13.6 GHz Ku-band and 5.3 GHz C-band scatterometer measurements of normalized radar backscatter to observe changes in the spatial pattern of snow accumulation and melting in the northwestern flank of Greenland during the periods 1978-1996 and 1997-2000. An increasing spatial extent of positive differences in the measured backscatter taken from the NASA and Seasat Scatterometers (NSCAT, SASS) was observed during a three-year period, providing further evidence of the cumulative effects of melting (Figure 2.4). This increase in the spatial extent of melting was thought to be responsible for the observed thinning of the periphery of the ice sheet seen by Krabill et al. (2000) and Abdalati et al. (2001).

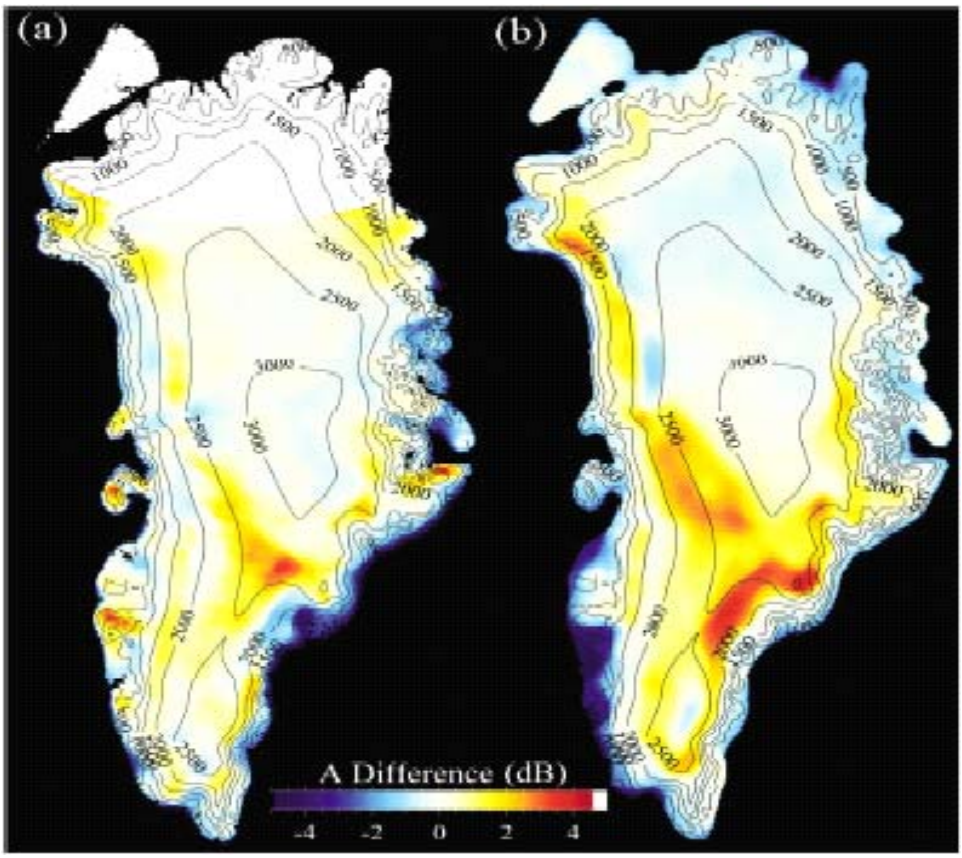

Figure 2.4 Images showing positive differences in V-polarization A backscatter values, indicating increases in scattering by buried ice lenses due to summer melt. The differences between a) SASS (1978) and NSCAT (1996) are substantially less than those between b) NSCAT (1997) and QSCAT (2000), as shown by Long et al. (2001).

Backscatter measurements from C-band Earth Remote Sensing satellites (ERS-1/2), Ku-band ADEOS-1 NASA Scatterometer (NSCAT), Ku-band SeaWinds on QuikScat (QSCAT), and Seasat-A (SASS) scatterometers are used to estimate the extent of snow and ice zones as well as the location of their boundaries. Backscatter of glacial ice is approximately a linear function of incidence angle, θ, with a range

between 20° and 60°, and the relationship of backscatter (in dB) to incidence angle can be represented by the following equation:

$$\sigma^{\circ}(\theta) = A + B(\theta - 40) \qquad (2.1)$$

where the backscatter component normalized to the mean incidence angle of 40° is A, and the dependence of backscatter on the incidence angle is B in dB deg^{-1}. These values of A and B are commonly used to produce enhanced resolution images, as both A and B have a notable correlation with land type and vary with surface conditions (Long et al. 1993, Long and Drinkwater 1994, and Drinkwater et al. 2001).

By applying resolution enhancements to scatterometer data, particularly to A and B, it was possible to take advantage of the overlap of multiple passes of the same area, according to Long et al. (1993). The scatterometer image reconstruction (SIR) and the SIR with filtering (SIRF) algorithms were applied to estimated A and B images from simulated backscatter (σ°) measurements (Long et al., 1993, Long and Drinkwater, 1994; Drinkwater et al., 2001), as these algorithms allowed for the depiction of fine details of objects or features in an image at the cost of some evident smoothing and noise. Enhanced resolution data were used by Drinkwater et al. (2001) to define relationships between backscatter and physical properties of the surface to infer snow accumulation estimates. Results demonstrated that the dry snow line may be defined at the -1.8 dB contour line, based on frequency difference images between EScat minus NSCAT data obtained simultaneously during the Julian days 267 to 272 (September 23 to 28), 1996 (Drinkwater et al. 2001).

It was also possible to examine distinct spatial variations in backscatter during summer surface melting due to the fact that melting creates dielectric changes in the

snowpack. Further, melting has a strong impact on C-band data, resulting in horizontal gradients within the percolation zone. In winter, intense backscatter is observed due to refreezing of downward percolating meltwater that leads to permanent buried ice lenses and ice pipes in the percolation zone (Drinkwater et al. 2001). There exists relatively low backscatter at 40° incidence angle within the dry snow zone of central Greenland, which is contrasted by a bright region along the periphery of the dry snow zone indicative of the percolation zone (Figure 2.5). Throughout this region, backscatter values approach 0 dB. The lowest estimates of snow accumulation based on predictions from NSCAT B values are found in northern Greenland; whereas, the highest estimates of snow accumulation are found along the southeastern flank of the dry snow line (Drinkwater et al. 2001).

Additionally, Long and Drinkwater (1994) identified snow and ice regions of the Greenland ice sheet using enhanced resolution SASS backscatter imagery. The SIRF algorithm created enhanced resolution images of SASS backscatter from about 50 km to 6 km resolution, which allowed for better depiction of the conditions on the Greenland ice sheet. Their results showed that the dry snow line was most noticeable during the transition from summer to fall, typically in late September, and the dry snow zone was characteristic of negligible change in surface properties throughout the year. They delineated the dry snow line at the 40° incidence backscatter value (A) of -5 dB, where there existed a strong gradient apparent between low values of A in the dry snow zone and high values of A in the percolation zone. Further, they found that the WSL appears most clearly typically in early July, and it separates the lowest backscatter wet snow zone and the relatively bright percolation zone upslope. By examining SASS time-

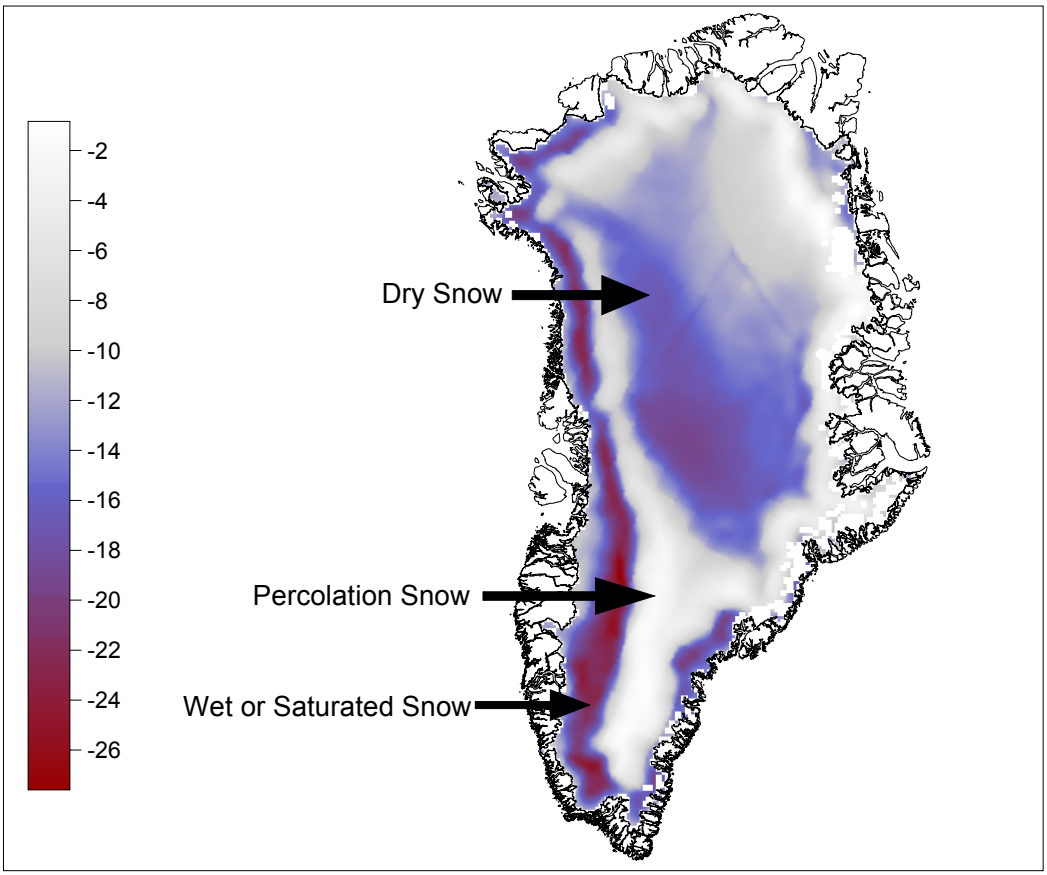

Figure 2.5 Sample image of ERS-1 backscatter A, in dB (July 21-26, 1995). Typical backscatter A values are illustrated for different regions of the ice sheet. From top to bottom, low values of A are found in the central region of dry snow, highest values of A are found in the region of percolating snow, and areas of wet or saturated snow are generally the darkest areas located near the margins of the ice sheet.

series images of Greenland from early July to late September of 1978, Long and Drinkwater (1994) were able to infer where the dry and wet snow lines exist but were less certain in the lower limit of the wet snow, i.e. the snow or firn line. The snow or firn line was characteristically not contiguous and appeared as mixed pixels in SASS imagery. Therefore, the authors recommended using higher-resolution SAR imagery in

conjunction with SASS data in order to more precisely locate the lower boundary of the wet snow zone.

This thesis uses 5.3 GHz C-band ERS-1/2 SAR data to identify the boundaries of the dry and wet snow zones. Typical penetration depths for C-band scatterometers in the dry snow zone are on the order of several meters. Early et al. (1994) found that C-band is sensitive to layering of the snow and also to slightly different scales of surface roughness. In the northern part of the dry snow zone, the higher backscatter and lower gradient indicated that the scattering characteristics differed greatly from more central and southern portions of the dry snow zone, and that layering was a much more dominant factor in signatures obtained in the northern part of the ice sheet. Early et al. (1994) implied that this was a result of different accumulation processes occurring in the northern region of the ice sheet, where lower annual precipitation and different wind patterns were observed. Further work has shown that C-band penetrates deeper than Ku-band in the percolation zone and is able to sense more buried scatterers, and melting has a larger impact on C-band, as it exhibits greater sensitivity to recent melting than Ku-band (Drinkwater et al. 2001).

2.7 Passive microwave studies

Passive microwave radiometers measure the amount of natural radiation emitted from the surface that is described by a blackbody equivalent radiometric temperature called a brightness temperature (T_b) (Mote, 1994), while microwave scatterometers use a radar sensor that transmits a microwave signal towards an object or surface and measures the amount of energy backscattered from a target. Because a substantial increase in the

emissivity of snow is observed during melt periods, monitoring the melt extent of the Greenland ice sheet can be performed by examining microwave emission patterns over time using satellite microwave radiometers. A rapid increase in brightness temperatures occurs as the snowpack melts, causing liquid water to form between individual snow grains and enhancing the surface scattering. Mote et al. (1993) analyzed time series of Special Sensor Microwave/Imager (SSM/I) data for three locations on the ice sheet and found a marked increase in brightness temperatures in late spring and early summer, with a decrease in brightness temperatures during late summer. Less variation was observed in brightness temperatures for the location within the region of dry snow. Melt threshold brightness temperature values were determined from SSMI/I 37 GHz brightness temperatures and used in a later study by Mote and Anderson (1995) to identify areas of melt on the Greenland ice sheet for the period 1979 to 1991. Their results illustrated a typical seasonal cycle of melt coverage with melt beginning in late April, a rapid increase in the melt extent from mid-May to mid-July, followed by a rapid decrease in melt area from late July through mid-August, and a termination of melt by late September. Increases in the mean melt extent observed over the ice sheet were confined largely to the west and southwest of the ice sheet.

Within the accumulation zone of the ice sheet, a peak in 37 GHz vertical and horizontal polarization brightness temperatures was shown from the Scanning Multichannel Microwave Radiometer (SMMR) during late July to early August of 1979, according to Zhang et al. (1989). Results showed that a seasonal trend becomes more pronounced with increasing frequency in the accumulation zone by comparing the 37 GHz data with 6.6 GHz data, which did not reveal a similar peak during the summer

months. Further, his results indicated different conditions in the ablation zone. In northwest Greenland near Melville Bay, the same polarization differences in the brightness temperature showed a similar trend but with lower values and a larger difference between the lowest and highest frequency. Bolzan and Jezek (1998) demonstrated that passive microwave brightness temperatures from the 18 GHz vertically polarized channel of the SMMR can be used to calculate average accumulation rates over decadal time scales to about 5% accuracy, which can be useful in mass balance calculations.

2.8 Surface mass balance measurements from climate models

Modeling may provide the most practical approach to obtain ablation and accumulation values, as continuous point measurements of mass balance are not available (Kaser et al. 2003). Various climatological and glaciological models have been applied to estimates of accumulation, runoff, and SMB of the Greenland ice sheet. Using ECMWF operational analyses data from 1992 to 1998 in conjunction with a meteorological model from Hanna et al. (2001) and a meltwater runoff/retention model from Jansenns and Huybrechts (2000), Hanna et al. (2002) produced annual maps of the Greenland ice sheet net runoff and SMB and compared their results with net runoff estimates made by Mote (2000) using SSM/I passive microwave data.

Annual estimates of accumulation, runoff, and SMB based on Hanna et al. (2002) are shown in the first three columns of Table 2.1 and passive microwave derived runoff rates are shown in the far right column. The different data sets agree well, although for all years except 1998, satellite derived ablation rates were higher than net runoff estimates

Table 2.1 Greenland ice sheet accumulation, runoff, and SMB estimates by Hanna et al. (2002) compared with satellite-derived net runoff, as shown by Hanna et al. (2002). All values are in m^{-1} yr water equivalent.

	ECMWF-based			SSM/I-based
Year	Accumulation	Net Runoff	SMB	Net Runoff
1992	0.333	0.049	0.283	0.077
1993	0.31	0.115	0.194	0.127
1994	0.245	0.062	0.186	0.105
1995	0.232	0.212	0.02	0.255
1996	0.326	0.121	0.205	0.125
1997	0.295	0.058	0.238	0.143
1998	0.269	0.28	-0.011	0.216
Mean	0.287	0.128	0.159	0.15
SD	0.039	0.087	0.111	0.063

produced by Hanna et al. (2002). Their results also indicated that during much of the 1990s, the SMB was in an overall state of positive SMB. Their estimates of SMB did not include ice mass lost due to iceberg calving. They further compared their results of the rate of change of the SMB with laser-altimetry surveys from Krabill et al. (2000), and revealed a similar pattern between the two data sets. Trends in the SMB and surface elevation were generally positive within the central portions of the ice sheet, but negative near the southeast and southwest margins. Additionally, Hanna et al. (2001) demonstrated the use of a simple meteorological model to derive accumulation estimates over Greenland, and these model-based estimates were found to provide more realistic values compared with independent data primarily developed by PARCA, although they were thought to be still too low over central Greenland.

Passive microwave observations were used in a SMB model by Mote (2003) to arrive at estimates of runoff rates, SMB, and elevation changes across the Greenland ice

sheet. Results indicated that years with higher accumulation are typically associated with overall low ablation for the ice sheet, whereas low ablation years are more likely associated with high accumulation. Further, SMB trends from 1988 to 1999 were in general agreement with elevation trends observed by Krabill et al. (2000), and, therefore, with results from Hanna et al. (2002). According to Mote (2003), the most substantial thinning during this period occurred in the southern and western portions of Greenland. Interestingly, thinning rates were found in excess of 25 cm per year in some locations, but thickening rates above 2000 m were generally in the range of only 2 to 6 cm per year.

Various surface mass balance models have proven effective in obtaining improved accumulation and runoff rates to arrive at surface mass balance estimates, demonstrated by Hanna et al. (2001, 2002) and Mote (2003). Scatterometer and radiometer satellite data have also proven useful in measuring the areal extents of the snow and ice zones of the Greenland ice sheet, as shown by Swift et al. (1985), Mote et al. (1993), Mote and Anderson (1995), Long and Drinkwater (1994), and Drinkwater et al. (2001), to name only a few. This study incorporates results from both Hanna et al. (2002) and Mote (2003) using surface mass balance model estimates and scatterometer satellite data available by the Scatterometer Climate Record Pathfinder project to examine variability in accumulation, ablation, and surface mass balance of the ice sheet for the period 1992 to 1999. From these data sets, the approximate locations of the equilibrium line were determined to assess the areal extents of the accumulation and ablation zones, which were then compared among the data sets over this period.

CHAPTER 3

DATA AND METHODOLOGY

This study compares patterns of the areal extents of the accumulation and ablation zones, and thus, the equilibrium line and surface mass balance of the Greenland ice sheet based on data previously compiled by the Brigham Young University (BYU) Scatterometer Climate Record Pathfinder (SCP) project and from results by Hanna et al. (2002) and Mote (2003). To compare accumulation and ablation areas across the ice sheet, data from Hanna et al. (2002) and a subset of data available from the BYU SCP project and Mote (2003) are employed here to compile a data set over a simultaneous temporal period of 1992 to 1999. This chapter describes each of the data sets utilized in this analysis, as well as methods used to compare the areal extents of the accumulation and ablation zones of the Greenland ice sheet between the data, largely based on the location of the equilibrium line.

3.1 ERS-1/2 scatterometer data

This study includes enhanced resolution 5.3 GHz C-band ERS-1/2 satellite data obtained from the NASA sponsored SCP project at BYU through the courtesy of David G. Long. ERS satellites are Earth observation satellites used to study phenomena over ocean and land. The ERS-1/2 satellites provide the longest continuous set of data for Greenland, as ERS-1 was fully operating from January 1, 1992 to June 3, 1996 and ERS-

2, identical to the first, had data available from May 1, 1996 to January 21, 2001. The shortest cross over time of the ERS satellite is about six days. Other satellite scatterometers are available for a limited number of years (Table 3.1). A detailed comparison of each of the sensor instruments is shown in Table 3.2.

Images of the Greenland ice sheet have been produced based on a time series of enhanced resolution images created using the SIRF algorithm. The SIRF algorithm is a non-linear resolution enhancement algorithm that maps backscatter values of A and B coefficients, where the effective resolution varies based on region and sampling conditions. Typical values of A are between 0 and -45 dB, but A is usually minimized at a value of -32 dB, where values less than -32 dB are used to indicate no data. Values of B typically fall within a smaller range between -0.2 and -0.1 dB, and B is limited to values above -3 dB, where values less than this denote no data. Original ERS images have a nominal resolution of 50 km on a 25 km sampling grid. The SIRF algorithm creates images of A and B with a pixel resolution of 8.9 km and an effective resolution at approximately 20-30 km. One cost of increasing the resolution is the addition of noise in resultant images of A and B. The SIRF algorithm was originally used to enhance SASS backscatter measurements and has been applied to other sensor measurements of A and B. The SIR and SIRF algorithms are described in detail by Long et al. (1993).

Backscatter (σ°) measurements are generally observed by spaceborne scatterometers over a wide range of incidence angles, and because of this wide range used, measurements of A and B coefficients (Equation 2.2) are more useful in common application than the measurement of backscatter directly (Long et al. 1993). Thus, ERS-1/2 A images are utilized in this study for the years 1992 to 1999. Results from this

Table 3.1 Summary of scatterometer data available from the Scatterometer Climate Record Pathfinder project at Brigham Young University (http://www.scp.byu.edu/data/regions/Grn.html)

Sensor	Mission Life
SASS	June 1, 1978 – Oct. 8, 1978
ERS-1	Jan. 1, 1992 – June 3, 1996
ERS-2	May 1, 1996 – Jan. 17, 2001
NSCAT	Sept. 14, 1996 – June 28, 1997
QuikSCAT (eggs)*	July 19, 1999 -
QuikSCAT (slices)*	July 19, 1999 -

Table 3.2 Comparison of sensor instrument characteristics from the Scatterometer Climate Record Pathfinder site (http://www.scp.byu.edu/data/scattscompare.html)

	SASS	ERS-1/2	NSCAT	SeaWinds
FREQUENCY	14.6 GHz	5.3 GHz	13.995 GHz	13.6 GHz
AZIMUTHS				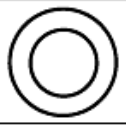
POLAR.	V-H, V-H	V ONLY	V, V-H, V	V-OUTER/H-INNER
BEAM RESOLUTION	FIXED DOPPLER	RANGE GATE	VARIABLE DOPPLER	PENCIL-BEAM
SCI. MODES	MANY	SAR, WIND	WIND ONLY	WIND/HI-RES
RESOLUTION	50/100 km	25/50 km	25/50 km	25 km/6x25km
SWATH	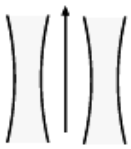		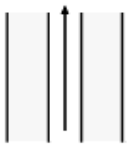	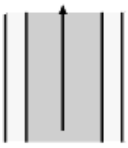
INCIDENCE ANGS	0° - 70°	18° - 59°	17° - 60°	45° & 54°
DAILY COVERAGE	VARIABLE	< 41 %	78 %	92 %
DATES	6/78 – 10/78	92–96 & 96–	8/96 – 6/97	5/99 & 11/01

eight-year analysis of ERS data can provide additions to historical data sets available from the SASS scatterometer as well as the NSCAT and more recent observations from the QuickScat scatterometers.

3.2 ECMWF ERA-40 and model data

Accumulation and net runoff rates, and thus, the SMB estimates of the Greenland ice sheet based on Hanna et al. (2002) are used in this study courtesy of Edward Hanna at the Institute of Marine Studies of the University of Plymouth, UK (personal communication). Runoff and accumulation compiled by Hanna et al. (2002) include ECMWF reanalyses (1974 – 1994) and operational analyses (1994 to 1998) data and have since been updated to include the years 1999 and 2000 based on "second generation" ECMWF reanalysis ERA-40 data. The new ERA-40 reanalysis project covers the period from 1957 to 2001 and includes previous ECMWF reanalysis ERA-15 data that spanned the period from 1979 to 1993.

Data compiled by Hanna et al. (2002) consist of net accumulation and net runoff estimates for the years 1992 to 1998 based on surface climate fields from high-resolution (~0.56° x 0.56°) ECMWF operational analysis data as well as meteorological and glaciological models. Forecasted snow amounts from ECMWF analyses were previously validated against ice-core and other data from work by McConnell et al. (2001). Hanna et al. (2002) net runoff values are based on a positive degree-day model to arrive at snow/ice melt. Runoff was calculated using a meltwater runoff/retention model based on work by Janssens and Huybrechts (2000), which incorporated ECMWF analyses annual precipitation and July 2-meter surface temperatures corrected using digital elevation

models (DEMs) from Ekholm (1996). Net runoff was defined as runoff of surface meltwater minus the portion that refreezes within or on the ice before being lost. Accumulation was defined as solid precipitation minus evaporation and sublimation. To arrive at SMB estimates, SMB was calculated as accumulation minus runoff. Hanna et al. (2002) stated that absolute values of accumulation were thought to be 20-30% too low in central Greenland and possibly too high near the margin of the ice sheet. Also, runoff values were likely underestimated primarily due to the ice mask used, which omitted approximately 6% of the ice sheet. By including all cells in the National Snow and Ice Data Center (NSIDC) polar grid using a ice mask from Abdalati and Steffen (1997), they found that net runoff values were substantially greater, by approximately 40-50%, than their initial results. They also suspected that the low resolution of the grid near the margins of the ice sheet might have missed areas of high runoff. For a more detailed description of this data set, refer to Hanna et al. (2002). When discussing results based on data from Hanna et al. (2002), runoff and accumulation refer to net runoff and net accumulation throughout the remainder of this thesis.

3.3 Passive microwave and surface mass balance model data

Additionally, this study employs annual estimates of accumulation, net runoff, and SMB from data previously compiled by Mote (2003) courtesy of Thomas Mote at the University of Georgia, Department of Geography, Athens, GA (personal communication). In his study, SMB estimates for the period 1988 to 1999 are primarily derived from passive microwave satellite data and accumulation based on ECMWF analysis precipitation data from Bromwich et al. (2001). Satellite data consisted of 37 GHz,

horizontal polarization, brightness temperatures on a 25x25 km grid from the Special Sensor Microwave/Imager (SSM/I) obtained from NSIDC. These brightness temperatures served as thresholds to estimate annual melt durations that represented the total number of days where the daily average brightness temperature exceeded a critical brightness temperature. To derive a critical brightness temperature associated with melting snow and ice, Mote used a radiative transfer model based on work by Mote and Anderson (1995). The total number of days classified as undergoing melt was summarized for each summer during the period 1988 to 1999 to arrive at annual melt durations. The error in runoff estimated from the SSM/I data was previously quantified by Mote (2000) at ±10% after comparison to stake ablation measurements, but that work assumed the use of individual swath brightness temperatures rather than the gridded product used by Mote (2003). Therefore, Mote (2003) stated that should be viewed as the lower bound for the potential error.

Mean summer (May – August) temperatures and positive degree days (PDDs) were calculated from annual melt duration and used in a SMB model in conjunction with accumulation rates to ultimately arrive at estimates of runoff rates, mass balance, and surface elevation changes for the twelve-year period 1988 to 1999. Annual accumulation values were derived from annual precipitation based on ECMWF analysis data from Bromwich et al. (2001) by subtracting from total precipitation sublimation and the fraction of liquid precipitation. A sublimation rate of 12% of precipitation was used based on findings by Box and Steffen (2001). Meltwater retention fraction was determined in a similar fashion as Hanna et al. (2002). Estimates utilized in this study are also in millimeters per year, and SMB values are calculated as accumulation minus runoff.

Discussions of results based on work by Mote (2003) hereafter in this thesis refer to net runoff and net accumulation, as mentioned for results based on data from Hanna et al. (2002).

3.4 Research methodology

Limitations inevitably exist when comparing accumulation and ablation estimates acquired from different sources due to differences in the nature of the data. Nevertheless, studying the SMB of the Greenland ice sheet from various types of data can contribute invaluable information toward a better understanding of its changing environment. This study looks at interannual variations in the SMB of Greenland as revealed by the three aforementioned data sets and aims to expand on results achieved from their work.

Identifying snow/ice boundaries from ERS-1/2 scatterometer observations

To examine the extent of the accumulation, ablation, and dry snow zones of Greenland using ERS-1/2 imagery, it was necessary to identify the locations of the boundaries of the snow and ice zones that reveal the extents of accumulation and ablation across the ice sheet. Since the dry snow line (DSL), wet snow line (WSL), and the equilibrium line (EL) boundaries are highly sensitivity to fluctuations in climate, monitoring shifts in their location over an extended period of time may prove beneficial in climate change research. During the summer to fall transition, summer melting and fall freeze-up have a distinct effect on backscatter signatures that reveal large gradients of A between adjacent snow/ice zones. This is mainly due to the presence of liquid water, which causes the greatest change in the dielectric properties of the snow and ice and

regulates the contribution of sub-surface or volume-scattering effects caused by absorption or extinction within the upper layers of the snowpack (Rott et al., 1985; Long and Drinkwater, 1994). Seasonal transitions in backscatter ERS data reflect these changes in the surface properties and were used in this study as the basis for the identification of the DSL, WSL and EL.

Defining the dry snow line

The dry snow zone, by definition, experiences little to no seasonal melting and, therefore, undergoes negligible change in microwave emissivity making it possible to map the extent of the dry snow zone using time-series data (Long and Drinkwater, 1994). In late September a strong delineation exists between the dry snow zone and the percolation zone downslope, where melt has occurred. Also, for regions of melt-induced inhomogeneities or layering, volume scattering is enhanced resulting in high values of A. The DSL is best mapped at the end of the summer-fall transition, approximately mid-September (Long and Drinkwater, 1994; Drinkwater et al. 2001). By observing SASS scatterometer data, the DSL was formerly delineated at the -5 dB contour, where a strong gradient between low values of A in the dry snow zone and remarkably higher values of A in the percolation zone was apparent (Long and Drinkwater, 1994).

In this study, a similar methodology was used in delineating the dry snow line. ERS scatterometer time-series data were analyzed through early and late fall of each year to assess where the gradient between low and high values of A existed, characteristic of the dry snow and percolation zones, respectively. In examining ERS-1/2 data during the months from late August through October of each year, sharp breaks in backscatter

values of A appeared to occur around -5 dB. Therefore, it is suggested that the -5 dB line sufficiently represents the boundary between the dry snow and percolation zones in ERS scatterometer data as well.

This backscatter value was further tested by examining a number of image histograms along a transect in the northwestern region of the ice sheet stretching across regions of dry and percolating snow, at 73°N, 51°W to 75°N, 47°W. Histograms were created using software applications provided by the Scatterometer Climate Record Pathfinder project at Brigham Young University written for Research Systems' IDL software. Figure 3.1a shows an example histogram of the ERS-1 backscatter pattern from September 7 to 12, 1995 (see appendix A.1 for other histograms). These histograms show backscatter values of A, in dB, against population or number of cells. The pattern of backscatter values in this region of the ice sheet reflects a gradual decline from lower values of A to increasingly higher values of A. Although a sharp break or minimum value in this graph was not apparent, the value of -5 dB provided a reasonable separation between higher and lower values of A (Figure 3.1). There was a sharp decline at values greater than -6 dB, indicating a sharp change in the backscatter signature along this area of the ice sheet. This change in the spatial pattern of backscatter is believed to represent a transition from areas of dry snow to areas of percolating snow. Thus, the -5 dB line is thought to be a sufficient marker for the location of the DSL from ERS-1/2 scatterometer observations.

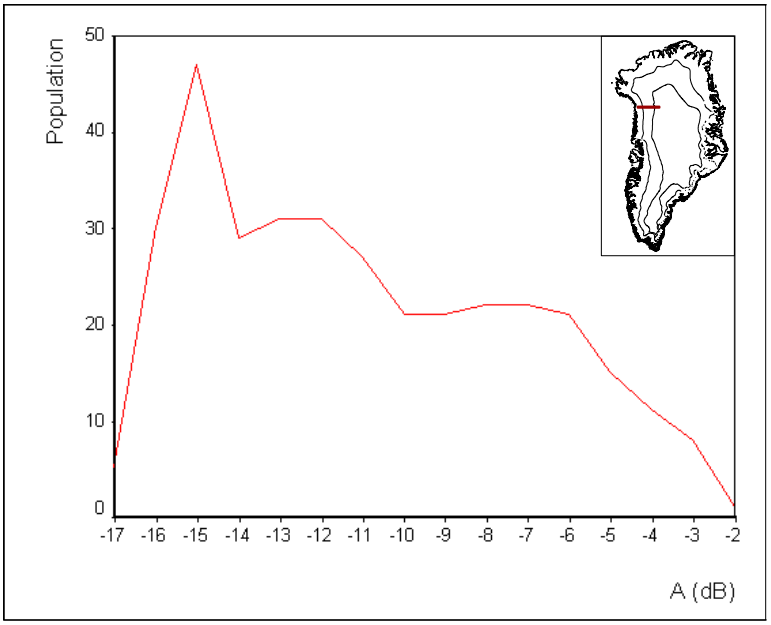

(a)

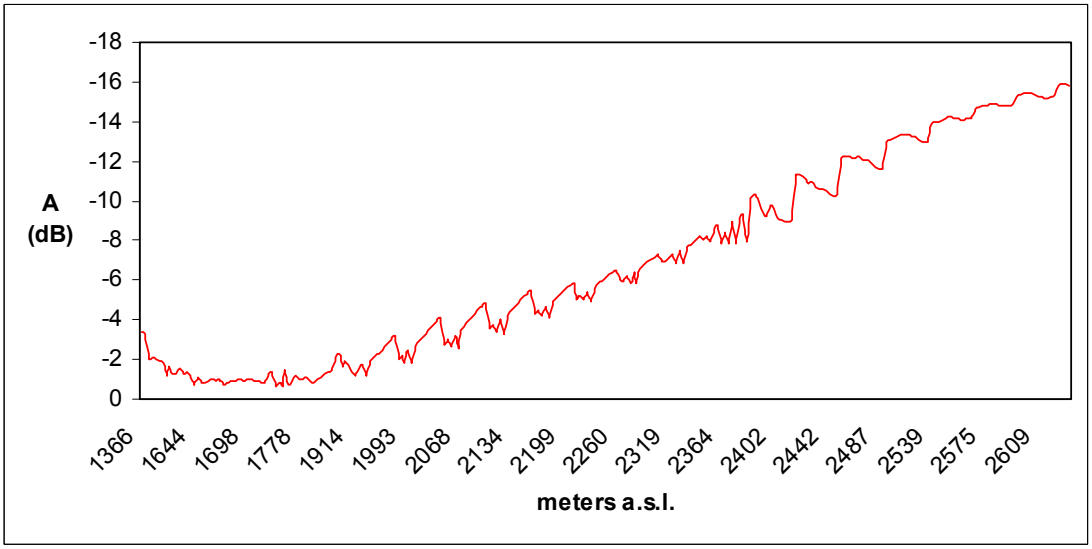

(b)

Figure 3.1 (a) ERS-1 image histogram from September 7 - 12, 1995, at 73°N, 51°W to 75°N, 47°W used in the delineation of the dry snow line, and **(b)** density slice for the same period and region.

Defining the wet snow line and equilibrium line

Since microwave backscatter and emission are highly sensitive to melt due to the fact that melting creates large changes in dielectric processes that are reflected in surface characteristics and backscatter signatures, this was used as the basis for identifying the WSL and EL. As previously mentioned, the WSL marks the boundary between the bright percolation zone from the darker wet snow zone downslope. Since values of A in the percolation zone are typically near zero and wet snow is characteristic of the lowest backscatter A values in microwave data, this results in the delineation of the WSL to be relatively straightforward. Mapping the wet snow region becomes optimal in late June to early July, when surface scattering, reflection, and surface roughness dominate backscatter signatures, as the liquid water content of the snowpack rises. Generally, the surface in the wet snow zone is covered by wet or saturated snow, as this is where the seasonal 0° C isotherm descends. The wet snow surface is relatively smooth compared to the dry snow, according to measurements by Rott et al. (1985).

The WSL and EL approximate the upper and lower extents of the wet snow zone, respectively. The snow or firn line bounds the area of wet snow from the ablation zone located along the outer extent of the ice sheet, and the EL was found to closely approximate the location of the snow or firn line during normal balance years (Long and Drinkwater, 1994). However, defining the snow or firn line is much more difficult in scatterometer data due to the low contrast observed in backscatter values between wet snow and bare glacial ice within the ablation zone. Nevertheless, during fall freeze-up the remaining glacial ice surface below the EL, i.e. the ablation zone, should have a different appearance from superimposed ice and snow covered regions. Generally, the EL can be

mapped as the downslope margin of the lowest backscatter region. The lower boundary of the wet snow zone, the firn/snow line or EL, also describes the end of continuous snow and the beginning of areas of discontinuous saturated snow, according to Long and Drinkwater (1994). They further emphasized that the location of the EL was most easily identifiable with the high resolution of SAR onboard ERS-1/2 satellites, so a long seasonal-change cycle of SAR data is optimal for the distinction between the ablation and wet snow.

Time series data from both ERS-1/2 for the months May to August were used in defining the WSL and EL. The WSL and EL were best mapped around the same period towards the end of summer, with the WSL optimal around early July and the EL best mapped around mid-July (Long and Drinkwater, 1994; Wismann, 2000). Therefore, this study observed backscatter signatures throughout summer with an emphasis on early to mid-July of each year to define the WSL and EL. In general, the contour lines -12 to -18 dB were found to best represent the WSL and EL, respectively, but these lines were found to vary slightly both interannually and throughout the summer season.

A similar approach used in testing the value of the DSL was used to test values of the WSL and EL. A number of ERS backscatter histograms were examined during early and mid-July of each year during the period 1992 to 1999 to determine the best demarcation of the WSL and EL. However, when observing image histograms along the southwestern part of the ice sheet, stretching across the percolation, wet snow and ablation regions, identifying relative backscatter minima becomes more ambiguous in this region. Long and Drinkwater (1994) defined the WSL at the -12 dB line in SASS imagery, which is thought to sufficiently delineate the WSL in ERS imagery as well.

Therefore, the -12 dB line was used to represent the WSL for purposes in this analysis. In the percolation zone of the ice sheet, backscatter A values were highest reaching near 0 dB observed over much of the region, contrasting with the area of lowest backscatter values in the wet snow zone, where values of A typically reach a minimum of -28 dB. Figure 3.2a shows an example of a backscatter histogram from June 30 to July 5, 1995 (see other histograms in Appendix A.2). This year was chosen somewhat arbitrarily, but 1995 is known as a high ablation year, which is reflected in these backscatter plots. Two peaks were apparent, one of high values of A and a larger peak existed at very low values of A. Minimum values were observed from -11 to -15 dB, and a relative minimum existed at -12 dB, which separated lower values of A found in the dry and wet snow zones from the highest values of A in the percolation zone.

Similarly, the EL was mapped where the lowest extent of the darkest backscatter region exists. Backscatter values appeared lowest in the wet snow zone, approaching values of -30 dB, and values of A slightly increased in the ablation zone downslope. Figure 3.3a shows an example image histogram for the same transect used in Figure 3.2 along the southwest region of the ice sheet for July 15 to 20, 1995 (see other histograms in Appendix A.3). Again, two peaks were obvious with several values representing relative minimum. The -18 dB line was chosen to represent the location of the EL, as this point reflected the separation between a large population of very low values of A from slightly higher values of A. The definition of the EL may be questioned, but it is believed to adequately separate the wet snow zone from the ablation zone, and slight deviations from this definition of the EL are not expected to produce significant changes in the extents of the snow and ice zones.

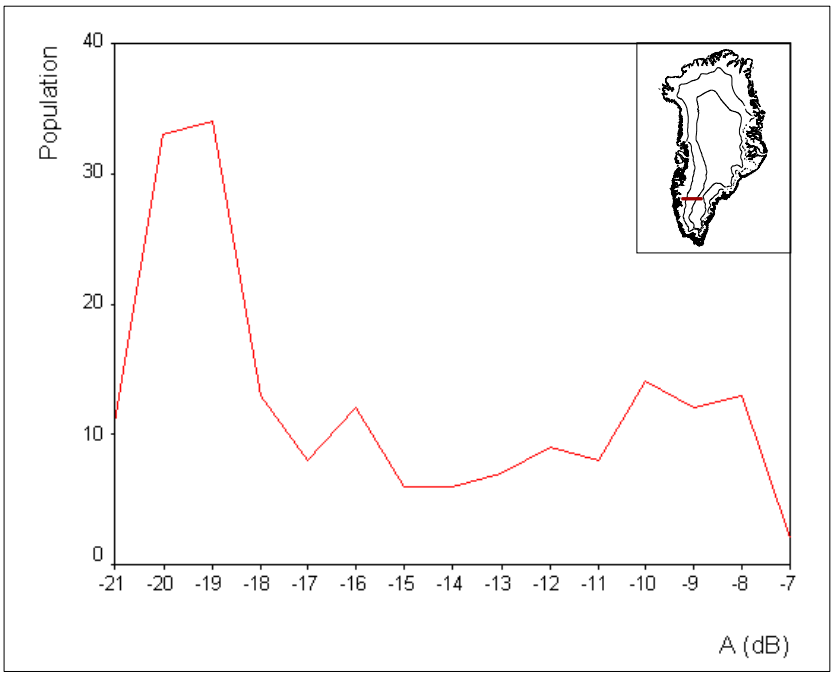

(a)

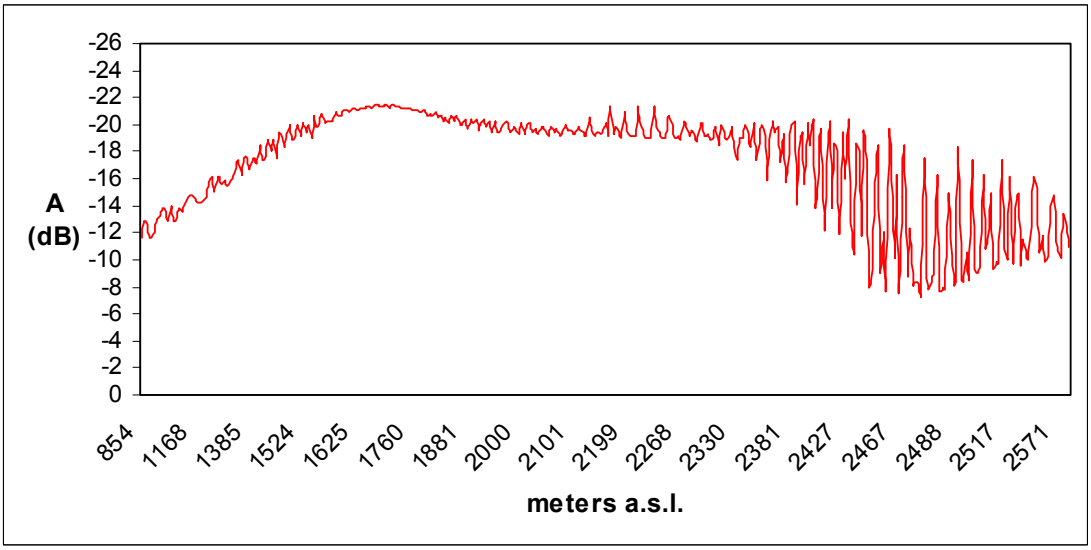

(b)

Figure 3.2 (a) ERS-1 image histogram from June 30 - July 5, 1995, at 65°N, 47°W to 66°N, 44°W used in the delineation of the wet snow line, and **(b)** ERS-1 density slice for the same period and region.

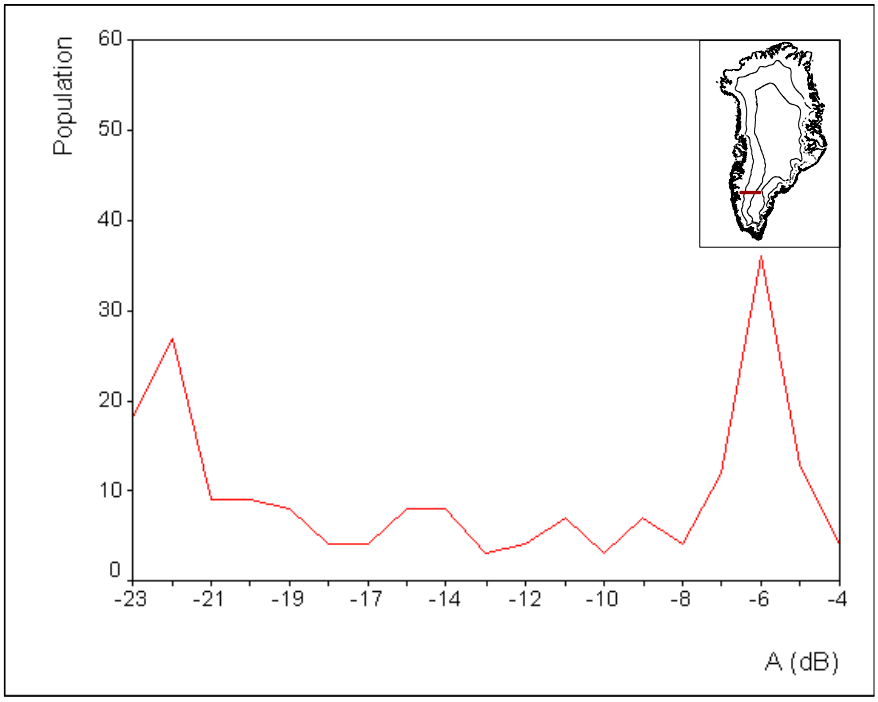

(a)

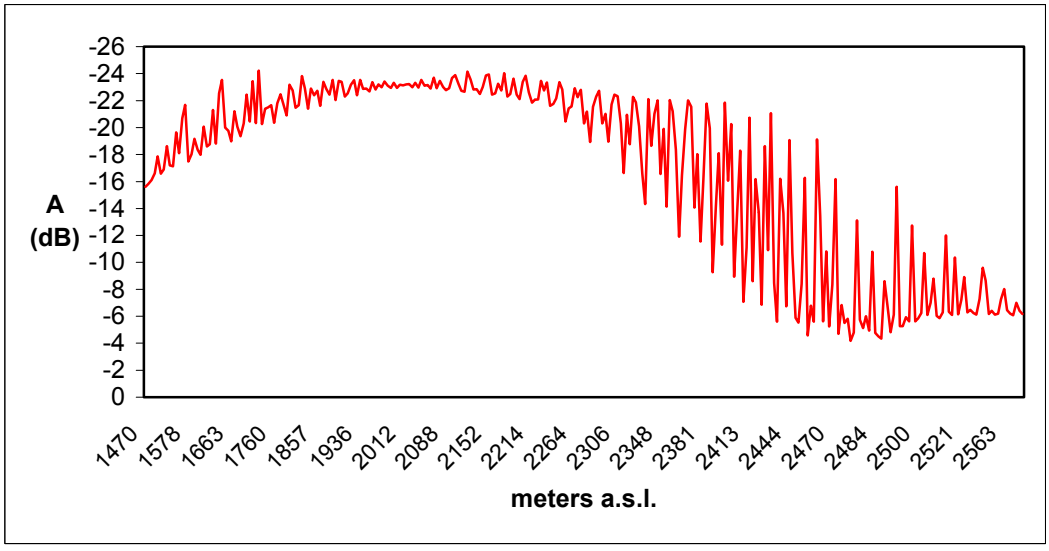

(b)

Figure 3.3 (a) ERS-1 image histogram from July 15 - 20, 1995 at 65°N, 47°W to 66°N, 44°W used in the delineation of the equilibrium line, and **(b)** ERS-1 density slice for the same period and region.

Relation of snow/ice zones with SMB estimates

A kriging method was utilized to produce maps from ERS satellite and SMB model data. Kriging is a geostatistical gridding method that attempts to express trends from irregularly spaced data (Cressie, 1990). The kriging technique interpolated the model and scatterometer data used in this study onto a 10 km x 10 km spacing grid of the Greenland ice sheet in Universal Transverse Mercator (UTM) projection. Kriging was selected as the method for spatial interpolation in order to preserve large gradients in the data, representing zone boundaries, which might be lost using inverse distance weighting or other similar interpolation techniques. Backscatter maps of the WSL and EL during the period of maximum melting were produced from ERS data to show the maximum extents of melting and ablation that occurred during each year. These boundaries of the WSL and EL identified in ERS scatterometer data were used to show the spatial pattern and maximum elevation that melting occurred across the ice sheet. From model-based estimates of the SMB, the EL was defined as areas where the SMB equals zero.

Evaluating changes in the SMB of the ice sheet between each of the data sets over an eight-year period is the primary focus of this research. One approach used to determine differences that may exist in estimates of the SMB was to compare the accumulation and ablation surface areas represented by each data set. The surface areas were represented as fractions of the accumulation and ablation areas to the total surface area of the ice sheet, shown as a percentage. For the model-based estimates from Hanna and Mote, the accumulation surface area for each year was calculated as the total surface area that fell above the zero SMB line, and the remaining surface area of the ice sheet represents the ablation surface area. Similarly, from scatterometer observations the

accumulation surface area was defined as that area of the ice sheet that fell above the -18 dB contour, with the area below this line used as the ablation surface area. The total surface area for each of the data sets was determined using a masked grid of the ice sheet obtained from Dr. Beata Csatho at the Byrd Polar Research Center, Ohio State University (personal communication).

The state of the SMB for any given year was found to vary by region of the ice sheet largely due to differences in accumulation and ablation rates (Mote, 2003). This study assessed the spatial differences between areas of positive and negative SMB across the ice sheet for the model-based estimates of SMB based on Hanna et al. (2002) and Mote (2003). Areas of positive and negative SMB were determined based on areas above and below the equilibrium line, respectively. Cell values were assigned a Boolean value of one if the SMB was positive and a value of zero was assigned to cells of negative SMB. New grids were created using the same kriging technique as described above for each year and data set to show the spatial distribution of positive and negative SMB and the grids were differenced to show the regions of the ice sheet where the sign of the SMB agree and where they disagree.

To further compare estimates of the SMB, the annual equilibrium line altitude (ELA) was determined for each data set along a transect in the west central region of the ice sheet along the elevation gradient at 69.1° N, 51.0° W to 70.2° N, 41.5° W, near the ETH Camp and Jakobshavn, closely following the EGIG traverse. This is a data rich region of the ice sheet that has been the subject of numerous investigations, where the long-term ELA is well established based on glaciological estimates. The EL signifies where the ice sheet is in a steady state, thus monitoring its position over time can provide

a good indication of the SMB changes occurring for either the entire ice sheet or individual regions. For purposes in this study, the ELA was defined as simply the elevation, in meters, where the SMB equals zero. To more accurately assess the elevation of the EL and the SMB gradient over this region of the ice sheet, SMB estimates were interpolated onto 5 km x 5 km spacing grids using a kriging technique, and SMB estimates were interpolated across grid cells to determine the approximate elevation at which the SMB equals zero. For scatterometer observations, the time of the approximate maximum melt extent during each year was used and interpolated onto a grid in the same fashion to determine the elevation of the -18 dB line to compare the ELA of the scatterometer data with the model-based estimates. In the case that backscatter values of A did not reach a low value of -18 dB in this region of the ice sheet, the elevation of the lowest backscatter value was shown instead to infer the most probable location of the EL.

Examining change in the location and elevation of the equilibrium line is an effective approach to assessing changes in the overall ice sheet and in localized areas of the ice sheet. These techniques are used to examine variability in the equilibrium line, and thus SMB, of the Greenland ice sheet in the following three chapters. The boundaries of the snow and ice zones defined using backscatter histograms of A (dB) are illustrated in the following chapter to demonstrate the temporal and spatial variability in the accumulation and ablation zones.

CHAPTER 4

GREENLAND SNOW AND ICE ZONES FROM ERS-1/2 SCATTEROMETERS

The delineation of the dry snow line (DSL), wet snow line (WSL), and equilibrium line (EL) from backscatter values of A based on ERS-1/2 scatterometer data is largely based on results from Long and Drinkwater (1994) and work by the Scatterometer Climate Record Pathfinder project. These snow and ice boundaries mark important transitions between melting and freezing processes, and thus net accumulation and ablation (Long and Drinkwater, 1994); therefore, their locations are used here to demonstrate the spatial and temporal patterns of the accumulation and ablation zones across the ice sheet from 1992 to 1999. The EL is of particular interest, as it distinguishes between areas of positive mass balance above this boundary from areas of negative mass balance below this boundary. Additionally, annual changes in backscatter values of A are shown to illustrate the spatial variability in melting across the ice sheet during the summer for the period 1992 to 1999.

4.1 The dry snow zone

An inverse relationship exists between backscatter values of A, the backscatter normalized to the mean incidence angle of 40°, and areas of accumulation, and this relationship becomes apparent in the backscatter signature patterns within the dry snow zone of the ice sheet. Within the region of dry snow, lowest values of A occur along the

high accumulation western flank of the dry snow zone, whereas highest values of A exist along the lower accumulation northeastern region of dry snow. According to Long and Drinkwater (1994), this relationship is the result of small-scale surface roughness associated with wind-scouring or wind-slab that becomes significant in areas of low accumulation. They stated that the mean value of A is about -11.93 ±0.75 dB in the southwestern part of the dry snow zone, whereas the mean of A is considerably lower at -4.02 ±0.22 dB in the northeast region of dry snow, based on SASS scatterometer observations.

Backscatter values of A were examined from the first and second ERS scatterometers to show the positions of the snow and ice boundaries over the period 1992 to 1996 (ERS-1) and 1996 to 1999 (ERS-2). The DSL was defined at the -5 dB contour based on the pattern of backscatter A values during mid-September of each year, as discussed in Chapter 3. The DSL and, thus, the extent of the dry snow zone, are shown during mid-September of 1992 through 1995 (Figure 4.1) and 1996 to 1999 (Figure 4.2). Throughout this period, the DSL closely followed the 1600 m contour in the north and south of about 75° N latitude its elevation increased to about 2000 m in the west and approximately 2400 m along the southern and eastern regions of the dry snow zone. Based on these scatterometer observations, backscatter A values generally reached a minimum in the southwestern portion of dry snow, with values mainly between -18 and -20 dB, and dry snow A values were typically highest in the northeastern region of dry snow, with values generally around -5 dB. The DSL and, thus, the extent of the dry snow zone did not vary much interannually, possibly due to the fact that greater penetration depths are generally experienced in dry snow and the transparency of the snow causes the

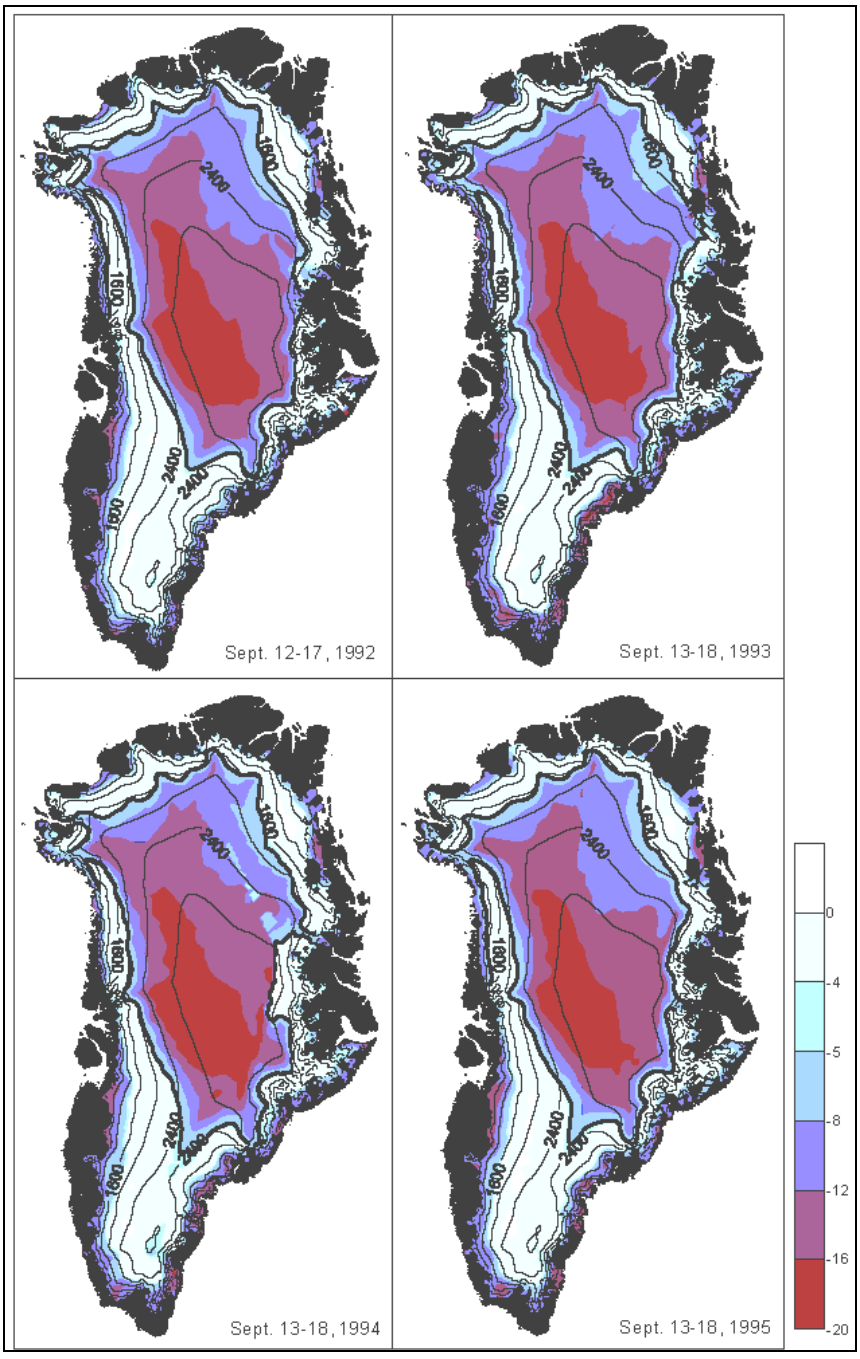

Figure 4.1 ERS-1 backscatter values of A (dB) from 1992 to 1995 with the dry snow line contoured in bold at the -5 dB line.

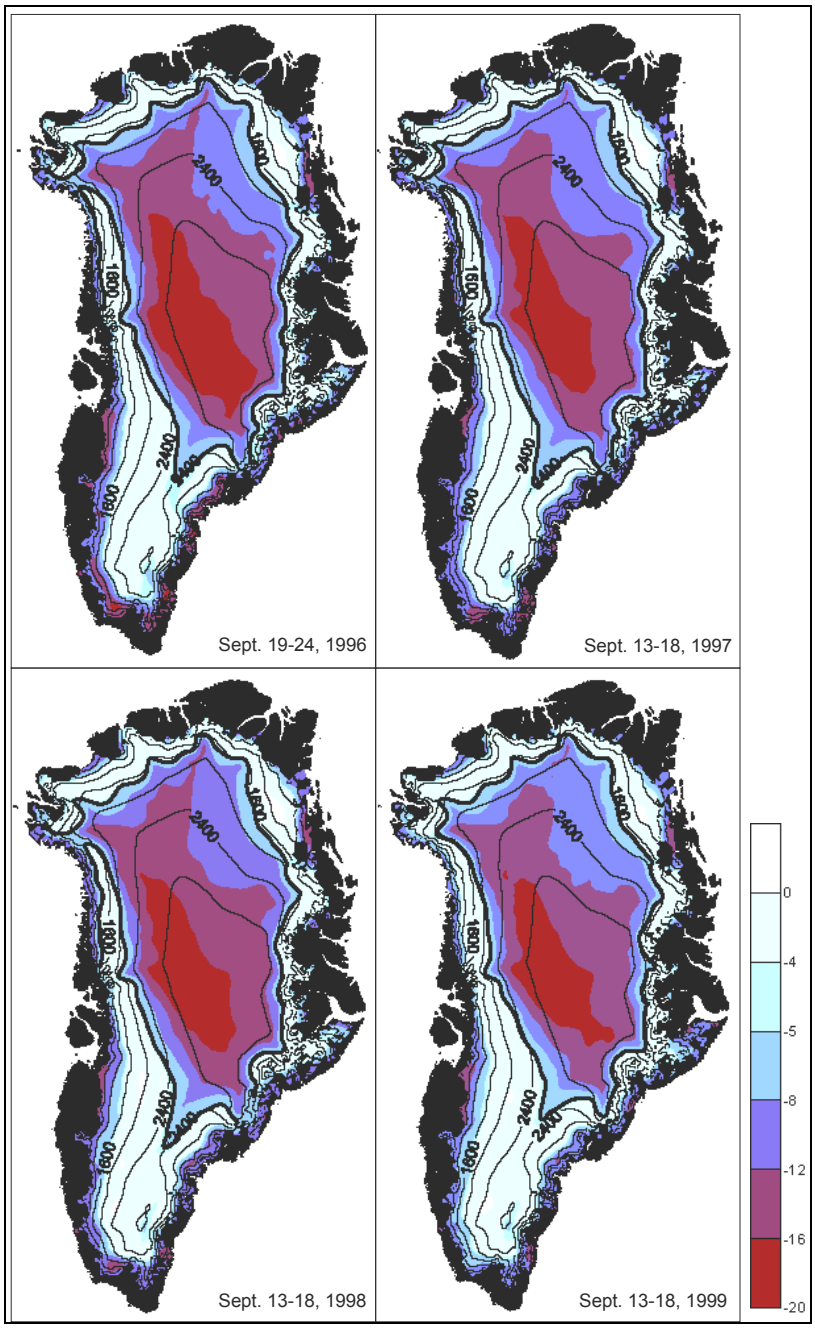

Figure 4.2 ERS-2 backscatter values A (dB) from 1996 to 1999 with the dry snow line contoured in bold at the -5 dB line.

backscatter to be determined by the volume scatter intensity from the summer surface and from the snow volume. The mean melt extent from 1979 to 1999 from results by Abdalati and Steffen (2001) showed that melt extent in the western portion of the ice sheet increased, while melt extent decreased in the east. In higher elevation regions of the ice sheet, they found that melt was mostly restricted to the south. There is an overall resemblance between the dry snow region defined over the longer-term period from 1979 to 1999 by Abdalati and Steffen (2001) with those from scatterometer observations during 1992 to 1999. The characteristic patterns of dry snow values of A revealed from ERS-1/2 scatterometers corresponded well with past observations by Long and Drinkwater (1994) using SASS scatterometer measurements and Drinkwater et al. (2001) using the NSCAT and SASS scatterometers.

4.2 The wet snow zone

The delineation of the WSL is optimal from late June to early July (Long and Drinkwater, 1994), and the WSL defined at the -12 dB contour is illustrated during 1992 to 1995 (Figure 4.3) and 1996 to 1999 (Figure 4.4). As the -12 dB contour line may also appear within the dry snow zone, manual interpretation was used to determine which contour line separated the percolation zone from the wet snow zone. The WSL was most discernible in the southwest region of the ice sheet where greatest melting typically occurs (Mote and Anderson, 1995; Abdalati and Steffen, 1995). The position of the WSL varies considerably from year-to-year compared with that observed in the DSL. This may be explained by the fact that as the liquid water content of the snow increases, backscatter becomes dominated by surface scattering and, therefore, is more sensitive to surface

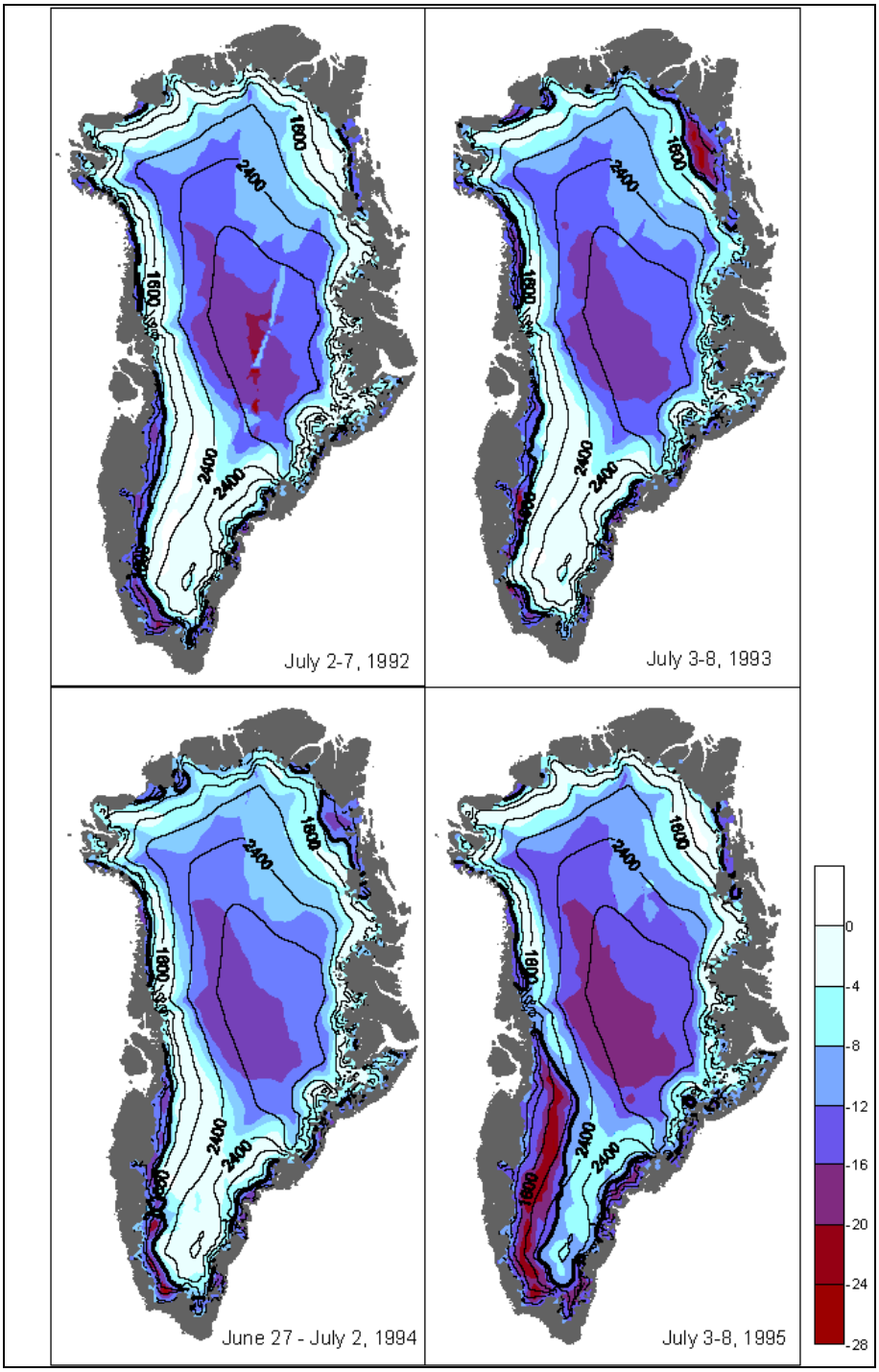

Figure 4.3 ERS-1 backscatter values of A (dB) for 1992 to 1995 with the wet snow line contoured in bold at the -12 dB line.

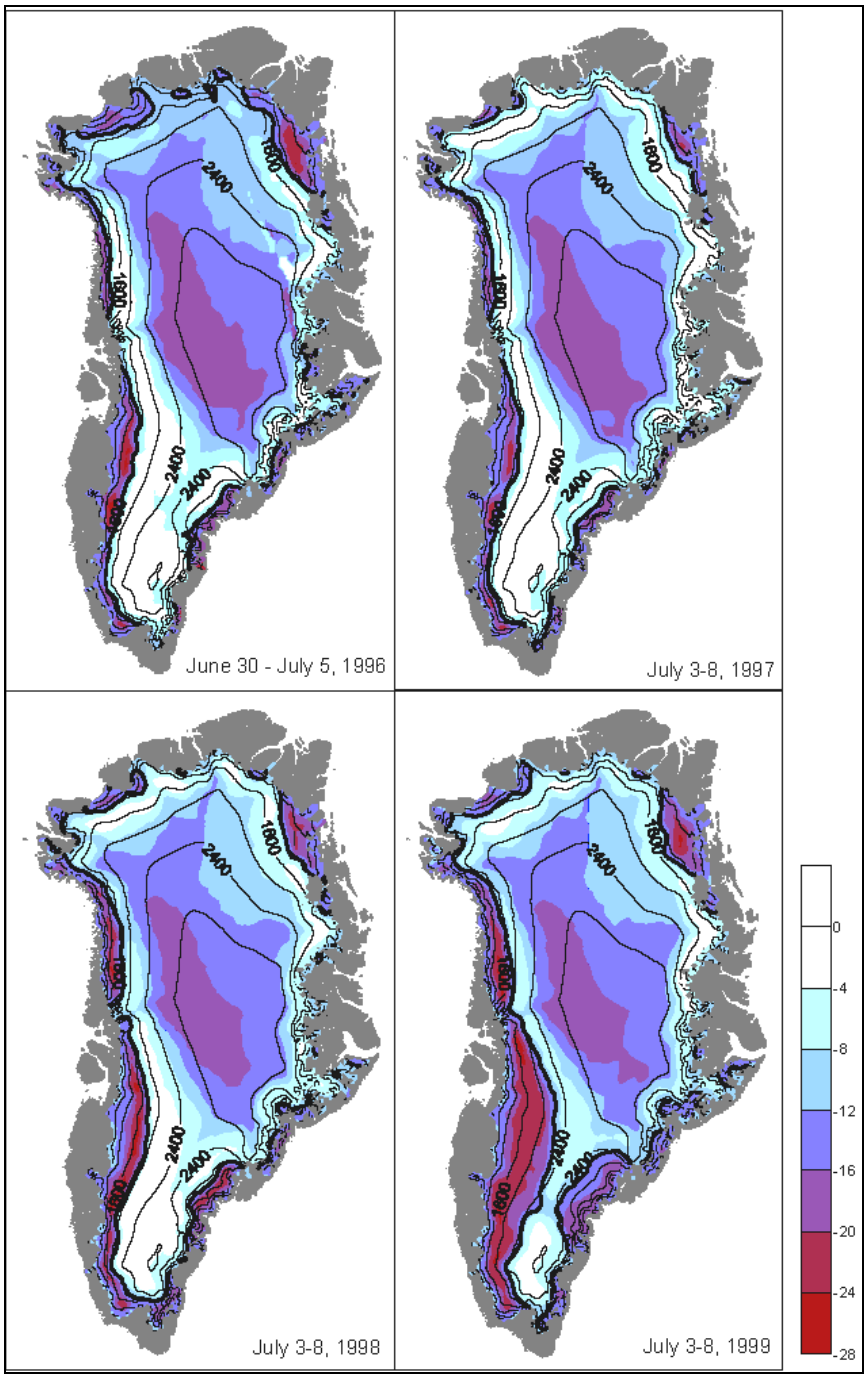

Figure 4.4 ERS-2 backscatter values of A (dB) from 1996 to 1999 with the wet snow line contoured in bold at the -12 dB line.

melting of the snow. In 1992, a year of relatively low melt, the WSL remained below the 1600 m contour mainly along the periphery of the ice sheet, and encroached upon the 2000 m contour at the extreme southern tip of the ice sheet from July 2-7 (Figure 4.3). A similar pattern existed in 1993 with the exception of the extreme northeastern region of the ice sheet, where greater melting occurred up to 1200 m evidenced by the presence of lower backscatter values of A. In early July of 1994 and 1995, the WSL was observed at high elevations in the southwest, around 2400 m, and at slightly lower elevations in the southeast close to 2000 m. In 1995, the WSL reached a maximum elevation of 2600 m near the southern dome of the ice sheet for the period (Figure 4.3).

In 1996, Figure 4.4, the WSL was observed at much lower elevations, about 1600 m, compared with 1995, and the position of the WSL in 1996 reflected a pattern similar to that seen in 1992, 1993, and 1994. During the latter part of this period from 1997 to 1999, the WSL in both the eastern and western flanks of the southern part of the ice sheet increased from 2000 m in 1997 to 2400 m in 1999. Also, the extent of the wet snow zone appeared to be greatest in 1995 and 1999 in the southwestern flank of the ice sheet, suggested by the large area of low backscatter values of A in this region (Figure 4.4). Over the entire period, years of relatively high melt occurred in 1995, 1998, and 1999, based on the upper extent of the wet snow zone as revealed by the WSL, which reached elevations greater than 1600 m. Years of relatively low melt were suggested to have occurred in 1992 to 1994, 1996, and 1997, when the WSL was observed at relatively low elevations of 1600 m or less.

4.3 The ablation zone

The ablation zone is characteristic of bare glacial ice, where surface scattering dominates and surface roughness is important in the pattern of observed backscatter (Long and Drinkwater, 1994). For purposes in this analysis, the EL was demarcated at the -18 dB contour line during mid-July of each year, based on the lower boundary of the region of lowest backscatter values of A. As with the WSL, the -18 dB contour line also lies within the dry snow zone, but manual interpretation was used to select the appropriate -18 dB contour. The EL depicts regions along the ice sheet where accumulation is exactly balanced by ablation; thus, monitoring shifts in this boundary can provide information on changes in the SMB of Greenland. The resulting EL defined in Figures 4.5 and 4.6 appeared as a discontinuous boundary and was most visible along the southwestern flank of the ice sheet in each year. The irregularity shown in the pattern of the EL may be a result of the nature of the ablation zone itself, which is generally described as patchy areas of slushy snow mixed with areas of bare ice where all the snow has melted away (Long and Drinkwater, 1994). This patchy type of surface is generally more difficult to distinguish from areas of wet or saturated snow that often takes on a more homogeneous appearance in backscatter signature patterns.

Variability in the EL, shown as a bold yellow line, is revealed for the years 1992 to 1995 (Figure 4.5) and 1996 to 1999 (Figure 4.6). For the beginning of this period in 1992 and 1993, the EL closely followed the 1200 m contour along the southwestern flank of the ice sheet. The EL reached an elevation of 1600 m in both 1994 and 1995. In 1995, the EL approximately followed the 1200 m line in the west and northwest margins of the ice sheet and this is the only year the EL was clearly visible in these regions. From 1996

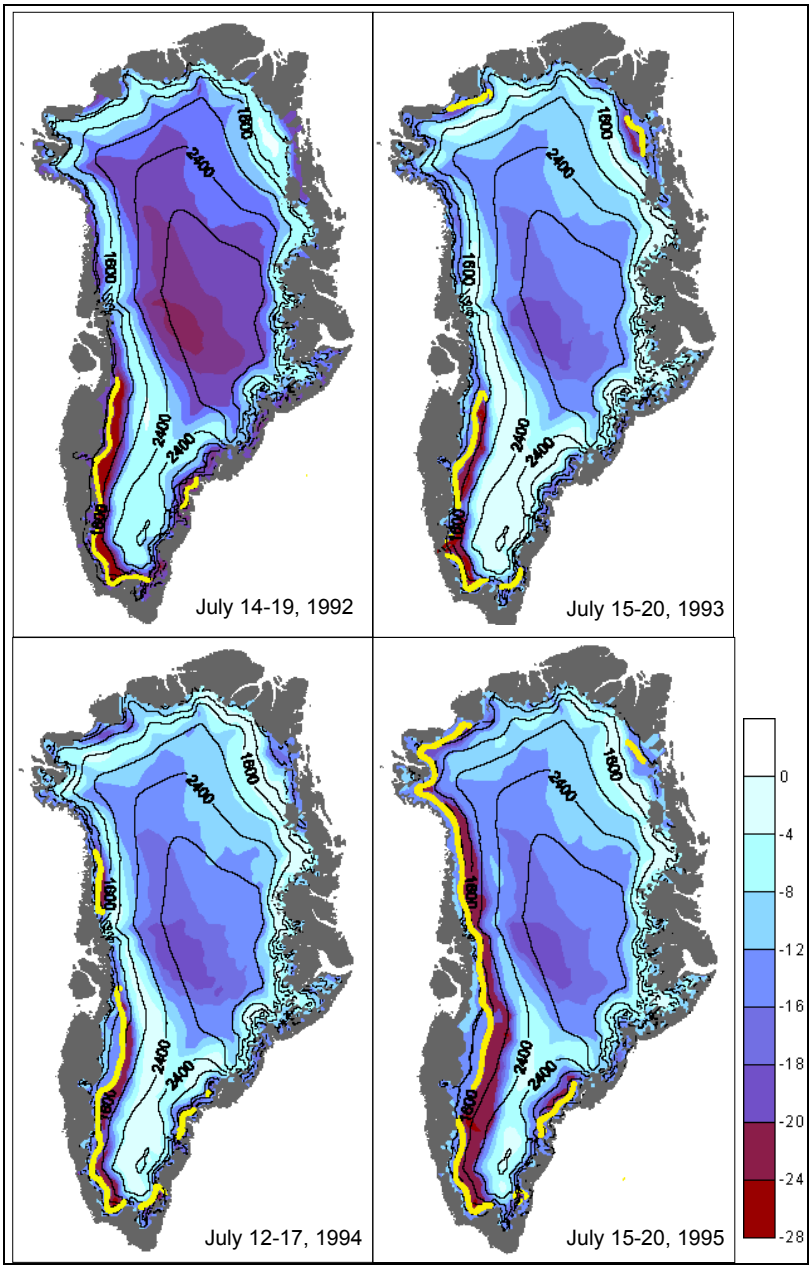

Figure 4.5 ERS-1 backscatter values of A (dB) for mid-July of 1992 to 1995 with the equilibrium line represented as a bold yellow contour at the -18 dB line.

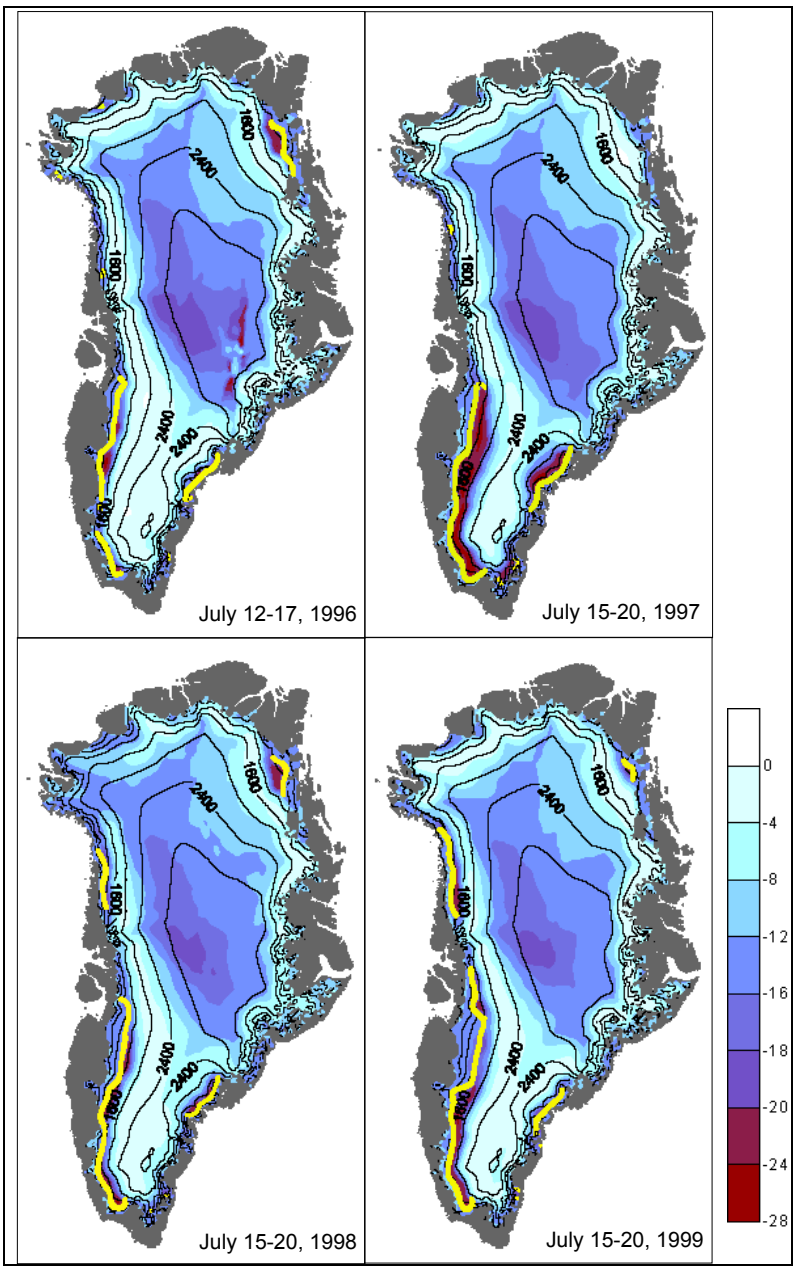

Figure 4.6 ERS-2 backscatter values of A (dB) for mid-July of 1996 to 1999 with the equilibrium line represented as a bold yellow contour at the -18 dB line.

to 1999 (Figure 4.6), the elevation of the EL was generally between 1200 and 1600 m along the southwestern flank. Throughout this period, the EL was not clearly discernable in the northwestern and northeastern regions, where it was observed at lower elevations between 800 and 1200 m. And, in most years during this period, the EL was only visible in the southwestern flank of the ice sheet, particularly for 1992 and 1997. Since the ablation zones was not clearly discernable from results shown here using the -18 dB contour as a demarcation of the EL, further investigation into an optimal mapping of the EL is recommended.

4.4 The wet snow line and equilibrium line during peak melt extents

The WSL, shown as a bold black line, and the EL, shown as a bold yellow line, were identified for each year during the period of the approximate maximum melt extent (Figures 4.7 and 4.8). These images reveal the variability in the WSL, EL, and thus the extent of the wet snow and ablation zones, as determined by scatterometer data during periods of high melt extent. For most of the period 1992 to 1999, the maximum melt extent appeared to be in mid- or late July, thus, these boundaries were delineated during this period for most of the years, except in 1996 when peak melting occurred earlier during late June, and in 1999 as the melt extent remained large through mid-August, according to ERS scatterometer observations. The WSL reached elevations between 1600 m and 2400 m during most of this period, and it reached a maximum elevation of 2600 m in the extreme southern portion of the ice sheet in mid-July of 1995. The position of the EL underwent minor shifts interannually over each approximate budget year, despite large interannual variability in the spatial extent of melting. The EL was generally

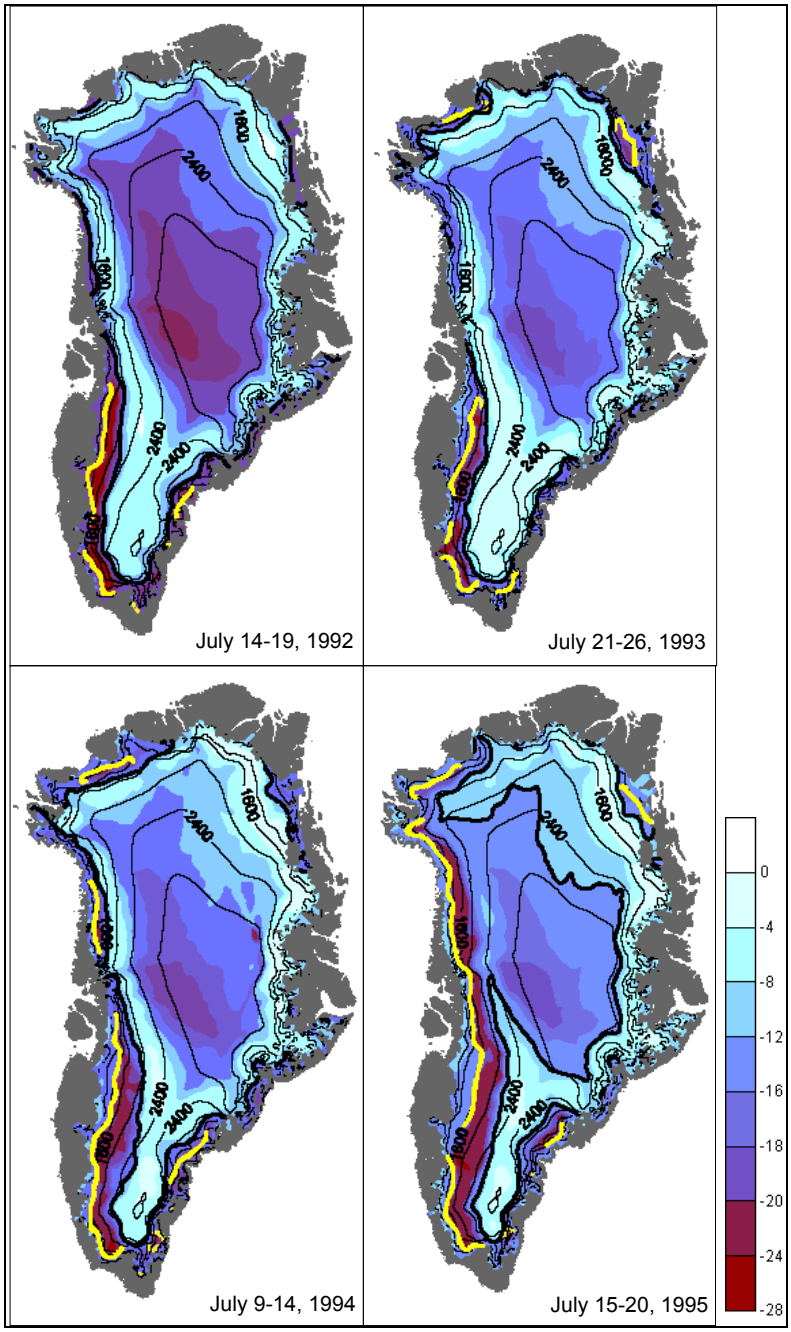

Figure 4.7 The wet snow line and equilibrium line defined from ERS-1 backscatter values of A (dB) during periods of high melt from 1992 to 1995. The WSL, defined at -12 dB, is contoured in a bold black line, and the EL, defined at -18 dB, is shown as a bold yellow line.

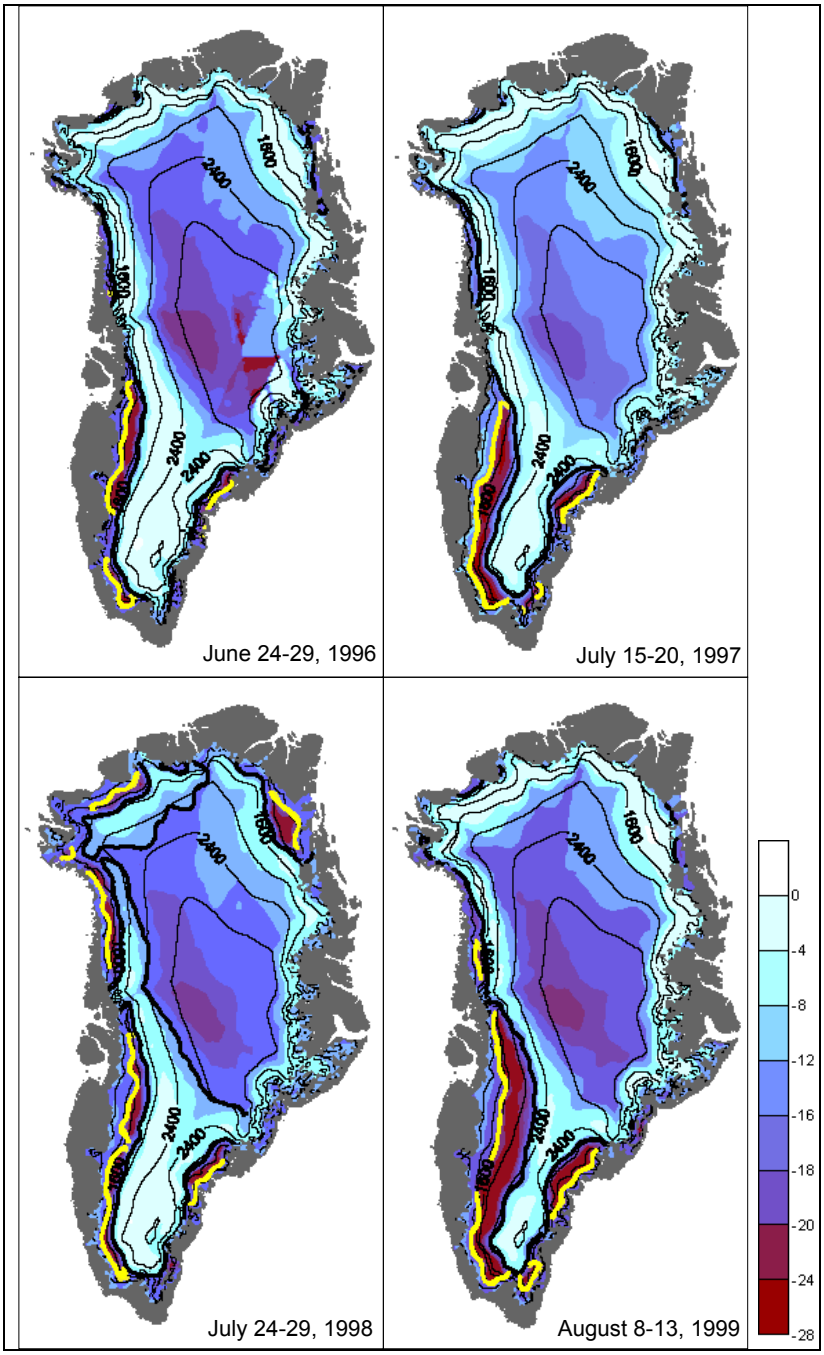

Figure 4.8 Same as in Figure 4.7, except ERS-2 backscatter values of A (dB) for the years 1996 to 1999.

observed at elevations between 1200 and 1600 m in the southwestern flank of the ice sheet. During 1995 and 1998, the EL was also visible along much of the western margin of the ice sheet and closely followed the 1200 m contour. Although the EL did not experience substantial shifts during this period, according to scatterometer data, the interannual variability in the EL followed a similar pattern to that of the WSL, reaching greater elevations during 1995, 1998, and 1999, and lower elevations during the other years during this period.

4.5 Spatial variation in backscatter values of A

This section examines changes in the spatial pattern of backscatter values of A over approximate budget years, for purposes in this study defined as the time of maximum melt extent from one year to the next. This period typically was observed around mid-July, although this varied. The resulting spatial variation in backscatter from year-to-year demonstrated areas repeatedly undergoing positive changes in backscatter, indicating that a decrease in the absolute value of A occurred, where it is expected that an increase in melt extent occurred. Conversely, areas of negative change in backscatter indicate increases in backscatter values of A, where it is expected that a decrease in the melt extent was experienced. Results showed greatest changes in A along the margins of the ice sheet. Within much of this region, positive changes in backscatter occurred as values of A decreased from year-to-year, suggesting that these areas of the ice sheet experienced an increase in melt over the one-year period. Conversely, negative changes in backscatter showed increasing values of A, which suggested that these areas experienced a decrease in melt over the period. This assumption relies on the fact that

lower values of A are typically observed with an increase in the liquid water content of the snow. Conversely, high values of A are generally observed in regions where liquid water has refrozen or percolated down into sub-layers of the snow.

Results showed that the patterns of positive and negative changes of A vary greatly interannually, but areas exhibiting the greatest change in backscatter generally occurred in the southwestern flank of the ice sheet (Figure 4.9). However, from July 14-19, 1992 to July 21-26, 1993, large differences in A were observed along the northern margin of the ice sheet, indicating an increase in melt within this region in 1993 compared with 1992. From July 21-26, 1993 to July 9-14, 1994, the northwest and southwest regions experienced an increase in A; whereas, the northeast and central regions showed a decline in backscatter. Within the southwestern flank of the ice sheet, greatest changes in backscatter were observed up to 2400 m. The west central and northwest regions of the ice sheet show the largest areas of positive change in A just beyond 2000 m between July 9-14, 1994 and July 15-20, 1995. The west and southwest regions experienced a negative change in A during only one period, from 1995 to 1996. A decline in melt area was suggested to have occurred above 1600 m in the southwest and up to 1600 m in the west and northwest from 1995 to 1996. During July 24-29, 1996 to 1997, increases in A were observed in the western and eastern portions of the southern part of the ice sheet, and this pattern was reversed from 1997 to 1998, as slightly negative changes were observed in the southern part of the ice sheet and positive changes in A were shown along the northern margins. The southern part of the ice sheet may have experienced an increase in melt up to 2400 m from 1998 to 1999, with a decline in melt

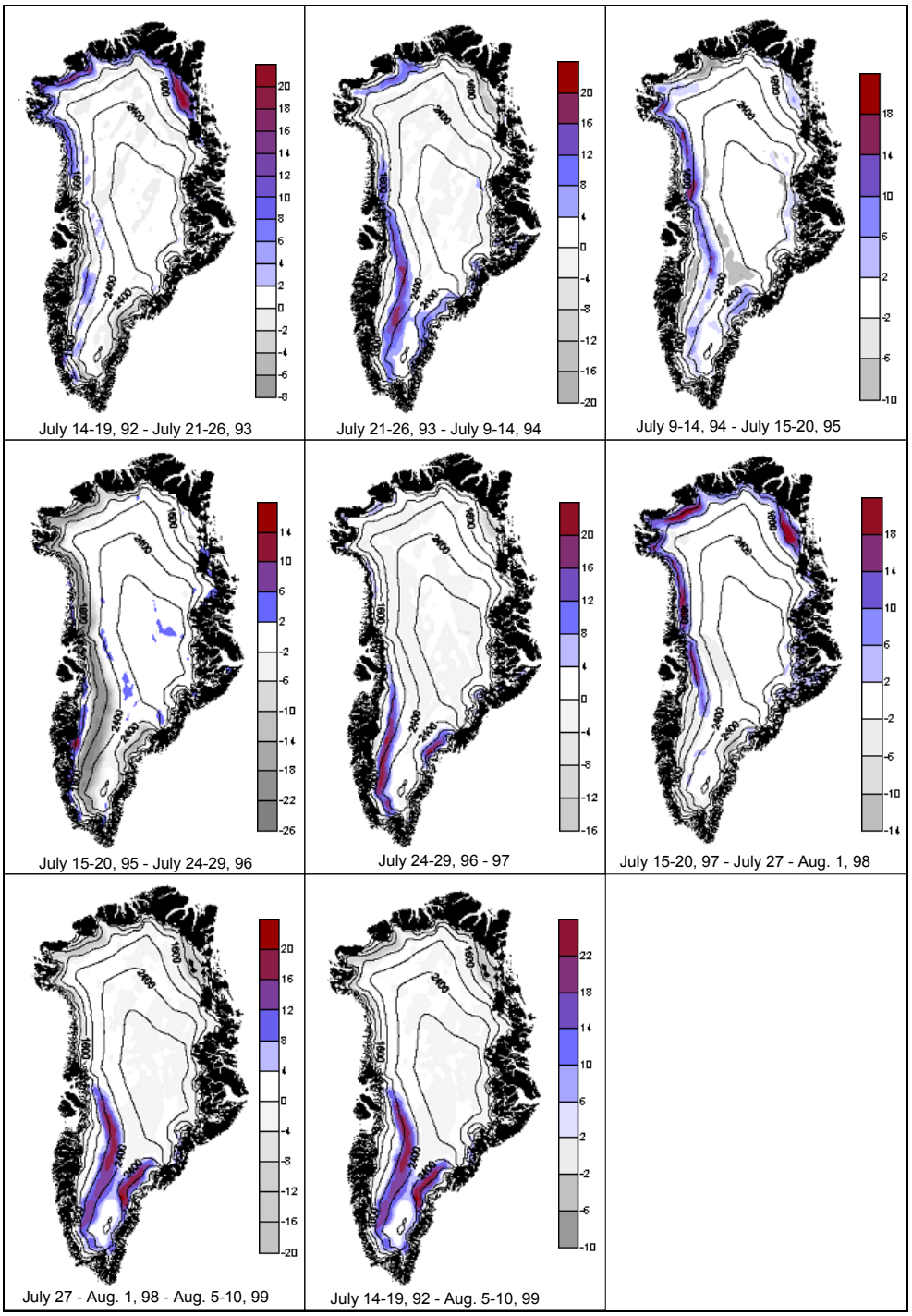

Figure 4.9 Change in backscatter values of A (dB) over approximate budget years, from 1992 to 1999. Positive changes in A indicate increases in melt, whereas negative changes show areas of decreasing melt.

area in the northern regions. Lastly, differences in A were determined over a longer eight-year period between 1992 and 1999. Substantial increases in A were experienced in the southern part of the ice sheet, suggesting an increase in the southern melt extent at elevations slightly greater than 2400 m over the period.

4.6 Summary and conclusions

The delineation of the DSL, WSL, and EL presented here show the spatial extents of the dry and wet snow zones, and thus the accumulation zone, and the ablation zone of the ice sheet. Generally, little interannual variability was experienced in the DSL, and the maximum elevation occurred in the southern and eastern regions of the dry snow zone at approximately 2400 m. Conversely, the position of the WSL showed relatively high interannual variability. The WSL experienced a maximum elevation of approximately 2600 m in the southern region of the ice sheet during mid-July of 1995. The EL was generally found at elevations between 1200 and 1600 m in the southwestern flank of the ice sheet, only reaching up to 1600 m during mid-July of 1994 and 1995. Therefore, results indicated that the EL typically experienced much less interannual variability and is thought to be less sensitive to melting rates than the WSL. Additionally, greatest year-to-year changes in backscatter values of A are observed along the margins of the ice sheet, and an overall increase in melt extent was suggested to have occurred within the southern region of the ice sheet up to 2400 m during this eight-year period.

This chapter showed results of the delineation of the DSL, based on the -5 dB, the WSL, based on the -12 dB, and the EL, based on the -18 dB, from ERS-1/2 scatterometer observations. To better determine if these backscatter values provide a sufficient and

accurate delineation of the boundaries of the snow and ice zones, the spatial extent of the accumulation and ablation zones were compared with the accumulation and ablation zones from model-based estimates. First, accumulation, runoff, and SMB estimates from results based on Hanna et al. (2002) and Mote (2003) are presented in the following chapter.

CHAPTER 5

ANNUAL ACCUMULATION, RUNOFF, AND SURFACE MASS BALANCE FROM MODEL RESULTS

Model derived estimates of Greenland accumulation, runoff, and thus the surface mass balance are shown for each year during the period 1992 to 1999 based on data from previous work by Hanna et al. (2002) and Mote (2003). Annual values of accumulation and runoff have been interpolated over the entire ice sheet using a kriging technique, as previously described, to show the spatial and temporal distribution of these mass balance components over this period according to each data set. The SMB was calculated as simply net accumulation minus net runoff, and the zero SMB contour line was used to identify the location of the EL and, therefore, the extents of the accumulation and ablation zones. Interannual spatial variability in accumulation and runoff rates are discussed here, as well as the location of the equilibrium line, which is used in further comparisons with scatterometer data in the subsequent chapter.

5.1. ECMWF ERA-40 and SMB model data

Annual estimates of accumulation, runoff, and SMB presented in this section are based on data from the ECMWF re-analysis project (ERA-40) and SMB model data that have been acquired from Hanna (personal communication). These estimates of accumulation refer to net snow accumulation, or solid precipitation minus

evaporation/sublimation (Hanna et al. 2002). Results showed little interannual variability in accumulation (Figure 5.1), and the overall spatial distribution of accumulation according to Hanna agrees well with results from Ohmura and Reeh (1991) and Bales et al. (2001). Accumulation ranged from 0 to 1200 mm/year for the entire period, with greatest accumulation existing along the extreme southeastern flank of the ice sheet and least accumulation in the north and northeastern regions of the ice sheet. This corresponded with observed backscatter A values from ERS estimates in the northern part of the dry snow zone, where higher values of A in this same region were also indicative of lower accumulation (Figures 4.1 and 4.2).

Net runoff was defined as surface meltwater minus that part which refreezes on or in the ice before being lost (Hanna et al. 2002). Results indicated that net runoff did not vary substantially spatially or temporally during 1992 to 1999 (Figure 5.2). Runoff ranged from 0 to 4000 mm/year, with little runoff occurring in the northern margin and greater runoff rates in the southwest margin of the ice sheet. Although interannual variation in the spatial extent of runoff was difficult to determine, results showed greatest runoff in the north during 1993 and 1998, and along the southwest margin a peak in net runoff occurred in every year, but to a lesser extent in 1992 and 1996. Further, results indicated that net runoff did not occur at elevations above 1600 m during this period. Runoff is suggested to have reached 1600 m along the northern margin of the ice sheet in 1993 and near 1600 m in the southwest during the years 1994, 1995 and 1997 – 1999.

The resulting annual SMB for the entire ice sheet is shown in Figure 5.3, and the zero contour line is shown in bold to represent the location of the EL. Overall, the southeast region of the ice sheet was in a positive balance during this period, whereas the

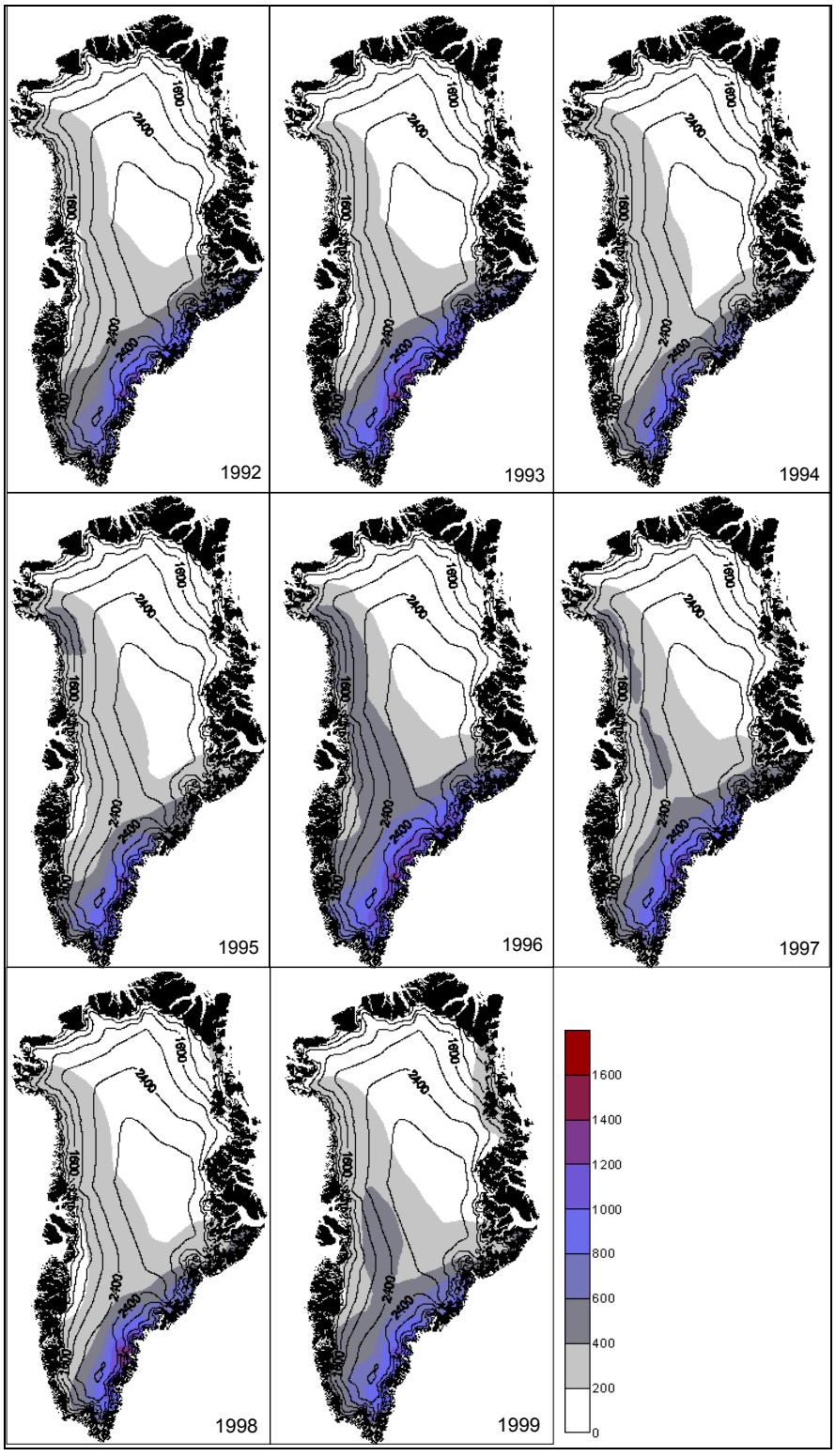

Figure 5.1 Annual accumulation estimates shown in mm per year for the period 1992 to 1999 based on ECMWF ERA-40 and SMB model data from Hanna et al. (2002).

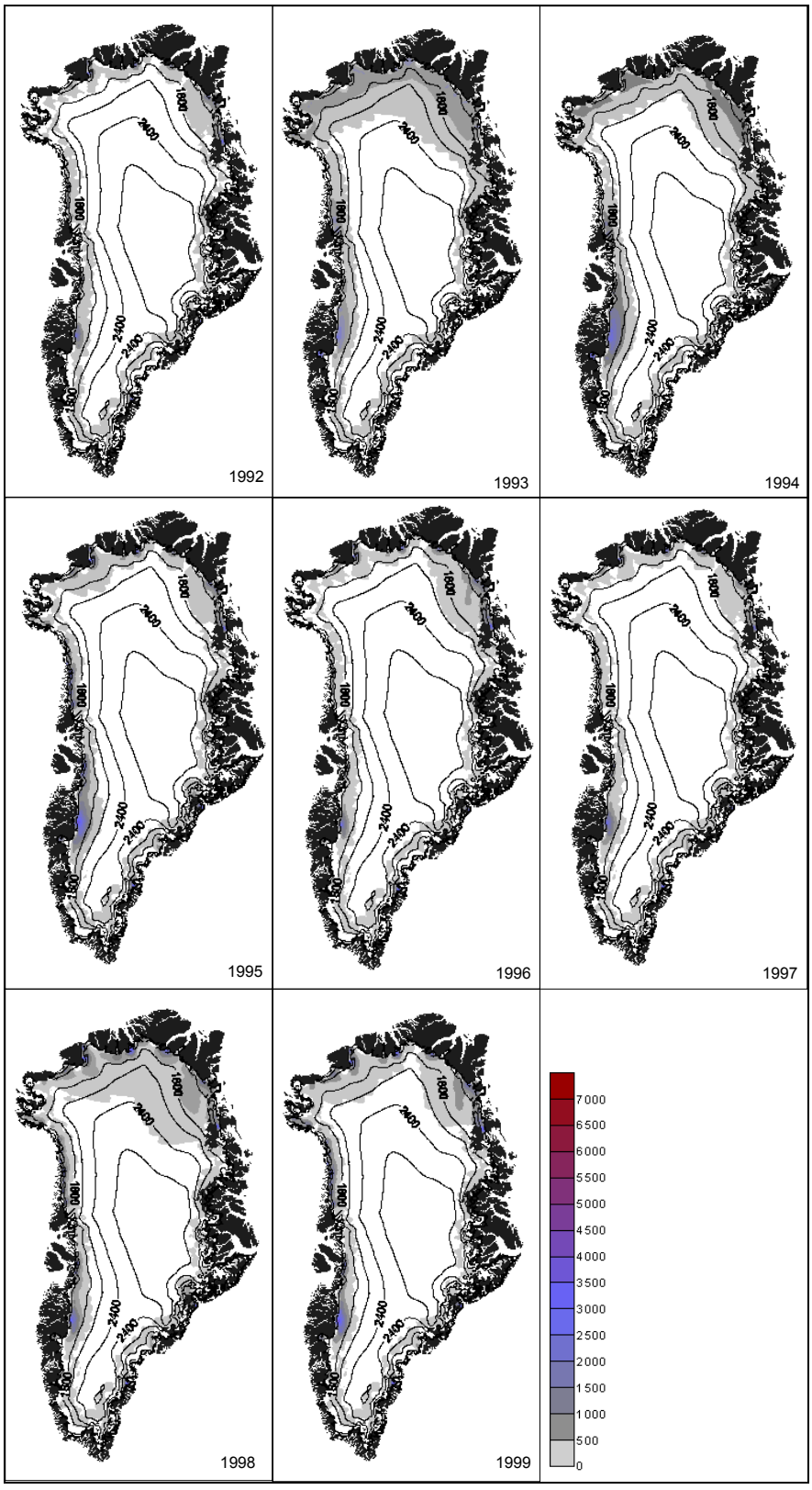

Figure 5.2 Annual net runoff estimates shown in mm per year for the period 1992 to 1999 based on ECMWF ERA-40 and SMB model data from Hanna et al. (2002).

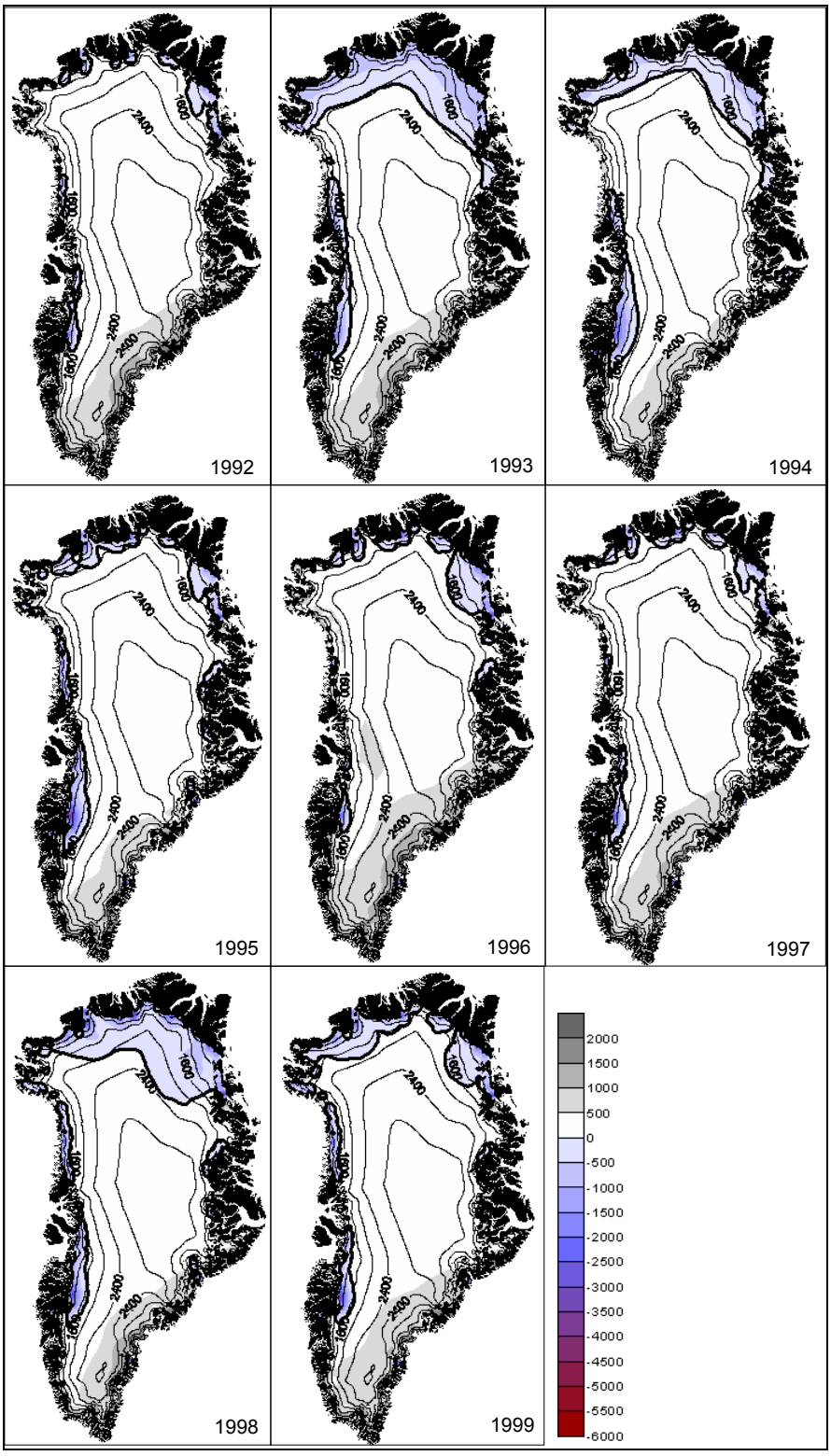

Figure 5.3 Annual SMB estimates shown in mm per year for the period 1992 to 1999 based on ECMWF ERA-40 and SMB model data from Hanna et al. (2002).

southwest margin and northern regions were in negative balance, and the EL experienced substantial shifts in elevation within the north and southwest regions. In 1998, the EL reached a maximum elevation close to 2400 m in the northeast, and in 1994 and 1995, the EL extended close to a high elevation of 2000 m in the southwest margin of the ice sheet. In 1992, 1996, and 1997, the SMB was generally positive in most parts of the ice sheet, and the maximum elevation of the EL was suggested to be about 1600 m in a small area of the southwest margin of the ice sheet in all three years.

5.2 Passive microwave and SMB model data

Additional estimates of Greenland accumulation, runoff, and SMB obtained from Mote (personal communication) are presented in this section. Figure 5.4 illustrates the distribution of annual accumulation rates that are based on annual precipitation data from Bromwich et al. (2001). There exists little spatial and temporal variability in accumulation during this period. A maximum rate of accumulation existed in the extreme south and southeast regions and lower accumulation rates in the central and northern regions, which is in general agreement with results from Hanna's data presented in the previous section, as well as Ohmura and Reeh (1991) and Bales et al. (2001). Much of the central and northern portions of the ice sheet experienced less than 400 mm/year accumulation, while the outer margins of the ice sheet generally received greatest accumulation. The maximum accumulation rate occurred in the southeast during 1992, with 1,753 mm, compared with 1,140 mm during 1995. There was also a relative peak in accumulation along the west central margin of the ice sheet, with values typically between 600 to 800 mm/year.

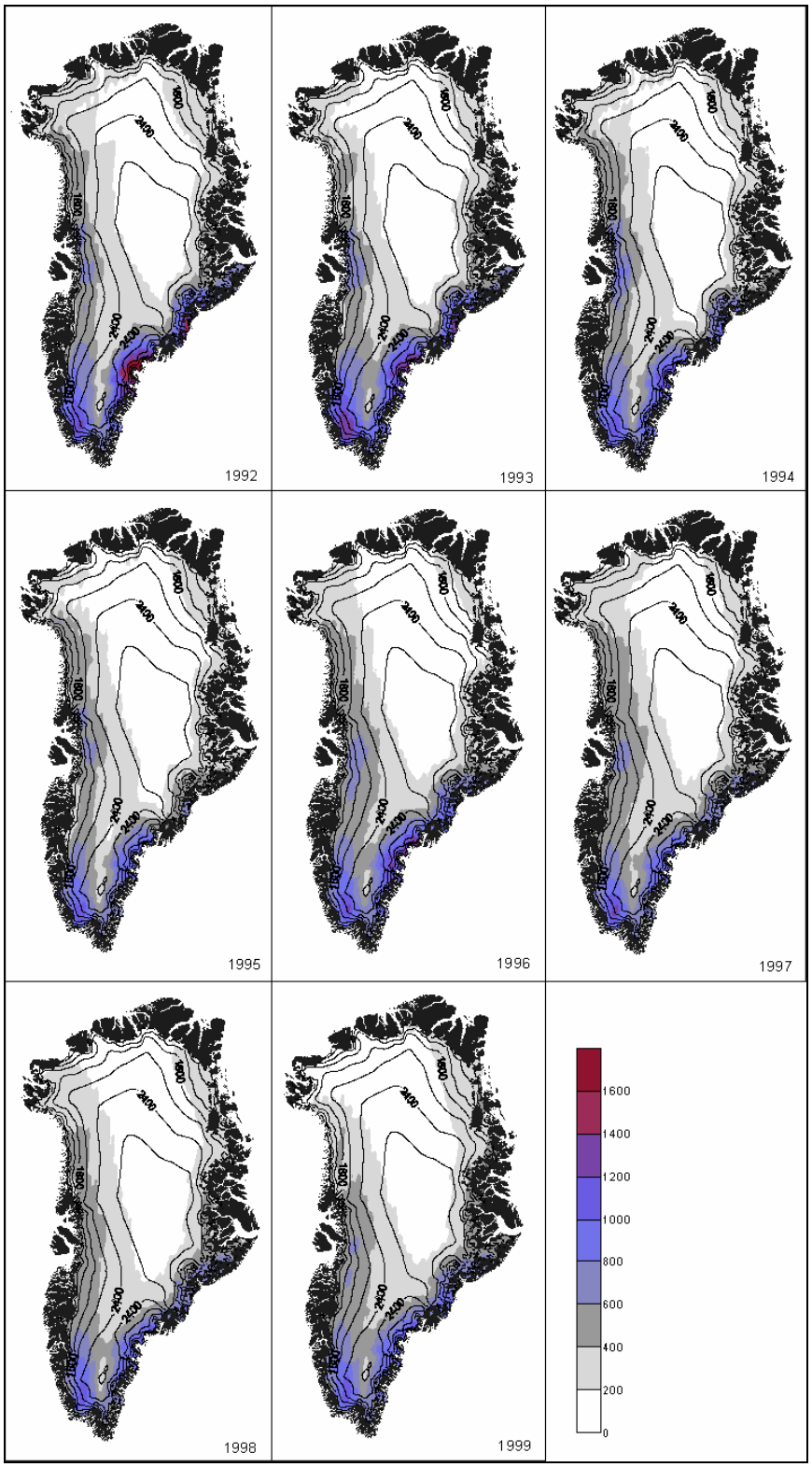

Figure 5.4 Annual accumulation estimates shown in mm per year for the period 1992 to 1999 based on passive microwave observations and SMB model data from Mote (2003).

Overall, greatest runoff rates over this period were experienced in the southwest region of the ice sheet (Figure 5.5). Peak runoff occurred in 1995 within the southwest region, with a maximum value of 5,879 mm, according to Mote (2003). Additionally, in 1995, 1997, and 1999, high runoff rates are suggested to have reached elevations at about 2000 m in the southwest. 1992 was a year of overall low runoff with a maximum runoff rate of only 2,009 mm. In 1995 and 1998, relatively high runoff rates occurred along the extreme west central margin of the ice sheet. During each year, little runoff was experienced in the north central, extreme northwest and southeast regions. Runoff in the central regions of the ice sheet was typically near zero or slightly positive and is not thought to be important in the overall spatial distribution of runoff.

The SMB of the Greenland ice sheet was generally positive for the ice sheet as a whole during this period, except during the years 1995 and 1998 when it was slightly negative, according to Mote (2003). Annual SMB estimates and the EL, in bold at the zero contour line, for Greenland are shown in Figure 5.6. During years of high runoff, the EL was shifted towards central regions of the ice sheet at higher elevations. Conversely, during low runoff years, the EL was found along the outer margins of the ice sheet at much lower elevations. For instance, in 1992 the EL closely followed the 800 m contour line within the northern region of the ice sheet and the 1200 m contour line in the southwest. However, during 1993 and 1994, the EL was located at higher elevations in the north and southwest regions of the ice sheet, where it existed between 1200 and 1600 m in the north and extends to 1600 m in the southwest. As expected, the greatest shift in the EL was experienced in 1995 in the southwest region, as this was a year of relatively

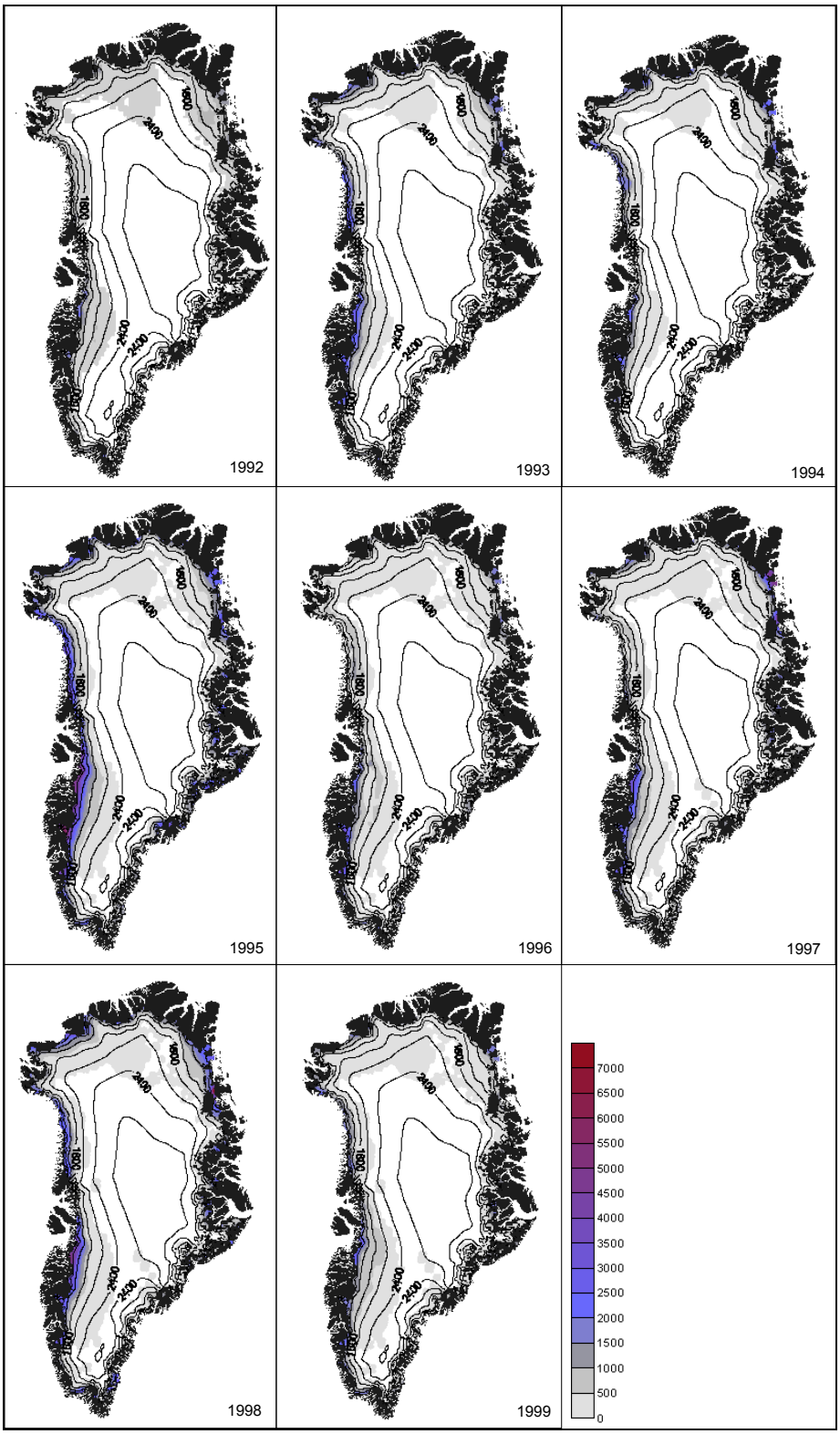

Figure 5.5 Annual net runoff estimates shown in mm per year for the period 1992 to 1999 based on passive microwave observations and SMB model data from Mote (2003).

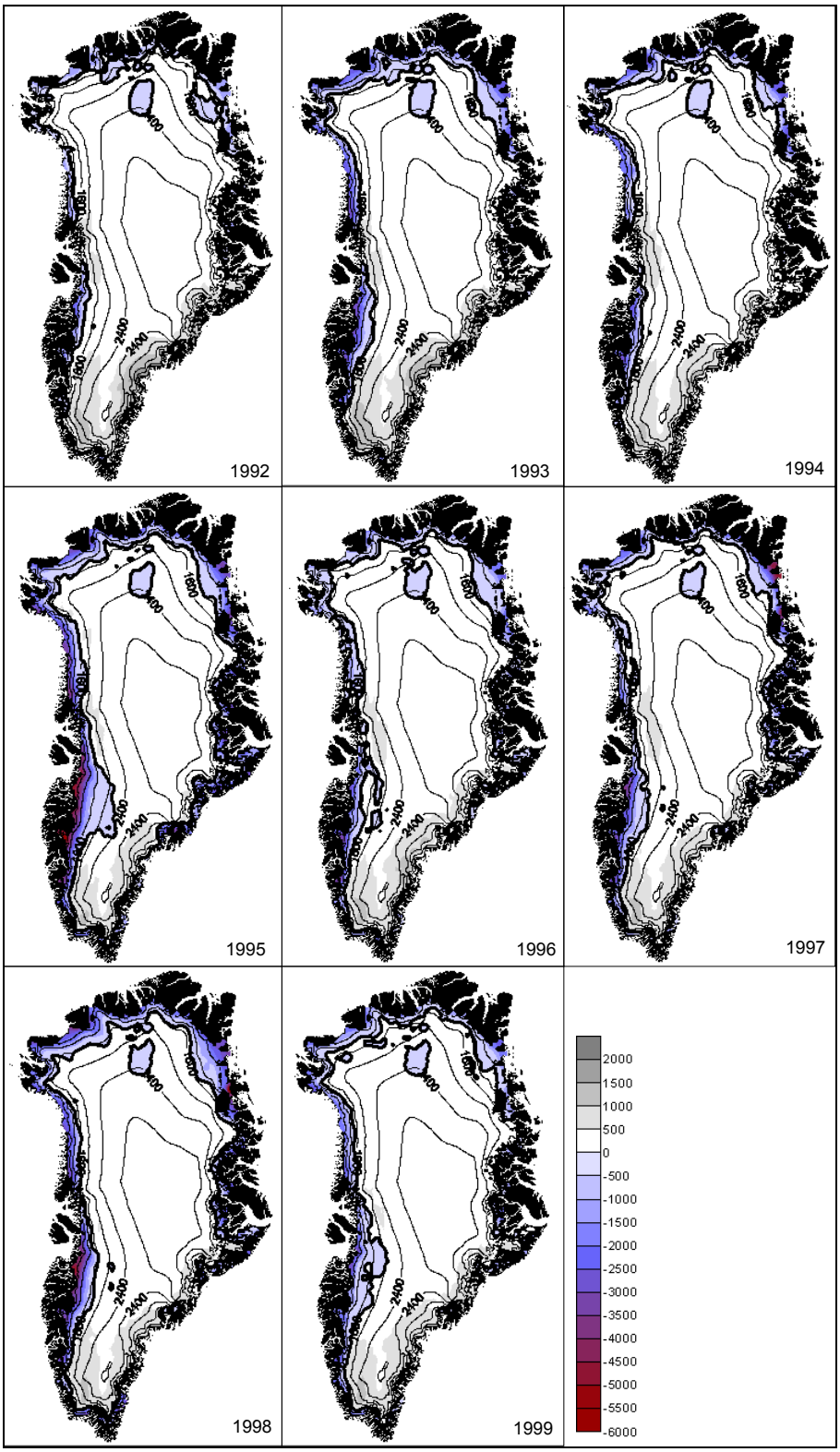

Figure 5.6 Annual SMB estimates shown in mm per year for the period 1992 to 1999 based on passive microwave observations and SMB model data from Mote (2003).

high runoff and the EL reached a maximum elevation of about 2400 m. In many years, including 1992, 1993, 1994, 1996, and 1998, the EL generally existed between 1200 and 1600 m in the southwestern margin of the ice sheet, but in 1997 and 1999 it encroached upon the 2000 m line in certain areas within the southwestern flank. In the northern region of the ice sheet, the EL reached a maximum elevation of 1600 m in 1998.

Results presented here from estimates by both Hanna and Mote showed similarities in the spatial pattern of accumulation, runoff, and SMB. Accumulation rates showed a maximum in the south and southeast of the ice sheet by both Hanna and Mote, as accumulation estimates in both studies were based on ECMWF reanalysis data. Likewise, ablation rates experienced little interannual variability and peaked in the extreme southwest margin of the ice sheet. The SMB also demonstrated similar patterns across the ice sheet between these two data sets. However, estimates from Hanna showed greater areas of negative SMB in the north, whereas estimates from Mote suggested that negative SMB was greatest in the southwest and western margins of the ice sheet. In the next chapter, the scatterometer data discussed previously in Chapter 4 are compared with these model-based results of annual SMB and location of the equilibrium line.

CHAPTER 6

COMPARISON OF GREENLAND SMB FROM SCATTEROMETER AND MODEL BASED ESTIMATES

By comparing model-based estimates with scatterometer observations, greater certainty and understanding may be gained in measurements of the surface mass balance of Greenland. To compare estimates of the SMB of the ice sheet for the period 1992 to 1999, the surface areas of the accumulation and ablation zones of the ice sheet were examined for ERS-1/2 scatterometer data from the Scatterometer Climate Record Pathfinder project, and for model-based estimates, including ECMWF ERA-40 reanalysis data from Hanna et al. (2002) and SSM/I-based melt frequency data from Mote (2003). Areas of positive and negative SMB across the ice sheet were determined and compared between the model-based data sets to show spatial differences in the sign of the SMB. Additionally, the elevation of the equilibrium line (EL) was determined for each data set and year during this period along the elevation gradient within the west central portion of the ice sheet, including the ETH Camp and Jakobshavn. These methods used here to compare estimates of the SMB from different data sources are expected to reveal both the strengths and shortcomings in the tools commonly used in estimating the SMB.

6.1 Accumulation and ablation surface areas

For purposes of this thesis, the accumulation zone is defined as simply the area of the ice sheet where the SMB is positive and the ablation zone is the area of negative SMB for each year during 1992 to 1999. To assess the extent of accumulation and ablation between each data set, annual surface areas were computed for the model-based estimates and scatterometer observations. These areas are expressed as fractions of the total area of the ice sheet. The total area of the ice sheet (Table 6.1) was defined using the ice mask mentioned in Chapter 3 and was determined separately for each data set. The total surface area defined as the ice sheet varied slightly between the data, most likely a result of the interpolation process onto the 10 km x 10 km grid spacing, but the difference in the total surface area is at most 0.1% of the ice sheet.

Table 6.1 Total surface areas of the ice sheet for each of the data sets, in square kilometers. The difference in the total surface area between these data sets is at most 0.1% of the ice sheet.

Source	Total Surface Area
ERS-1/2	1,609,299.05 km²
Hanna	1,611,856.15 km²
Mote	1,611,178.98 km²

Model-based estimates acquired from Hanna and Mote represent annual SMB, whereas SMB estimated from scatterometer observations are represented during the time of maximum melt extent for each year. The ablation season was defined as May through August of each year by Mote (2003), and runoff rates based on Hanna et al. (2002) were derived from a melt model that used annual and July temperatures to arrive at the sum of

degree days. Additionally, the time of maximum melt extent was found to occur generally during mid-July based on ERS-1/2 scatterometer data, although this also varied slightly interannually. Therefore, the definition of the ablation season, and thus the balance year, differs between each of the data sets and the duration of the ablation season is likely inconsistent from year-to-year. Despite these limitations, surface areas presented in this section should provide an indication of the interannual changes in the accumulation and ablation extents experienced during this period according to each data set.

In general, annual accumulation surface areas from the ERS-1/2 scatterometers varied least during this period, and the fractions of the accumulation area from scatterometer estimates remained considerably higher than model-based estimates over the entire period (Table 6.2). Annual accumulation surface areas from ERS-1/2 scatterometers showed a minimum of 92.1% in 1995 and a maximum of 97.3% in 1996.

Table 6.2 Annual accumulation surface areas from 1992 to 1999 represented as a fraction (%) of the total surface area of the ice sheet.

Year	MMDD (ERS only)	ERS-1/2 (-18 dB)	ERS-1/2 (-12 dB)	Hanna	Mote
1992	0714 - 0719	95.6	90.8	95.4	91.2
1993	0721 - 0726	96.7	85.5	79.0	85.9
1994	0709 - 0714	96.1	80.6	83.5	89.2
1995	0715 - 0720	92.1	74.4	89.8	78.7
1996	0630 - 0705	97.3	89.1	92.4	85.6
1997	0715 - 0720	96.9	88.3	94.5	85.6
1998	0724 - 0729	94.4	83.2	78.6	81.5
1999	0808 - 0813	95.0	82.8	87.4	84.3
Mean		95.5 ±1.7	84.3 ±5.3	87.6 ±6.6	85.2 ±3.9

A corresponding increase was found in accumulation rates during 1995 to 1996 by McConnell et al. (2001), with an increase of 37%. Accumulation surface areas based on ECMWF ERA-40 and SMB model estimates from Hanna suggested that a much larger range was experienced during this period, with a minimum surface area of 78.6% in 1998 and a maximum area of 95.4% during 1992. Similarly, annual accumulation surface areas from SSM/I and SMB model estimates by Mote (2003) suggested that a minimum accumulation area of 78.7% occurred in 1995, and a maximum accumulation surface area also occurred in 1992, at 91.2%. Thus, the year in which the accumulation zone occupied the largest area of the ice sheet agreed between estimates from Hanna and Mote, both indicating that it was experienced in 1992. Estimates of accumulation surface areas given by both Hanna and Mote also indicated that a similar range was experienced during the period, at 16.8% and 12.5% respectively.

Because the lower boundary defined as the ice sheet varied somewhat for each of the data sets, the resulting ablation surface areas should be compared among the data sets with discretion. Annual ablation surface areas defined by scatterometer observations reflect relatively low values compared with that from estimates by Hanna and Mote (Table 6.3). The fractions of the ablation area to the area of the entire ice sheet based on ERS-1/2 scatterometer data are much lower and showed the least interannual variability compared with model-based estimates. Overall, the ablation surface area occupied the largest surface area of the ice sheet in 1998 based on estimates from Hanna. However, according to ERS-1/2 scatterometer observations and estimates by Mote, the year in which the ablation zone occupied the largest area of the ice sheet is 1995, although the magnitude of the fraction of the ablation area to the area of the entire ice sheet differed

Table 6.3 Annual ablation surface areas from 1992 to 1999 represented as a fraction (%) of the total surface area of the ice sheet.

Year	MMDD (ERS only)	ERS-1/2 (-18 dB)	ERS-1/2 (-12 dB)	Hanna	Mote
1992	0714 - 0719	4.1	9.2	4.7	8.8
1993	0721 - 0726	3.3	14.5	21.0	14.2
1994	0709 - 0714	3.9	19.4	16.5	10.8
1995	0715 - 0720	7.9	25.6	10.2	21.3
1996	0630 - 0705	2.7	10.9	7.6	14.5
1997	0715 - 0720	3.1	11.7	5.5	14.4
1998	0724 - 0729	5.6	16.8	21.4	18.5
1999	0808 - 0813	5.0	17.2	12.7	15.7
Mean		4.5 ±1.7	15.7 ±5.3	12.4 ±6.6	14.8 ±4.0

substantially, at 21.3% according to Mote and only 7.9% from ERS-1/2 scatterometer observations.

Based on glaciological observations from snow pits, Benson (1962) found that the long-term accumulation zone occupied approximately 84% of the total surface area of the ice sheet, while the remaining 16% of the ice sheet accounts for the ablation zone where a net annual mass loss was experienced. More recently, Zwally (1989) indicated that 85% of the Greenland ice sheet existed above the equilibrium line, suggesting that about 15% of the ice sheet was occupied by the ablation zone. These past measurements of the accumulation and ablation zones show good agreement with mean accumulation and ablation surface areas over the period 1992 to 1999 shown here from estimates by Hanna and Mote, with a mean accumulation surface area of 87.6% and 85.2%, respectively (Table 6.2). The comparison of the surface areas determined here with past published results suggests that, while large interannual variability may exist in the extent of the

accumulation and ablation areas for the ice sheet, mean accumulation and ablation areas over a longer period generally vary by much less.

Results of the accumulation and ablation surface areas determined from the ERS-1/2 scatterometer observations differed substantially from the model-based estimates presented here and from surface areas based on published work. The estimated accumulation and ablation surface areas were dependent on the definition of the equilibrium line, which was defined at the -18 dB line for each year in this study. This backscatter value of A may not reflect an optimal demarcation of the equilibrium line from ERS scatterometer data, and it is possible that a more realistic definition of the equilibrium line may vary interannually, as the melt extent and subsequent ablation zone change from year-to-year. Further investigation of the delineation of the ablation zone and equilibrium line is recommended to acquire more accurate estimates of scatterometer-based accumulation and ablation surface areas.

The annual accumulation and ablation surface areas are shown graphically to illustrate annual trends between the data sets and to more clearly demonstrate the variability in the fraction of the accumulation and ablation areas to the total surface area of the ice sheet during this period (Figures 6.1 and 6.2). In 1992, the fractions of the accumulation and ablation areas of the entire ice sheet agreed, but for other years, such as 1993, there were significant differences between the data sets. The accumulation and ablation surface areas experienced large interannual variability during this period, causing any longer-term trends difficult to discern.

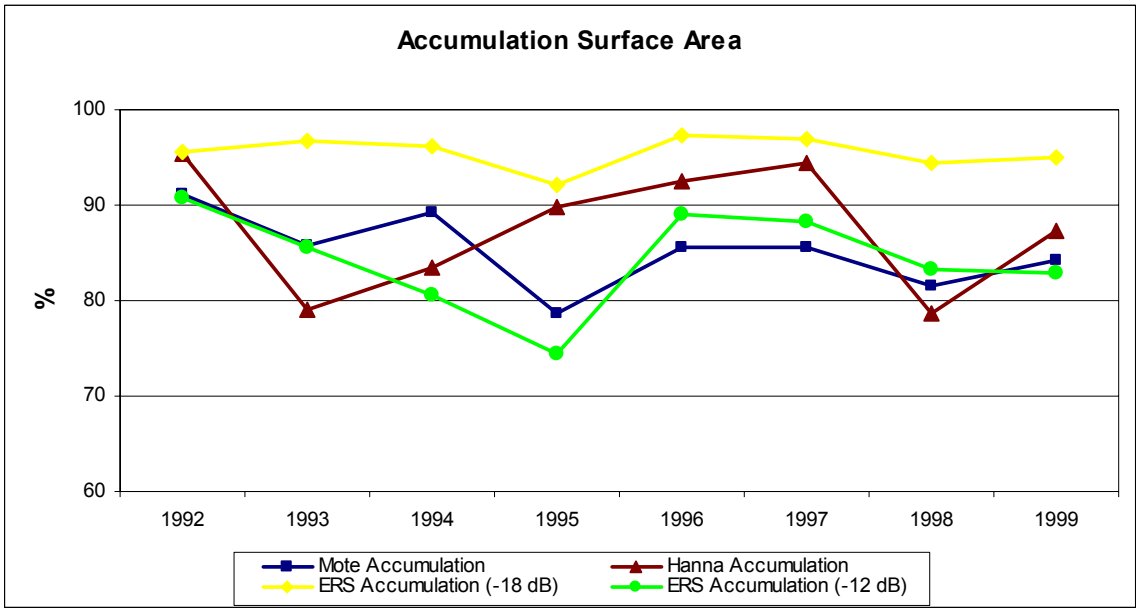

Figure 6.1 Accumulation surface areas over the period 1992 to 1999 from Table 6.1.

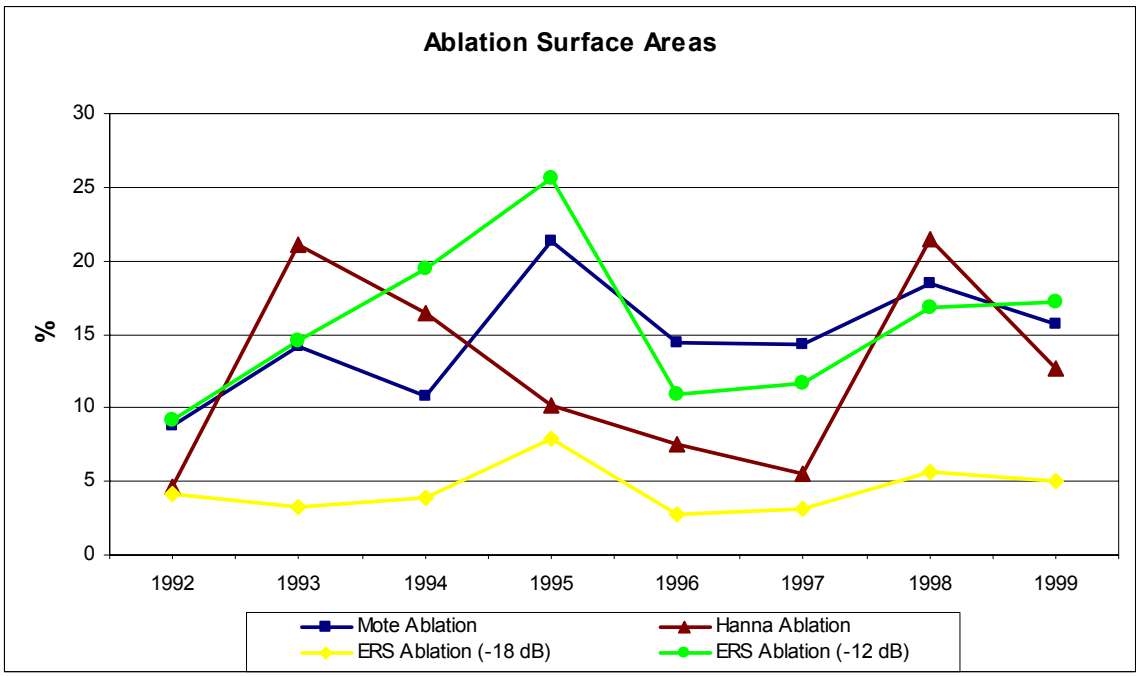

Figure 6.2 Ablation surface areas over the period 1992 to 1999 from Table 6.2.

6.2 Spatial comparisons of SMB and equilibrium lines

Differences in areas of positive and negative SMB of each year were determined between the model-based data sets to show areas along the ice sheet where the state, or sign, of the SMB agreed. Results of the spatial differences in the sign of the SMB between Hanna and Mote are shown in Figure 6.3. Areas of the ice sheet shaded in red indicate where the SMB was positive according to Hanna but negative according to Mote, and areas shaded in blue show the reverse. Areas not shaded represent agreement between the two data sets, where the SMB was either positive or negative according to both data sets. Results showed that differences exist in the southwest and northern margins of the ice sheet. Data from Hanna suggests that the SMB was negative within much of the northeast and southwest portions; whereas, Mote (2003) indicated the opposite sign in the SMB within these regions. However, their estimates agreed for the central, east, and extreme southwest portions of the ice sheet during the entire period.

Differences in the EL between peak melting periods from ERS scatterometer data and estimates from Hanna are shown in Figure 6.4. As previously mentioned, the EL was defined at the –18 dB contour in ERS-1/2 images, and areas above the -18 dB backscatter contour were defined as the accumulation zone and areas below this line were defined as the ablation zone. For comparison, the EL from Hanna, defined as areas of zero SMB, was overlayed to show spatial differences in the EL during low and high melt years. Greatest discrepancies were shown in the northern regions of the ice sheet in both low (1992) and high (1995, 1998, and 1999) melt years, where the SMB was positive according to ERS scatterometer estimates but negative based on estimates from Hanna.

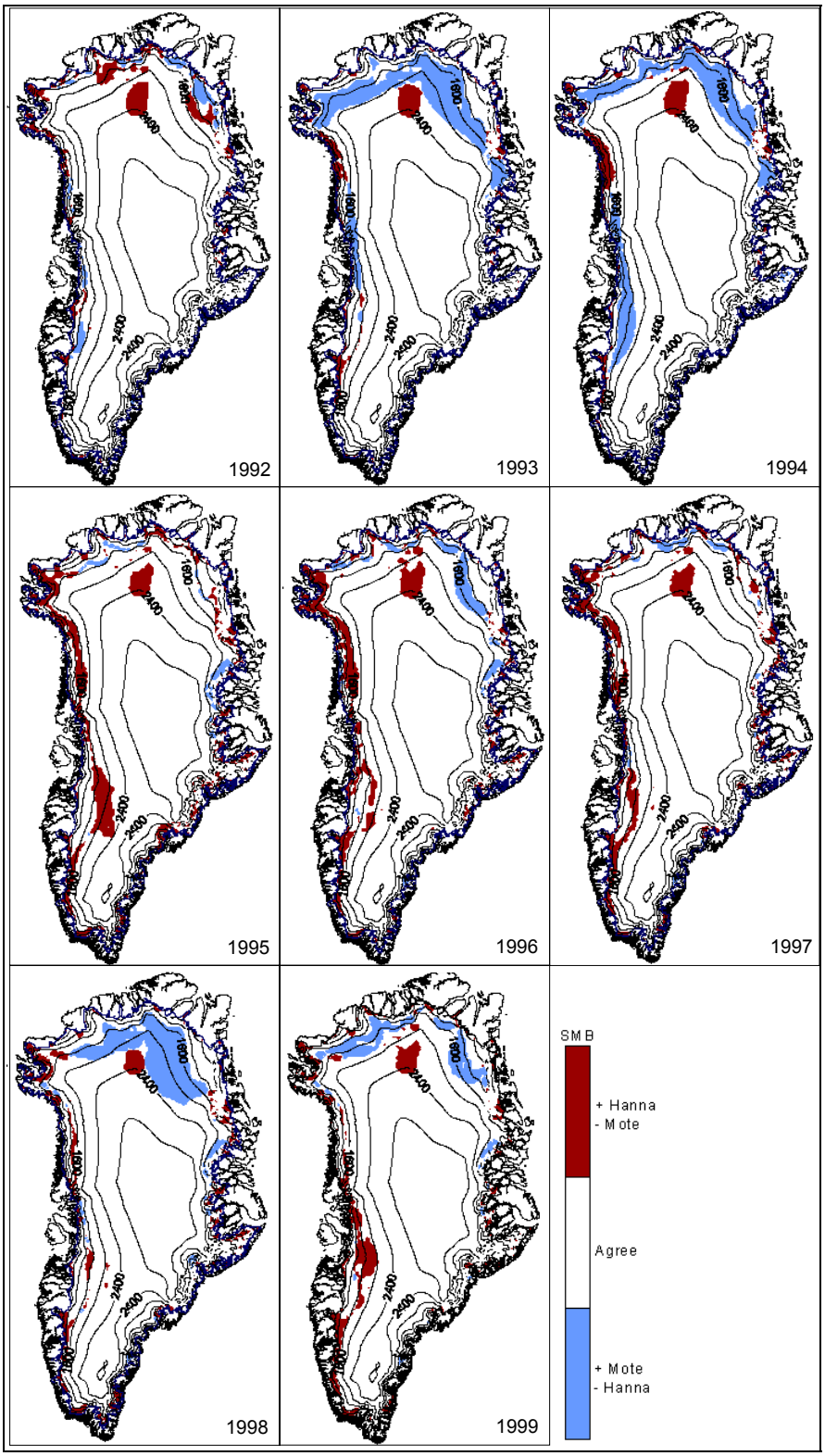

Figure 6.3 Annual differences between SMB estimates from Hanna and Mote for each year, with areas shaded in red indicating where the SMB was positive according to Hanna and negative for Mote, and areas shaded in blue indicate the reverse.

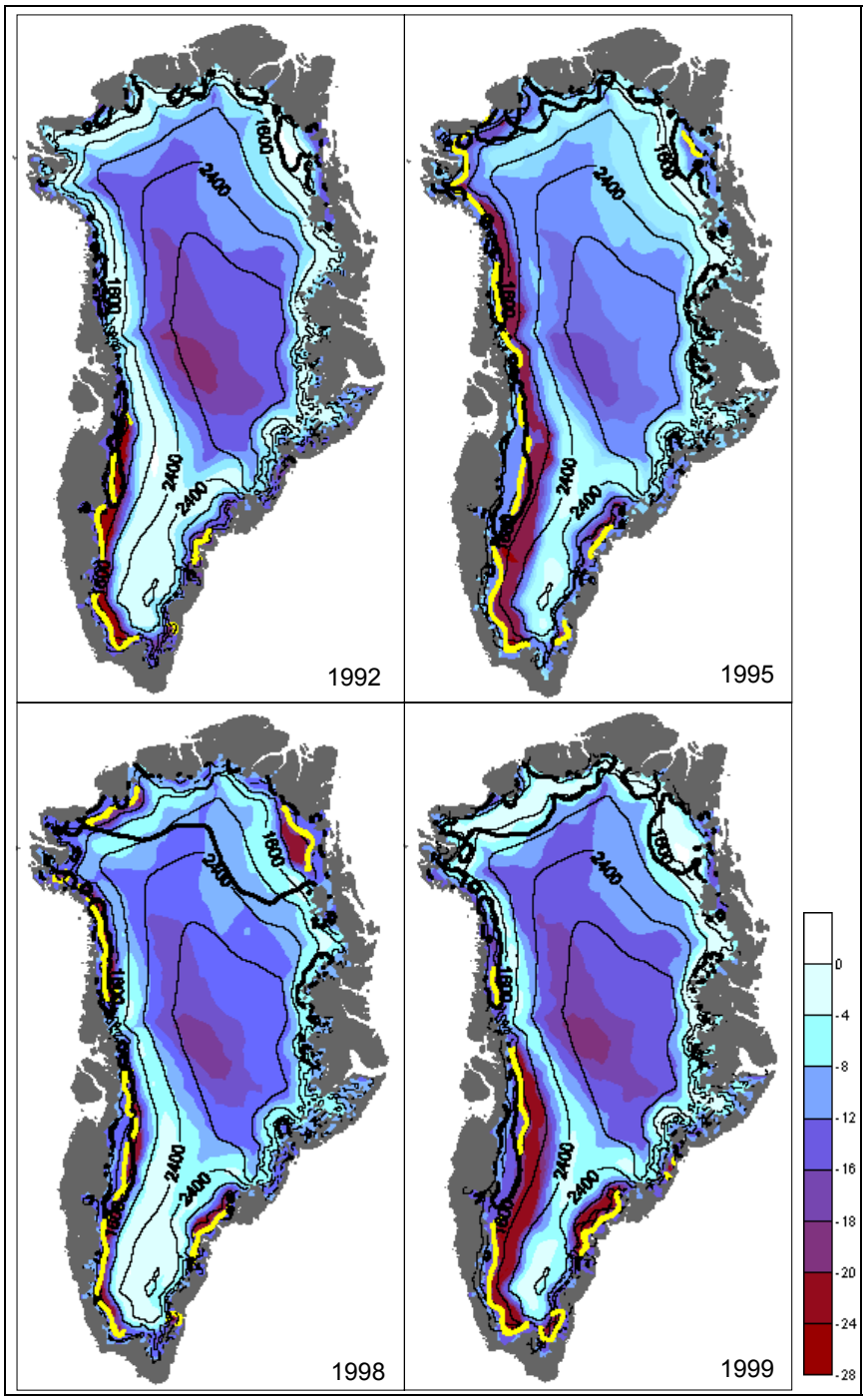

Figure 6.4 Equilibrium lines shown for ERS-1/2 observations, yellow contour line at –18 dB, and from estimates by Hanna, bold solid line, for the years 1992, 1995, 1998, and 1999.

Conversely, the EL along the southwest and western margins of the ice sheet showed similar patterns, except within the extreme southwest flank where negative SMB was suggested by scatterometer observations and positive SMB based on estimates from Hanna.

The EL from ERS-1/2 scatterometer observations and estimates from Mote (2003) were also compared for the same four years, 1992, 1995, 1998 and 1999 (Figure 6.5). Generally, the EL according to each data set followed a similar pattern within the southwest portion of the ice sheet, with the exception of 1995. However, the northern portions of the ice sheet showed greater discrepancies between the location of the EL. Along the northern regions of each year, the SMB was mostly positive based on scatterometer estimates but negative according to Mote. The EL based on these two data sets agrees within the extreme southern and southeastern margins of the ice sheet.

Lastly, differences in annual EL between model-based estimates from Mote, green bold contour, and Hanna, black bold contour, were examined (Figure 6.6). During 1992, a relatively low melt year, the pattern of the EL was similar for the two data sets across much of the ice sheet. However, during years of relatively high melt, 1995, 1998, and 1999, discrepancies existed in both the northern and southwestern portions of the ice sheet. In 1995, the EL reached an elevation near 2400 m in the southwest where the elevation of the EL was below 2000 m according to estimates from Hanna. In 1998, much of the northern portion of the ice sheet was in negative SMB according to Hanna and the EL reached a maximum elevation of near 2400 m in this region. The SMB was also negative along the northern margins of the ice sheet based on Mote, but the EL

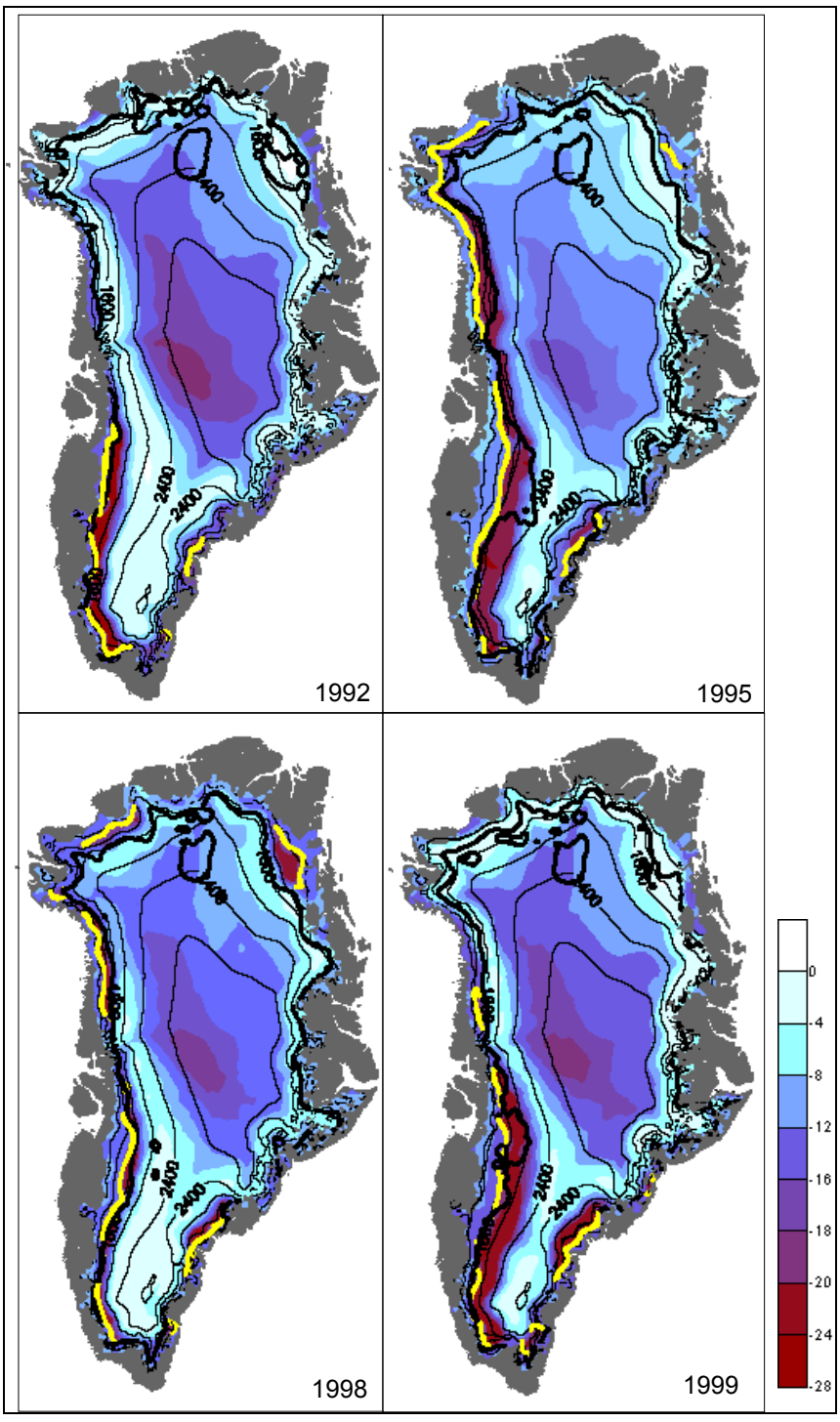

Figure 6.5 Equilibrium lines shown for ERS-1/2 observations, yellow contour at the –18 dB line, and Mote (2003), solid bold contour, for the years 1992, 1995, 1998, and 1999.

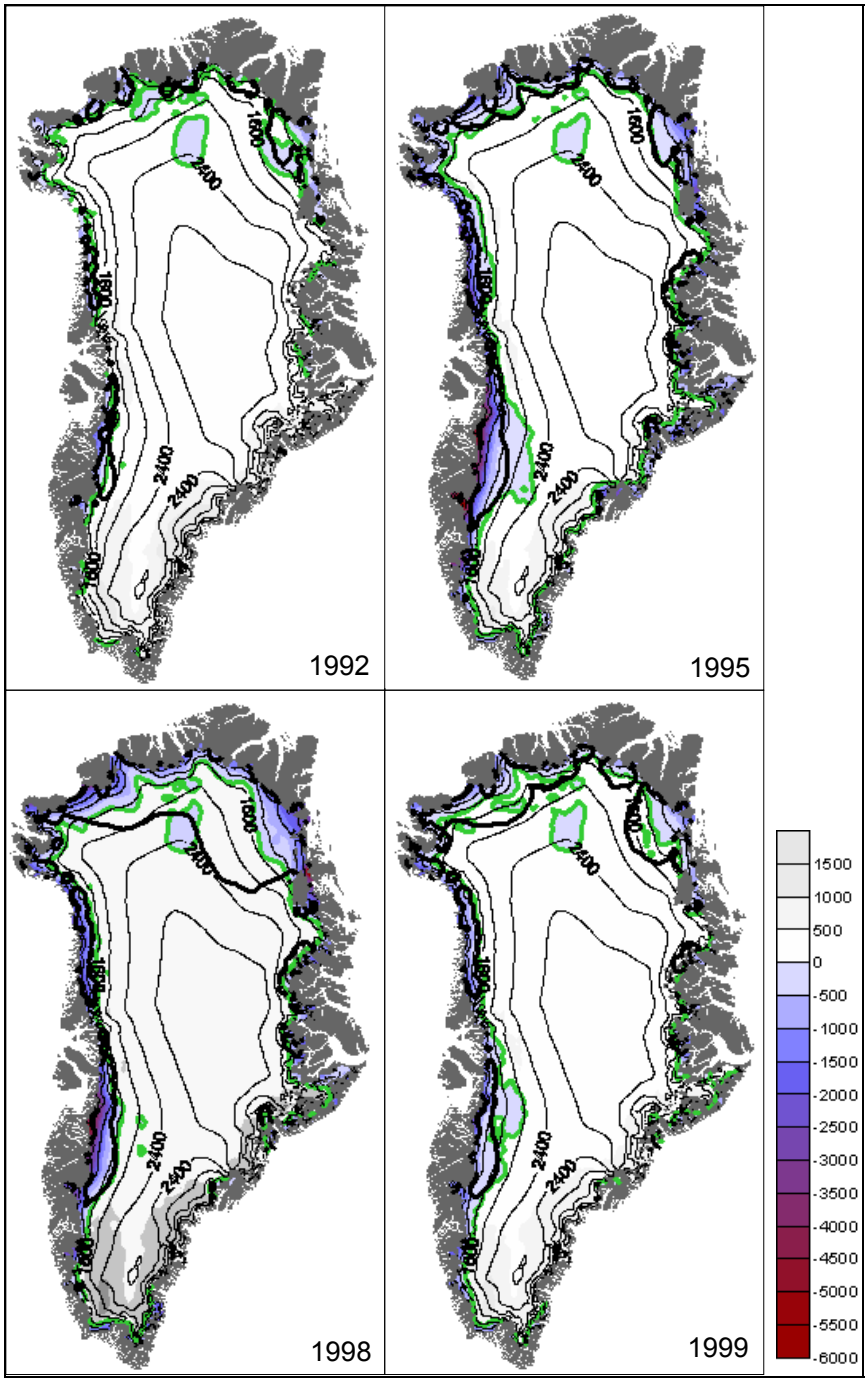

Figure 6.6 Equilibrium lines from estimates by Hanna, bold black contour, and Mote, bold green contour, for the years 1992, 1995, 1998, and 1999.

closely followed the 1600 m elevation contour. Zwally (1989) stated that the EL is generally assumed to lie between 1200 and 1500 m a.s.l., but each of the data sets deviated from this range over some portion of the ice sheet during each year.

6.3 Equilibrium line altitude

The equilibrium line altitude (ELA) is the height where the net mass change is zero (Kaser et al. 2003) for a given location of the ice sheet. The ELA is useful in examining changes in the surface mass balance of an ice sheet, as an increase in the ELA indicates that a larger portion of the ice sheet is in the ablation zone and that the ice sheet is retreating. The opposite can be said for a decrease in the ELA, indicating that more of the ice sheet is in the accumulation zone and the ice sheet is growing. For purposes in this study, the annual ELA shows the height, in meters, where the SMB equals zero along the elevation gradient in the west central region of the ice sheet from 69.13°N, 51.03°W (71 m) to 70.2°N, 41.5°W (2,804 m) for each year during 1992 to 1999. It is important to note that the ELA determined in this manner may not agree with long-term glaciological measurements of ELA. Nevertheless, annual ELA determined for each data set provides further information on how the SMB changed during this period and how these changes compare between each of the data sets.

Annual ELA estimates according to each data set are shown in Figures 6.7 to 6.14. The elevation at which the SMB equals zero according to estimates by Hanna and Mote are shown along the primary y-axis, and for comparison, the scatterometer backscatter values of A are plotted along a secondary y-axis to show the height at which the -18 dB contour line was reached. Overall, the maximum ELA was 1,958 m in 1999,

according to estimates from Mote (2003), and a minimum ELA was suggested to have occurred in 1996 at 854 m based on scatterometer observations. The ELA along a nearby transect at Pâkitsoq was approximately 1,200 m a.s.l. based on surface observations from Braithwaite et al. (1994). For the period 1979 to 1986, Mote (2000) estimated the long-term ELA at the same region of the ice sheet as 1,200 m a.s.l. using SMMR data and a surface mass balance model data, and 1,190 m a.s.l. using surface temperature data. In comparison, the mean ELA was 1,448 ±337 m a.s.l. according to estimates from Mote (2003), 1,193 ±245 m a.s.l. according to estimates from Hanna et al. (2002), and 1,110 ±148 m a.s.l. based on ERS observations. The data sets showed greatest similarity in the ELA for the years 1993, 1997, and 1999. These figures also revealed that estimates of the SMB differed substantially at lower elevations between estimates by Hanna and Mote, but their estimates showed greater similarity at higher elevations of the ice sheet. This suggests that SMB estimates differed more substantially along the margin of the ice sheet within the ablation zone.

6.4 Summary and conclusions

SMB comparisons between these three data sets showed large interannual variability in short-term estimates of the SMB. The year in which the accumulation zone occupied the largest area of the ice sheet occurred during 1996 based on scatterometer observations and 1992 based on model estimates from Hanna and Mote. The year in which the ablation zone was largest agreed for scatterometer observations and estimates by Mote, occurring in 1995, where estimates by Hanna indicated that the ablation zone was largest during 1998. Although interannual variability existed in the surface areas of

the accumulation and ablation zones for each of the data sets, they all showed the same general change of a decrease in the accumulation surface area from 1992 to 1999 and a corresponding increase in the ablation surface area.

Generally, the sign of the SMB according to Hanna and Mote was in good agreement for much of the central, southeast and extreme southern portions of the ice sheet, but it differed in the north and southwest regions. Likewise, the north and southwest regions also disagreed when compared with scatterometer-based estimates. Since these two regions of the ice sheet were typically where greatest melting was experienced during this period, discrepancies in estimates of the SMB of the ice sheet are likely due to uncertainties that remain in estimates of net runoff or ablation. To further quantify this comparison in the SMB of the ice sheet between these data sets, the ELA was determined along the elevation gradient of the west central region of the ice sheet. ELA estimates from Hanna and Mote were similar during 1992, 1993, and 1998, but for most of the years during this period the ELA differed substantially between each data set. A large range in the ELA was also revealed in each data set, indicating that the equilibrium line and, therefore, the SMB experienced large shifts interannually in this region of the ice sheet.

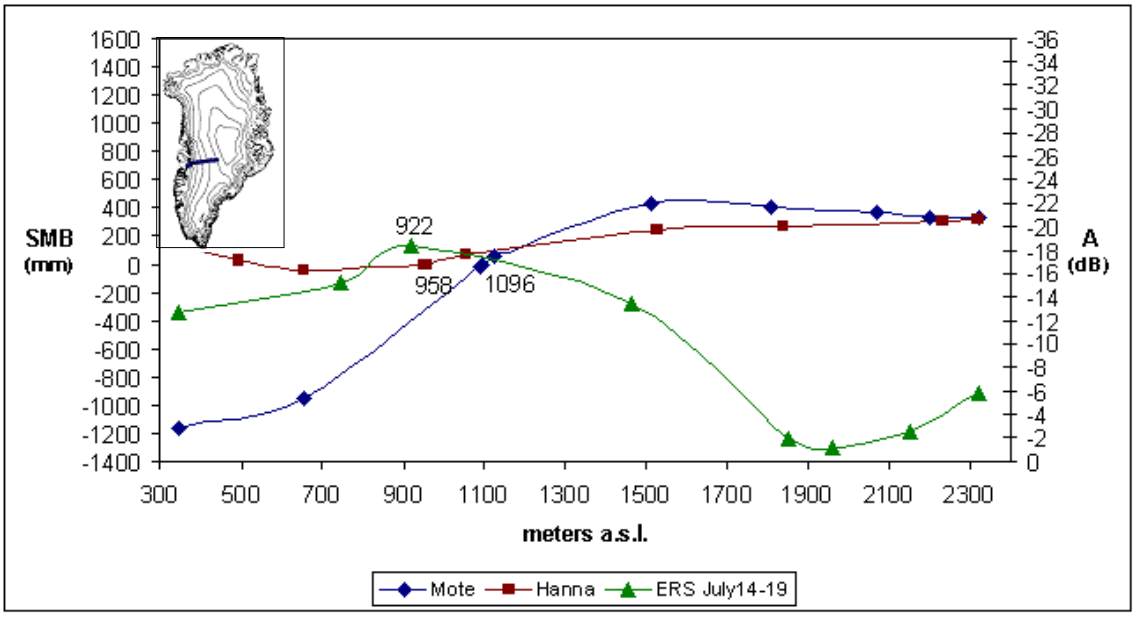

Figure 6.7 SMB and equilibrium line altitude (m a.s.l.) in west central Greenland at 69.1° N, 51° W to 70.2° N, 41.5° W, in 1992 for Mote (2003) (blue diamonds), and Hanna et al. (2002) (red squares). Also shown are scatterometer backscatter A values (dB) (green triangles).

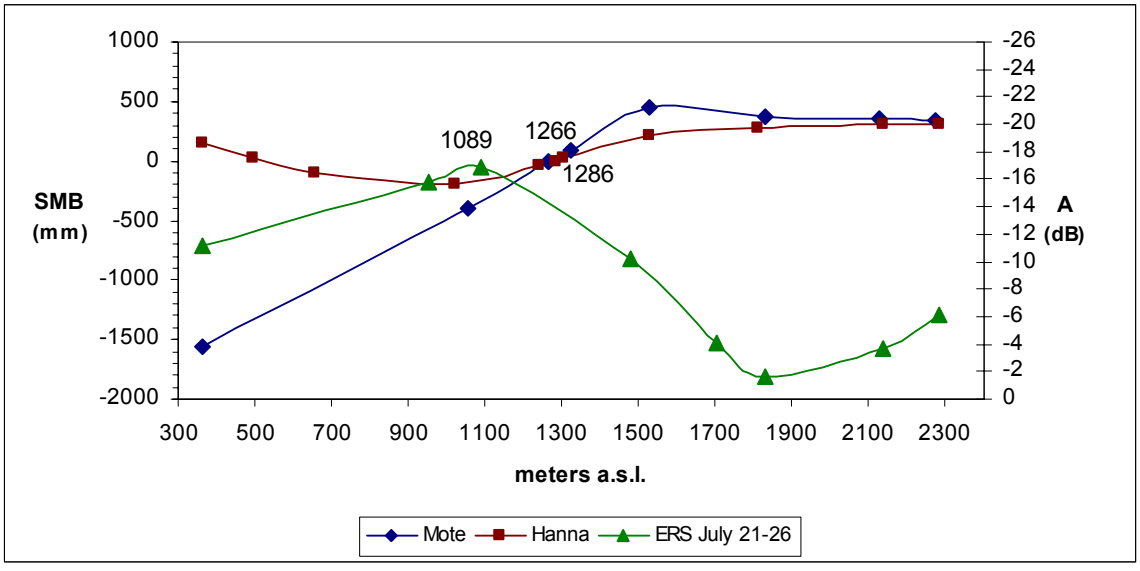

Figure 6.8 Same as that shown in Figure 6.7 for 1993.

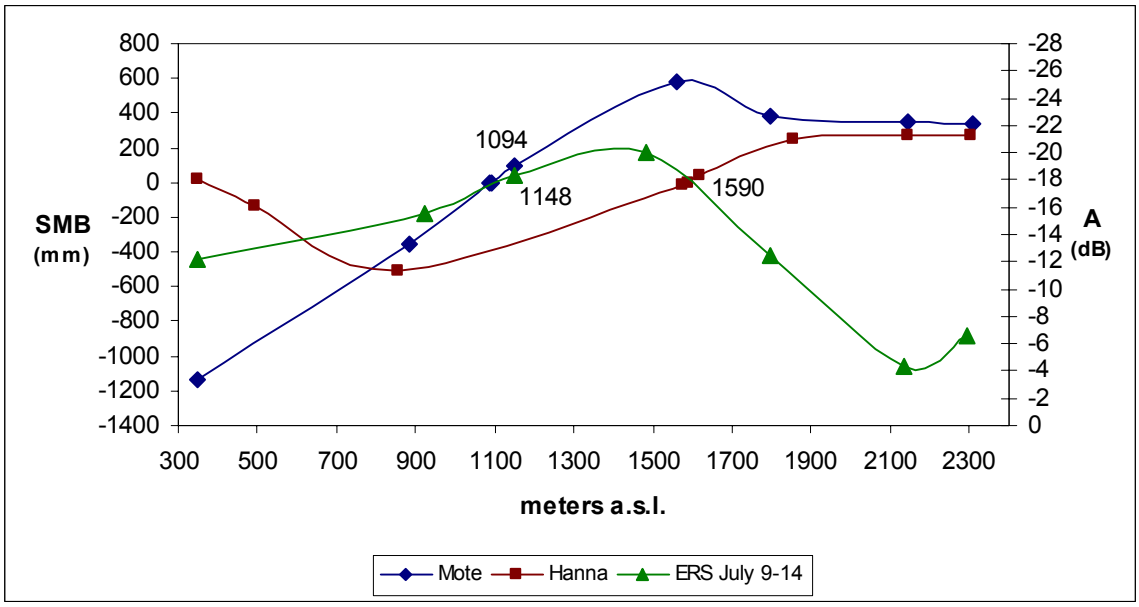

Figure 6.9 Same as that shown in Figure 6.7 for 1994.

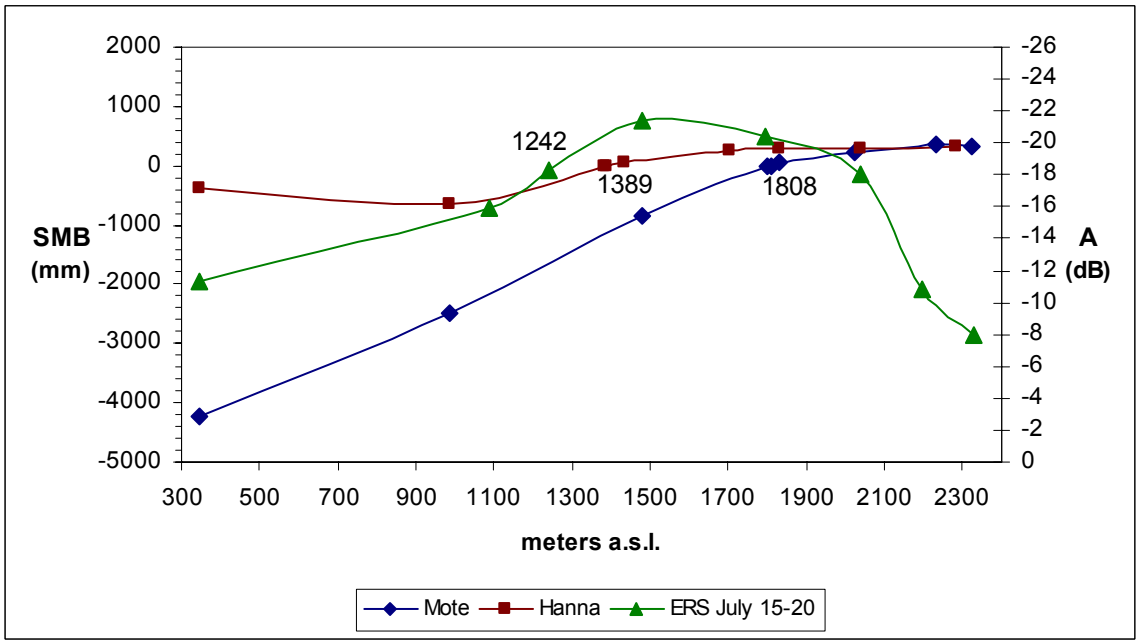

Figure 6.10 Same as that shown in Figure 6.7 for 1995.

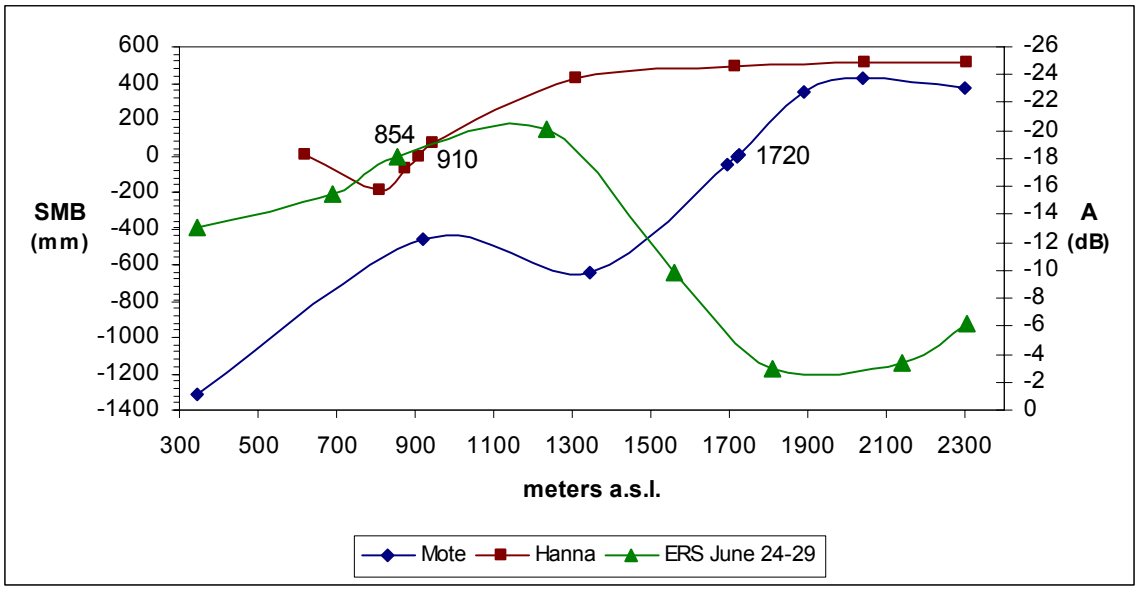

Figure 6.11 Same as that shown in Figure 6.7 for 1996.

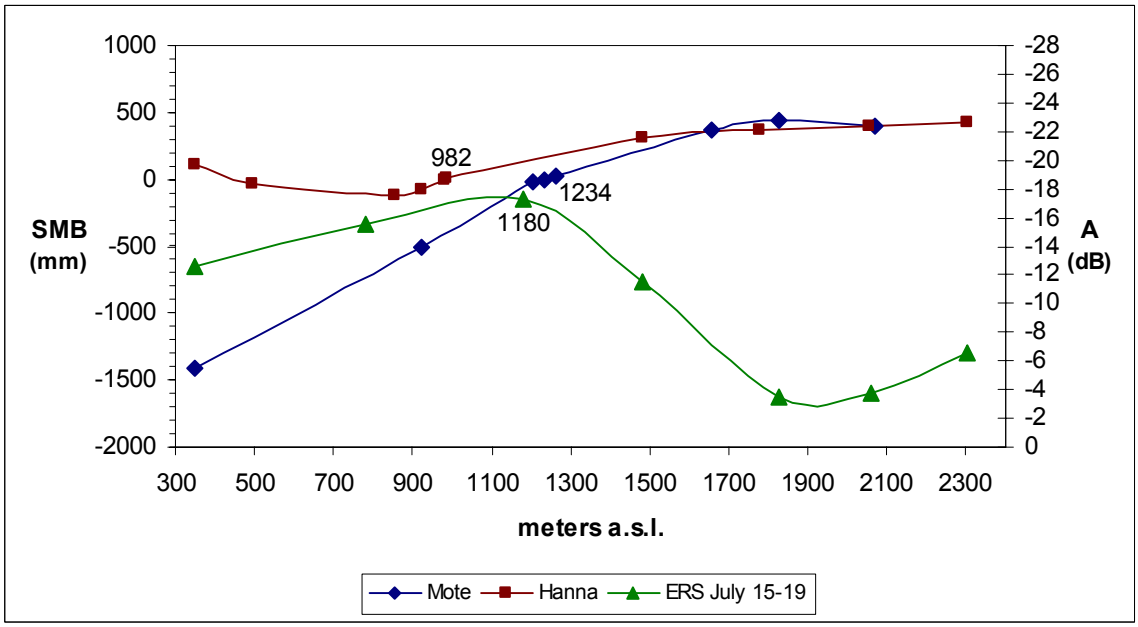

Figure 6.12 Same as that shown in Figure 6.7 for 1997.

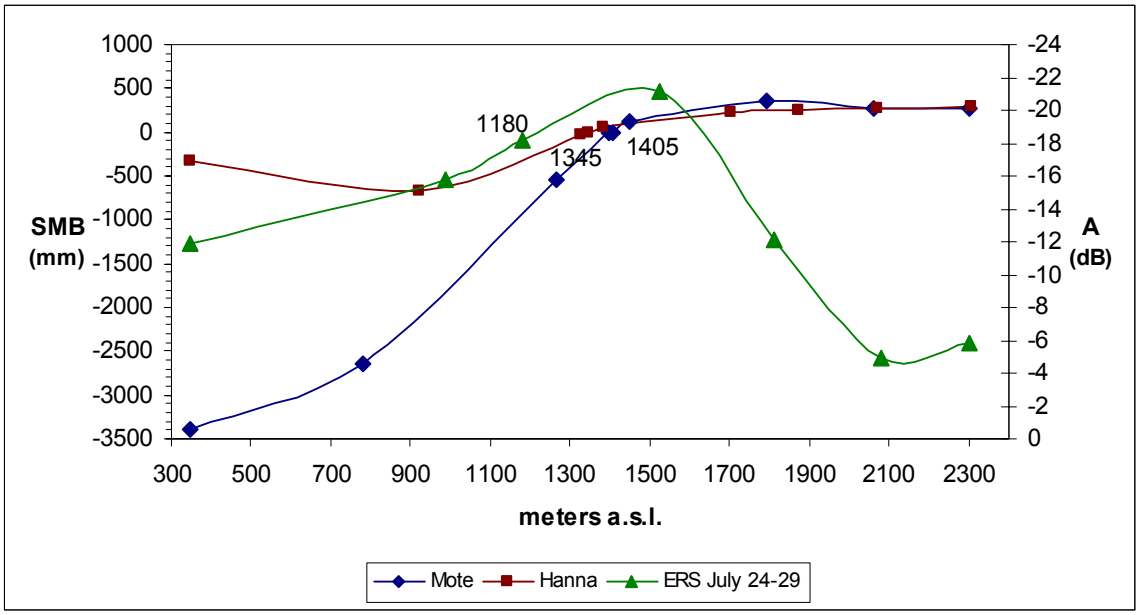

Figure 6.13 Same as that shown in Figure 6.7 for 1998.

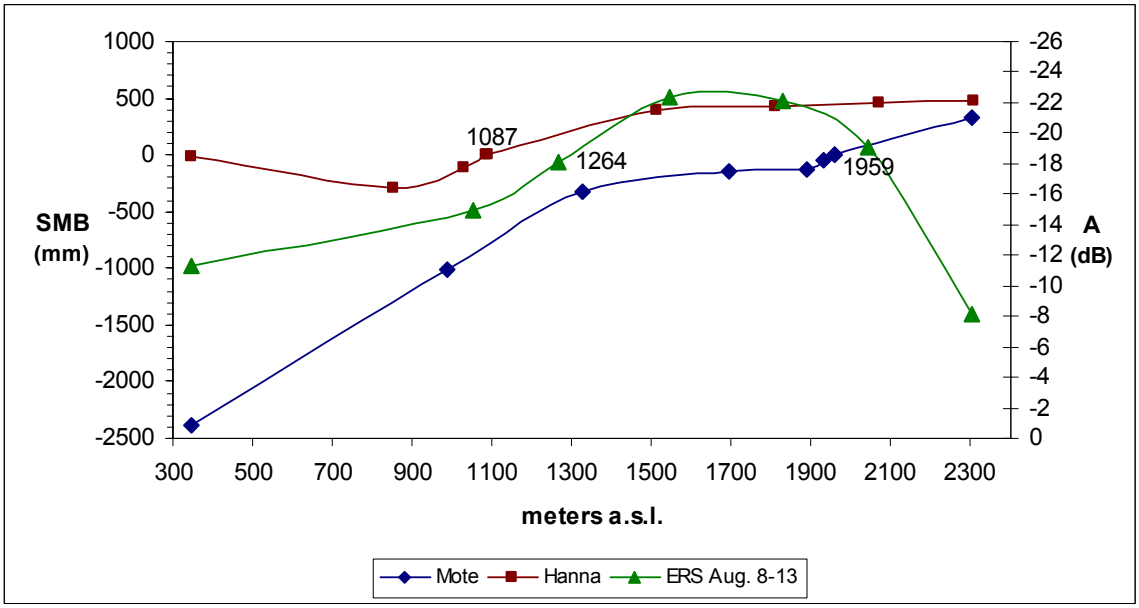

Figure 6.14 Same as that shown in Figure 6.7 for 1999.

CHAPTER 7

SUMMARY AND CONCLUSIONS

During the 1990s, the SMB of the Greenland ice sheet changed largely based on growing rates of ablation near the lower elevations and margins of the ice sheet (Hanna et al., 2002). Average thickening rates above 2000 m of 14 ±7 mm per year in the north and -11 ±7 mm in the south were observed during 1994 to 1999, according to Krabill et al. (2000). These results showed some of the uncertainties that remain over the long-term sign change of the surface mass balance of the Greenland ice sheet. To address these questions in the overall change in the SMB, obtaining reliable rates of accumulation and ablation is required to better predict which of these SMB components will be larger in the long-term.

This study examined the interannual variability in the SMB of the Greenland ice sheet based on results from Hanna et al. (2002), Mote (2003), and scatterometer data acquired from the Scatterometer Climate Record Pathfinder project. These results were used to compare the SMB over the period 1992 to 1999 between each of the data sets. Model-based estimates of accumulation, runoff, and the SMB of the ice sheet were examined based on ECMWF ERA-40 reanalyses data acquired from Edward Hanna, and SSM/I observations acquired from Thomas Mote and compared with the accumulation and ablation zones defined from scatterometer observations.

Scatterometer data from the first and second Earth Remote Sensing (ERS-1/2) satellites were utilized for purposes in this study to span the years 1992 to 1999. The dry snow line (DSL), wet snow line (WSL), and the equilibrium line (EL) were defined in the scatterometer data largely based on work by Long and Drinkwater (1994) and Drinkwater et al. (2001). These boundaries are important in assessing the equilibrium line altitude of the ice sheet from scatterometer observations and therefore the extent of the accumulation and ablation zones. By examining backscatter signature patterns over transitional zones of the ice sheet from the ablation zone near the margins up to the dry snow zone in central regions of the ice sheet, the boundaries of the snow and ice zones were delineated. For purposes in this study, the DSL was defined at the backscatter A value of -5 dB during mid-September, the WSL was defined at the -12 dB line in early July, and the EL was identified at -18 dB during mid-July of each year. Thus, the area of the ice sheet above the -18 dB contour was used to represent the accumulation zone and the area below this line defined the ablation zone, making comparisons with model-based estimates of the SMB by Hanna and Mote possible.

Little interannual variability was observed in the positions of the DSL and EL during this period, and greatest shifts were found in the WSL boundary likely due to fluctuations in annual melt extent of the ice sheet. As a result, the extents of the accumulation and ablation zones did not change substantially over the period based on results from scatterometer observations, and the extent of the ablation zone appeared too small using a backscatter value of -18 dB in the delineation of the EL. In general, the DSL was found to closely follow the 1600 m contour in the north and about 2000 m in the south below about 75° N latitude. The location of the WSL varied both spatially

across the ice sheet and temporally during 1992 to 1999. The WSL reached a maximum elevation of about 2600 m near the southern dome of the ice sheet in 1995. In years of low melt, such as 1992 and 1996, the WSL was generally observed at elevations near 1600 m. Conversely, the EL based on scatterometer observations was generally observed between 1200 and 1600 m in the southwest flank of the ice sheet during the entire period. Differences in backscatter values of A from one year to the next were also examined to show areas of the ice sheet undergoing positive changes in A and, thus, increases in melt areas, and areas of negative changes in A and decreasing areas of melt. Results showed greatest positive changes occurring along the margins of the ice sheet, particularly in the southwest and western portions, suggesting that increases in melt extents were observed interannually over much of the period in these regions.

Spatial patterns of accumulation, runoff, and SMB for the entire ice sheet were examined during this period based on results from Hanna et al. (2002) and Mote (2003). These annual estimates represented by both Hanna and Mote were interpolated onto a 10 km x 10 km based grid to show the spatial and temporal distribution of each over the period. Their results showed that greatest accumulation rates occurred in the southeast region and lowest accumulation rates were experienced in the north central region of the ice sheet during this period. The spatial distribution of net runoff also agreed between the two data sets, with greatest runoff rates occurring in a small portion of the southwest and a second maximum along the northern margin of the ice sheet. Results from all three data sets showed that melting dominated much of the southwest portion of the ice sheet during 1992 to 1999, which had been previously found by Mote and Anderson (1995) and Abdalati and Steffen (1995). Likewise, the pattern of SMB estimates based on results

from Hanna and Mote show good similarity. The EL, represented as the areas of the ice sheet where the SMB equals zero, reached a maximum elevation of about 2400 m in 1998 along the northeast region of the ice sheet according to estimates by Hanna, whereas the EL was suggested to have reached a maximum elevation of 2400 m in 1995 based on estimates by Mote (2003). However, the EL reached much greater elevations during this period according to both Hanna and Mote than was observed from scatterometer observations.

To compare the spatial extents of the accumulation and ablation zones between each of these data sets, the surface areas of both zones were determined for each year and expressed as a fraction of the total surface area of the ice sheet. Greater confidence was placed in the accumulation surface areas, since the lower boundary defined as the ice sheet varied among each of the data sets, likely causing the ablation surface areas to be in error, although the amount of error is unknown. These results demonstrated that large interannual variability existed in the accumulation and ablation surface areas, but each data set showed a similar trend over the eight-year period of an increasing ablation zone and a subsequent decreasing accumulation zone. According to scatterometer observations, the mean accumulation and ablation surface areas were 95.5% ±1.7% and 4.5% ±1.7%, respectively. Based on estimates by Hanna et al. (2002), mean accumulation and ablation surface areas were 87.6% ±6.6% and 12.4% ±6.6%, and from estimates by Mote (2003) mean accumulation and ablation surface areas were 85.2% ±3.9% and 14.8% ±4.0%, respectively.

Annual equilibrium line altitude determined for each data set along a transect within the west central region of the ice sheet, near Jakobshavn and the ETH Camp,

emphasized a longer-term change of an increasing ablation zone over the eight-year period. Despite substantial interannual variability in the ELA, each data set showed an overall increase in the ELA in this region of the ice sheet over the period 1992 to 1999, indicating that a larger portion of the ice sheet existed in the ablation zone by the end of the period then had existed at the beginning. Also, estimates of the SMB along this elevation gradient contained large differences between Hanna and Mote at lower elevations, but their estimates were in better agreement at higher elevations likely due to the fact that accumulation rates were both derived from ECMWF reanalysis data.

To further compare the SMB between the data sets, spatial differences in areas of positive and negative SMB were examined between model-based estimates from Hanna et al. (2002) and Mote (2003). Results showed that much of the central, southeast and extreme southern portions of the ice sheet were in agreement among the two data sets, indicating that the SMB was either positive or negative according to both Hanna and Mote. Conversely, the sign of the SMB of the ice sheet differed mainly in the southwestern, northern, and western margins of the ice sheet. As a result, it is expected that these discrepancies shown in the sign of the SMB within the margins of the ice sheet are likely due to differences in estimates of ablation. A comparison of the equilibrium lines between each of the data sets for the years 1992, 1995, 1998, and 1999 showed similar results, with discrepancies in the location of the EL mainly in the southwestern and northern regions of the ice sheet.

This research showed that during the period 1992 to 1999, SMB estimates were in better agreement within higher elevation regions. However, inconsistencies remain in estimates of the SMB within the lower elevation ablation regions, particularly along the

southwestern and northern margins of the ice sheet. The accumulation and ablation zones defined by the -18 dB backscatter contour from ERS-1/2 scatterometer observations may not adequately represent the location of the equilibrium line. Since the definition of the equilibrium line is crucial in studies of the SMB of the ice sheet, it is recommended that further analysis be performed to determine the most optimal demarcation of the equilibrium line from ERS scatterometer data. The comparison of annual ELA among the three data sets performed in this study demonstrated an effective method by which to infer differences in the SMB between each of the data sets. Therefore, it is also recommended that annual ELA be calculated for several other basins within the ice sheet to illustrate change in the SMB over more regions of the ice sheet and to provide a more detailed comparison between these data sets utilized in this study as well, as with other published results.

The inclusion of three unique data sets to examine variability in the SMB of the Greenland ice sheet over an eight-year period is the primary focus of this work. By comparing results from separate studies, disagreement in SMB estimates between the different data sets may be more clearly identified and can be useful in an ongoing effort to obtain more reliable rates of accumulation and ablation. Greenland plays a critical role in climate change, serving as in indicator of long-term climate trends, and with approximately 85% of the island covered by snow and ice it has the potential of contributing substantially to global sea levels, equivalent to 6-7 m of global sea-level rise according to Hvidberg (2000). This research re-emphasizes the need to acquire more accurate estimates of the surface mass balance of the ice sheet, especially within the lower elevation north and southwest margins of the ice sheet.

REFERENCES

Abdalati, W. and K. Steffen, 1995: Passive Microwave-Derived Snow Melt Regions on the Greenland ice sheet. *Geophys. Res. Lett*., 22, 787-790.

_____, and _____, 1997: Snowmelt on the Greenland Ice Sheet as Derived from Passive Microwave Satellite Data. *J. Clim*., 10, 165-175.

_____, and _____, 2001: Greenland ice sheet Melt Extent: 1979-1999. *J. Geophys. Res*., 106, 33,983-33,989.

_____, W. Krabill, E. Frederick, S. Manizade, C. Martin, J. Sonntag, R. Swift, R. Thomas, W. Wright, and J. Yungel, 2001: Outlet Glacier and Margin Elevation Changes: Near-Coastal Thinning of the Greenland ice sheet. *J. Geophys. Res*., 106, 33,729-33,742.

Ambach, W., 1993: Effects of Climatic Perturbations on the Equilibrium-line Altitude, West Greenland. *J. Glaciol.*, 39, 5-8.

Bales, R. C., J. McConnell, E. Mosley-Thompson, and G. Lamorey, 2001: Accumulation Map for the Greenland ice sheet: 1971 – 1990. *Geophys. Res. Lett.*, 28, 2967-2970.

Benson, C.S., 1962: Stratigraphic Studies in the Snow and Firn of the Greenland Ice Sheet. U.S. Army CRREL Research Report 70, U.S. Army Cold Regions Research and Engineering Laboratory, Hanover, NH, 93 pp.

_____, 1967: Polar Regions Snow Cover. In *Physics of snow and ice. International conference on Low Temperature Science, 1966, Proceedings,* 1, 1039-1063.

Bindschadler, R. A., 1984: Jakobshavns Glacier Drainage Basin: A Balance Assessment. *J. Geophy. Res*., 89, 2066-2072.

_____, 1985: Contribution of the Greenland Ice Cap to Changing Sea Level: Present and Future. *Glaciers, Ice Sheets, and Sea Level*, Washington DC: National Academy Press.

_____, K. C. Jezek, and J. Crawford, 1987: Glaciologic Investigations Using the Synthetic Aperture Radar Imaging System. *Ann. Glaciol.*, 9, 11-19.

Bolzan, J.F, and K.C. Jezek, 1998: Accumulation Rate Changes in Central Greenland from Passive Microwave Data. Byrd Polar Research Center, The Ohio State University.

Box J., K. Steffen, 2001: Sublimation on the Greenland Ice Sheet from Automated Weather Station Observations. *J. Geophys. Res*., 106, 33,965-33,982.

Braithwaite, R. and B. Olesen, 1989: Calculation of Glacier Ablation from Air Temperature, West Greenland. In Oerlemans, J., ed. Glacier fluctuations and climate change. Dordrecht, Kluwer Academic Publishers, 219-233.

_____, and _____, 1990: Response of the Energy Balance on the Margin of the Greenland ice sheet to Temperature Changes. *J. Glaciol.*, 36, 217-221.

_____, and _____, 1992: Seasonal Variation of Ice Ablation at the Margin of the Greenland ice sheet and its Sensitivity to Climate Change, Qamanârssûp Sermia, West Greenland. *J. Glaciol*., 39, 267-274.

_____, M. Laternser, and W. Pfeffer, 1994: Variations of Near-Surface Firn Density in the Lower Accumulation Area of the Greenland Ice Sheet, Pâkitsoq, West Greenland. *J. Glaciol*., 40, 477-485.

Bromwich, D. H., Q. Chen, L. Bai, E. N. Cassano, and Y. Li, 2001: Modeled Precipitation Variability over the Greenland ice sheet. *J. Geophy. Res*., 106, 33,891-33,908.

Cressie, Noel A. C., 1990: The Origins of Kriging. *Mathematical Geology*, 22, 239-252.

Drinkwater, D., D. Long, and A. Bingham, 2001: Greenland Snow Accumulation Estimates from Satellite Radar Scatterometer Data. *J. Geophys. Res*., 106, 33,935-33,950.

Early, D., D. Long, and M. Drinkwater, 1994: Comparison of Enhanced Resolution Images of Greenland from the ERS-1 and Seasat Scatterometers. *Proc. IGARSS '94*, Vol. 4, IEEE Cat. No. 94CH3378-7, 2382-2384.

Ekholm, E., 1996: A Full Coverage, High-Resolution Topographic Model of Greenland Computed from a Variety of Digital Elevation Data. *J. Geophys. Res*., 101, 21,961-21,972.

Hanna, E., P. Valdes, and J. McConnell, 2001: Patterns and Variations of Snow Accumulation over Greenland, 1979 – 98, from ECMWF Analyses and Their Verification. *J. Clim*, 14, 3521 – 3535.

_____, P. Huybrechts, and T. Mote, 2002: Surface Mass Balance of the Greenland Ice Sheet from Climate Analysis Data and Accumulation/Runoff Models. *Ann. Glaciol*., 35, 67-72.

Hvidberg, C.S., 2000: When Greenland Ice Melts. *Nature*, 404, 551 – 552.

Janssens, I. and P. Huybrechts, 2000: The Treatment of Meltwater Retention in Mass-Balance Parameterizations of the Greenland ice sheet. *A. of Glaciol*., 31, 133-140.

Jezek, K., J.P. Crawford, R. Bindschadler, M.R. Drinkwater, and R. Kwok, 1990: Synthetic Aperture Radar Observations of the Greenland ice sheet. *Proceedings of the Second Airborne Synthetic Aperture Radar (AIRSAR) Workshop*, June 7 and 8, 1990. JPL Publ. 90-56, 21-28.

_____, M.R. Drinkwater, J.P. Crawford, R. Bindschadler, and R. Kwok, 1993: Analysis of Synthetic Aperture Radar Data Collected over the Southwester Greenland ice sheet. *J. Glaciol*., 39, 119-132.

Kaser, G., A. Fountain, and P. Jansson, 2003: A manual for monitoring the mass balance of mountain glaciers. IHP-IV, *Technical Documents in Hydrology*, No. 59, UNESCO.

Krabill, W., W. Abdalati, E. Frederick, S. Manizade, C. Martin, J. Sonntag, R. Swift, R. Thomas, W. Wright, and J. Yungel, 2000: Greenland ice sheet: High-Elevation Balance and Peripheral Thinning. *Science*, 428 – 430.

Long, D., P. Hardin, and P. Whiting, 1993: Resolution Enhancement of Spaceborne Scatterometer Data. *IEEE Trans. Geosci. and Rem. Sens*., 31, 700-715.

_____, and M.R. Drinkwater, 1994: Greenland Ice-Sheet Surface Properties Observed by the Seasat-A Scatterometer at Enhanced Resolution. *J. Glaciol*., 40, 213-230.

_____, M. R. Drinkwater, B. Holt, S. Saatchi, and C. Bertoia, 2001: Global Ice and Land Climate Studies Using Scatterometer Image Data. *EOS Transactions*, AGU, 82, 503.

McConnell, J. R., G. Lamorey, E. Hanna, E. Mosley-Thompson, R. Bales, D. Belle-Oudry, and J. Kyne, 2001: Annual Net Snow Accumulation Over Southern Greenland from 1975 to 1998. *J. Geophys. Res.*, 106, 33,827 – 33,836.

Mitrovica, J.X., M. E. Tamisiea, J. L. Davis, and G. A. Milne, 2001: Recent Mass Balance of Polar Ice Sheets Inferred from Patterns of Global Sea-Level Change. *Nature*, 409, 1026-1029.

Mote, T. L., M. R. Anderson, K. C. Kuivinen, and C. M. Rowe, 1993: Passive Microwave-Derived Spatial and Temporal Variations of Summer Melt on the Greenland ice sheet. *Ann. Glaciol*., 17, 233-238.

_____, 1994: Variations in Passive Microwave Measurements of Melt on the Greenland Ice Sheet and Associated Northern Hemisphere Atmospheric Circulation. Dissertation, University of Nebraska, Lincoln Nebraska.

_____, and M. R. Anderson, 1995: Variations in Snowpack Melt on the Greenland Ice Sheet Based on Passive-Microwave Measurements. *J. Glaciol*., 41, 51-60.

_____, 1998a: Mid-Tropospheric Circulation and Surface Melt on the Greenland Ice Sheet. Part I: Atmospheric Teleconnections. *Int. J. Clim.*, 18, 111-129.

_____, 1998b: Mid-Tropospheric Circulation and Surface Melt on the Greenland Ice Sheet. Part II: Synoptic Climatology. *Int. J. Clim.*, 18, 131-145.

_____, 2000: Ablation Rate Estimates over the Greenland Ice Sheet from Microwave Radiometric Data. *Prof. Geog.*, 52, 322-331.

_____, 2003: Estimation of Runoff Rates, Mass Balance, and Elevation Changes on the Greenland ice sheet from Passive Microwave Observations. *J. Geophys. Res.*, 108, 4056, doi:10.1029/2001JD002032.

Ohmura, A. and N. Reeh, 1991: New Precipitation and Accumulation Maps for Greenland. *J. Glaciol.*, 37, 142 – 148.

Partington, K.C., J.K. Ridley, C.G. Rapley, and H.J. Zwally, 1989: Observations of the Surface Properties of the Ice Sheets by Satellite Radar Altimetry. *J. Glaciol*., 267-275.

Paterson, W.S.B, 1981: The Physics of Glaciers, Second Edition. Pergamon, Oxford.

Reeh, N. Ørsted: Greenland Ice Sheet Mass Balance. *Technical University of Denmark*, Lyngby, Denmark.

Rott, H., G. Domik, C. Mätzler, H. Miller, and K. G. Lenhart, 1985: Study on the use and Characteristics of SAR for Land Snow and Ice Applications. Final report. Paris, European Space Agency. (ESA Report 5441/83/D/IM/SC).

Swift, C. T., P. S. Hays, J. S. Herd, W. L. Jones and V. E. Delnore, 1985: Airborne Microwave Measurements of the Southern Greenland ice sheet. *J. Geophys. Res.*, 90, 1983-1994.

Thomas, R., T. Akins, B. Csatho, M. Fahnestock, P. Gogineni, C. Kim, and J. Sonntag, 2000: Mass Balance of the Greenland ice sheet at High Elevations. *Science*, 289, 426 – 428.

Weidick, A., 1985: The Ice Cover of Greenland. *Gletscher-hydrol. Meddelelser* nr. 85/4, Grønlands Geol. Undersøgelse, Copenhagen.

Williams, R. S. Jr., D. K. Hall, and C. S. Benson, 1991: Analysis of Glacier Facies using Satellite Techniques. *J. Glaciol*., 37, 120-127.

Wismann, V. R., 2000: Monitoring of seasonal snowmelt in Greenland with ERS scatterometer data. *IEEE Trans. Geosci. Remote Sens*., 38, 1821-1826.

Zhang, H., L. Pedersen, and P. Gudmandsen, 1989: Microwave Brightness Temperatures of the Greenland ice sheet. *Adv. Space Res*., 9, 277-287.

Zwally, J. H., 1989: Growth of Greenland Ice Sheet: Interpretation. *Science*, 246, 1589-1591.

APPENDIX A

ANNUAL ERS-1/2 HISTOGRAMS FROM 1992 TO 1999

Annual histograms of ERS-1/2 backscatter (σ°) values of A along two sample regions, I and J, of the ice sheet used in the delineation of the dry snow line, wet snow line, and the equilibrium line during the period 1992 to 1999. Transect I is located at 73° N, 54° W to 75° N, 50° W, and transect J is located at 65° N, 47° W to 66° N, 44° W.

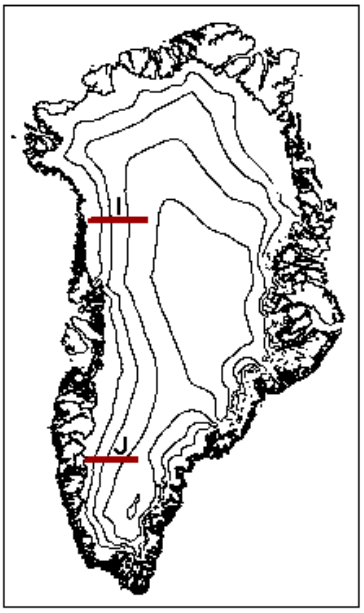

A.1 Delineation of the dry snow line at I

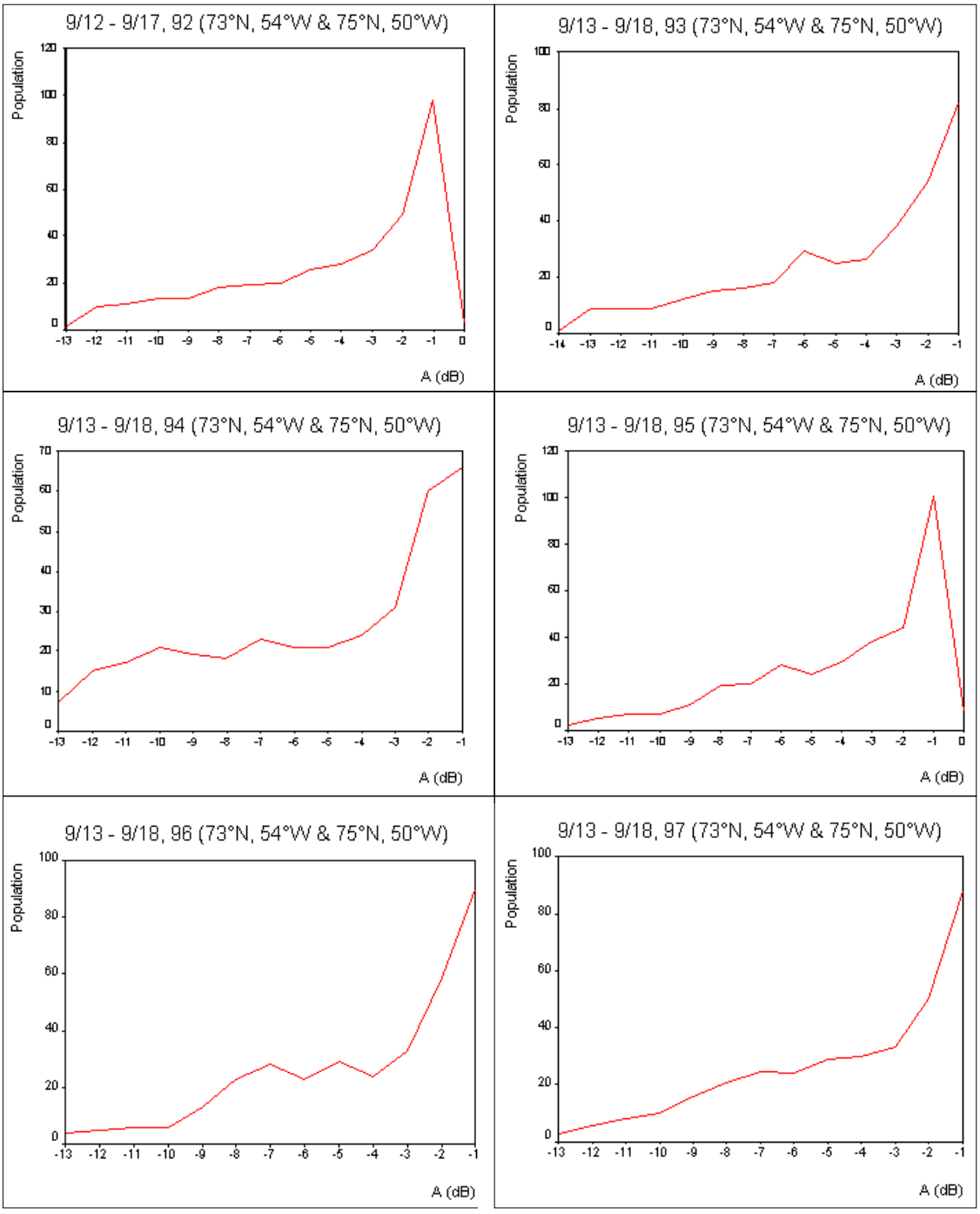

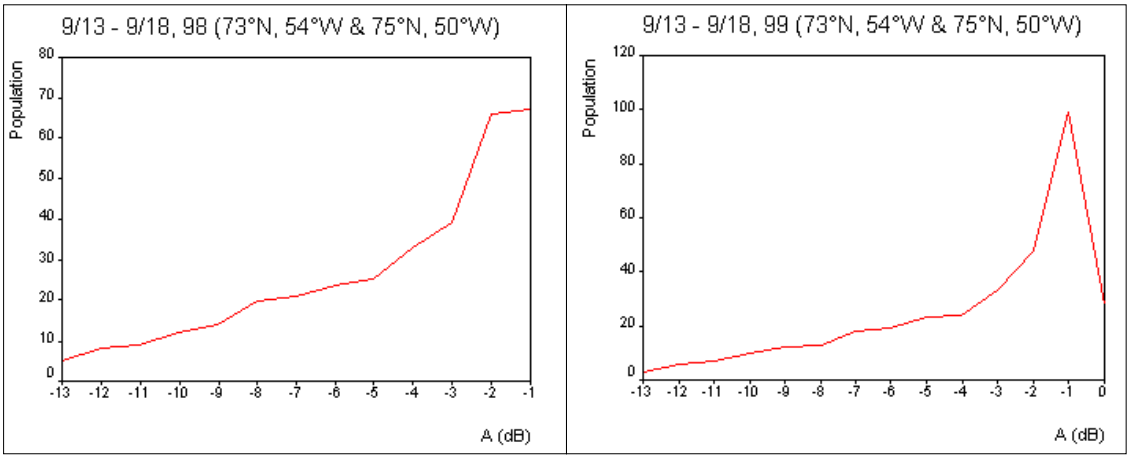
9/13 - 9/18, 98 (73°N, 54°W & 75°N, 50°W)
Population
80
70
60
50
40
30
20
10
0
-13 -12 -11 -10 -9 -8 -7 -6 -5 -4 -3 -2 -1
A (dB)
9/13 - 9/18, 99 (73°N, 54°W & 75°N, 50°W)
Population
120
100
80
60
40
20
0
-13 -12 -11 -10 -9 -8 -7 -6 -5 -4 -3 -2 -1 0
A (dB)

A.2 Delineation of the wet snow line at J

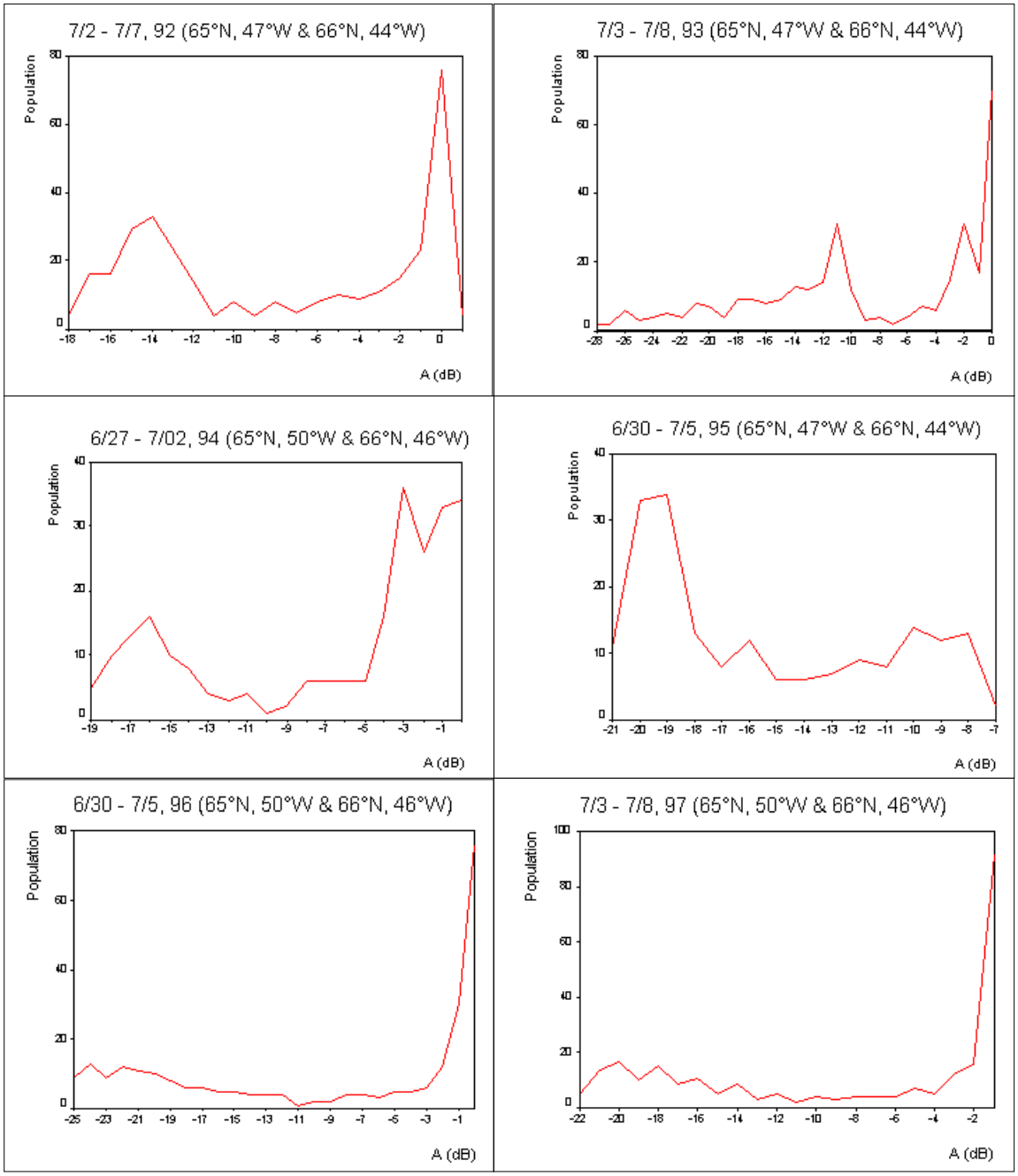

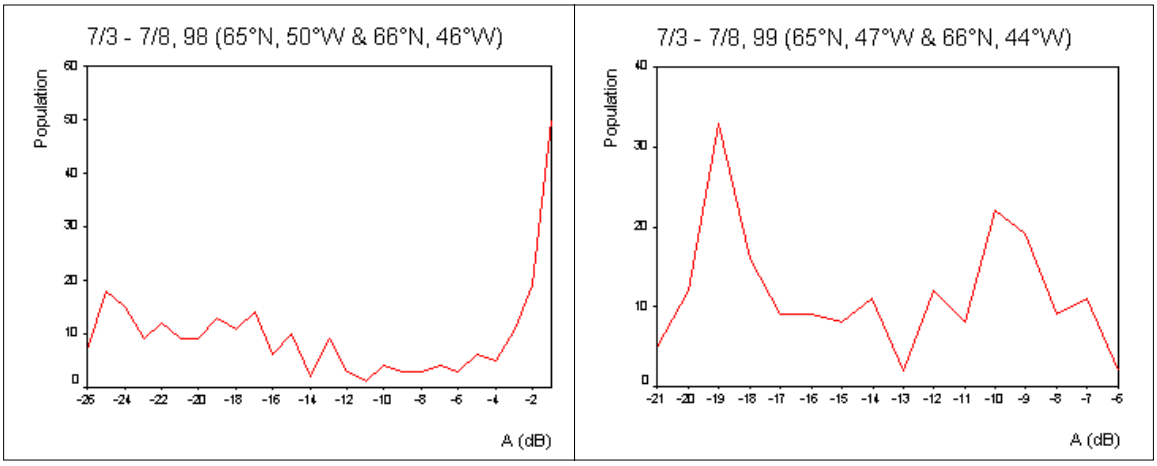
7/3 - 7/8, 98 (65°N, 50°W & 66°N, 46°W)
Population
A (dB)
7/3 - 7/8, 99 (65°N, 47°W & 66°N, 44°W)
Population
A (dB)

A.3 Delineation of the equilibrium line at J

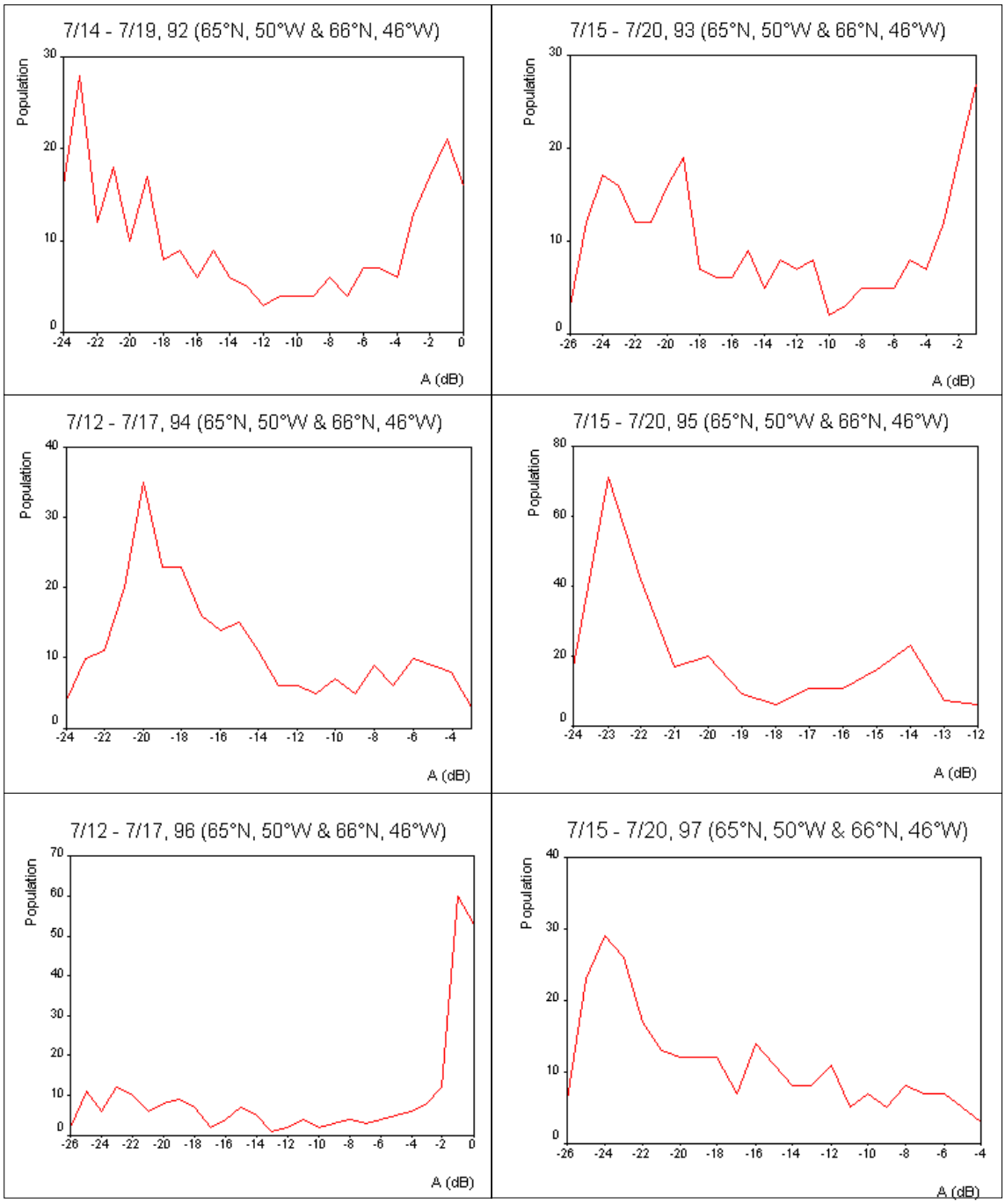

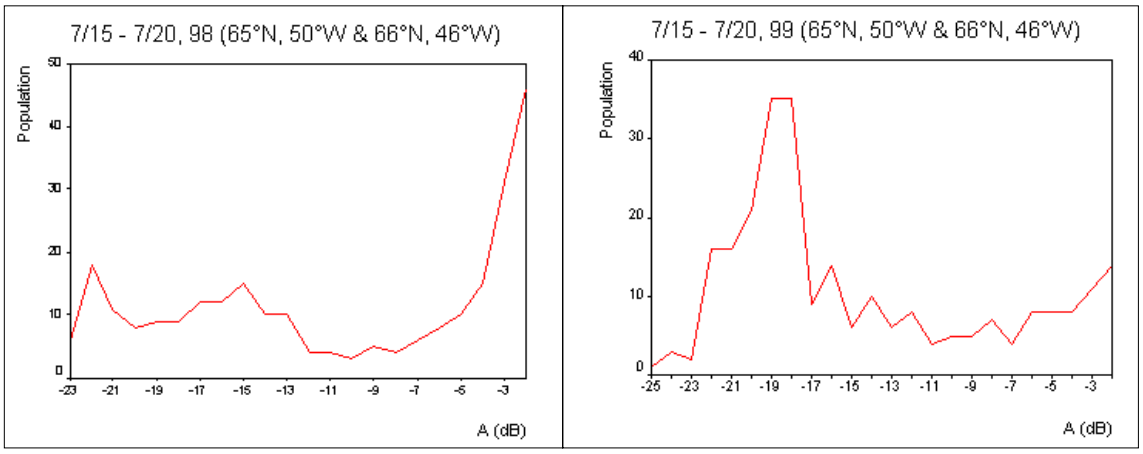
7/15 - 7/20, 98 (65°N, 50°W & 66°N, 46°W)
Population
0
10
20
30
40
50
-23
-21
-19
-17
-15
-13
-11
-9
-7
-5
-3
A (dB)
7/15 - 7/20, 99 (65°N, 50°W & 66°N, 46°W)
Population
0
10
20
30
40
-25
-23
-21
-19
-17
-15
-13
-11
-9
-7
-5
-3
A (dB)